USGS
science for a changing world

Gallery of Melt Textures Developed in Westerly Granite During High-Pressure Triaxial Friction Experiments

By Diane E. Moore, David A. Lockner, Brian D. Kilgore, and Nicholas M. Beeler

Open-File Report 2016–1059

U.S. Department of the Interior
U.S. Geological Survey

U.S. Department of the Interior
SALLY JEWELL, Secretary

U.S. Geological Survey
Suzette M. Kimball, Director

U.S. Geological Survey, Reston, Virginia: 2016

Suggested citation:
Moore, D.E., Lockner, D.A., Kilgore, B.D., and Beeler, N.M., 2016, Gallery of melt textures developed in Westerly Granite during high-pressure triaxial friction experiments: U.S. Geological Survey Open-File Report 2016–1059, 75 p., http://dx.doi.org/10.3133/ofr20161059.

ISSN 2331-1258 (online)

Contents

Figures

Gallery of Melt Textures Developed in Westerly Granite During High-Pressure Triaxial Friction Experiments

By Diane E. Moore, David A. Lockner, Brian D. Kilgore, and Nicholas M. Beeler

Introduction

Melting occurred during stick-slip faulting of granite blocks (fig. 1) sheared at room-dry, room-temperature conditions in a triaxial apparatus at 200–400 megapascals (MPa) confining pressure (Lockner and others, 2010). Petrographic examinations of melt textures focused largely on the 400-MPa run products. This report presents an overview of the petrographic data collected on those samples, followed by brief descriptions of annotated versions of all the images.

Scanning electron microscope (SEM) images of the starting materials and the three examined 400-MPa samples are presented in this report. Secondary-electron (SE) and backscattered-electron (BSE) imaging techniques were used on different samples. The SE images look down on the sawcut surfaces, yielding topographic and three-dimensional textural information. The BSE imaging was done on samples cut to provide cross-sectional views of the glass-filled shear band (or zone) that developed along the sawcut. Brightness in the BSE images increases with increasing mean atomic number of the material. Additional chemical information about the quenched melt and adjoining minerals was obtained using the energy dispersive system (EDS) of the SEM during BSE examinations. However, the very narrow shear-band thicknesses and common occurrence of very fine lamellar compositional layering limited the usefulness of this technique for estimating melt chemistry.

To determine the nature of the starting surfaces, one of the sawcuts was examined with SE techniques. In addition, two granite disks were prepared in the same manner as the driving blocks (see below). The roughened surfaces of the disks were then epoxied together and sliced perpendicular to the plane of the surfaces for polished thin-section preparation and BSE examination.

The run products featured in this report were examined in one of two ways. The jackets were removed from two samples and the two driving blocks were separated. The narrow end of one of the half cylinders was then broken off and mounted on a glass slide, such that the sawcut was facing up and roughly horizontal. The third, still-jacketed sample was impregnated with epoxy resin before being sliced parallel to the axis of the cylinder and perpendicular to the plane of the sawcut. The surface of one of the sliced half cylinders was polished for SEM examination.

Mineral abbreviations used in the figures, after Whitney and Evans (2010), are listed below.

Mineral Abbreviations

Ab	albite
Aln	allanite
Ap	apatite
Bt	biotite
Cal	calcite
Chl	chlorite
Ep	epidote
Fl	fluorite
Ilm	ilmenite
Mt	magnetite
Kfs	K-feldspar
Mu	muscovite
Pl	plagioclase
Qz	quartz
Ttn	titanite (sphene)

Figure 1. Photograph of Westerly Granite driving blocks used in the experiments. The two halves of the granite cylinder are fitted together in a polyurethane jacket for the experiments, and shear is concentrated along the synthetic fault.

Starting Material

Westerly Granite is a granodiorite that contains ~40 modal percent plagioclase, ~25 percent quartz, and ~25 percent K-feldspar (for example, Moore, 1993). Biotite is the most abundant phyllosilicate mineral, at ~6 percent; lesser amounts of muscovite and secondary chlorite, after biotite, are also present. For the experiments, cylinders of Westerly Granite, 25.4 mm in diameter and 60 mm long, were sliced into two pieces at a 30° angle to the cylinder axis (fig. 1). The sawcut surfaces were ground with 600-grit alumina (Al_2O_3) powder, yielding a slightly roughened texture with several somewhat deeper pits (fig. 2). The largest depression in the examined samples of starting material was nearly 30 micrometers (μm) deep and slightly more than 100 μm wide.

Viewing the sawcut surfaces in cross section (figs. 3, 4), the amount of surface damage is seen to vary with the type, size, and orientation of the mineral exposed on the sawcut. However, the damaged zone has a minimum or baseline width of ~1.8–2 μm, produced by chipping of the mineral surfaces. This narrow disturbed zone is marked by the white dashed lines in figures 3 and 4 (see also fig. 2*B*). Fracturing and, in places, plucking of loose pieces (fig. 3*B*) commonly widens the damaged layer to 2.7–5.5 μm on a side (black lines in figs. 3, 4). Essentially undamaged rock is present at distances ≥10 μm from the sawcut (red line in fig. 4).

During initial shearing most of this initial surface roughness probably is broken off the sawcut and ground by frictional wear to form fine-grained gouge that will subsequently be involved in melting. However, considerably wider damage zones of fracturing and fragmentation develop during the high-pressure experiments.

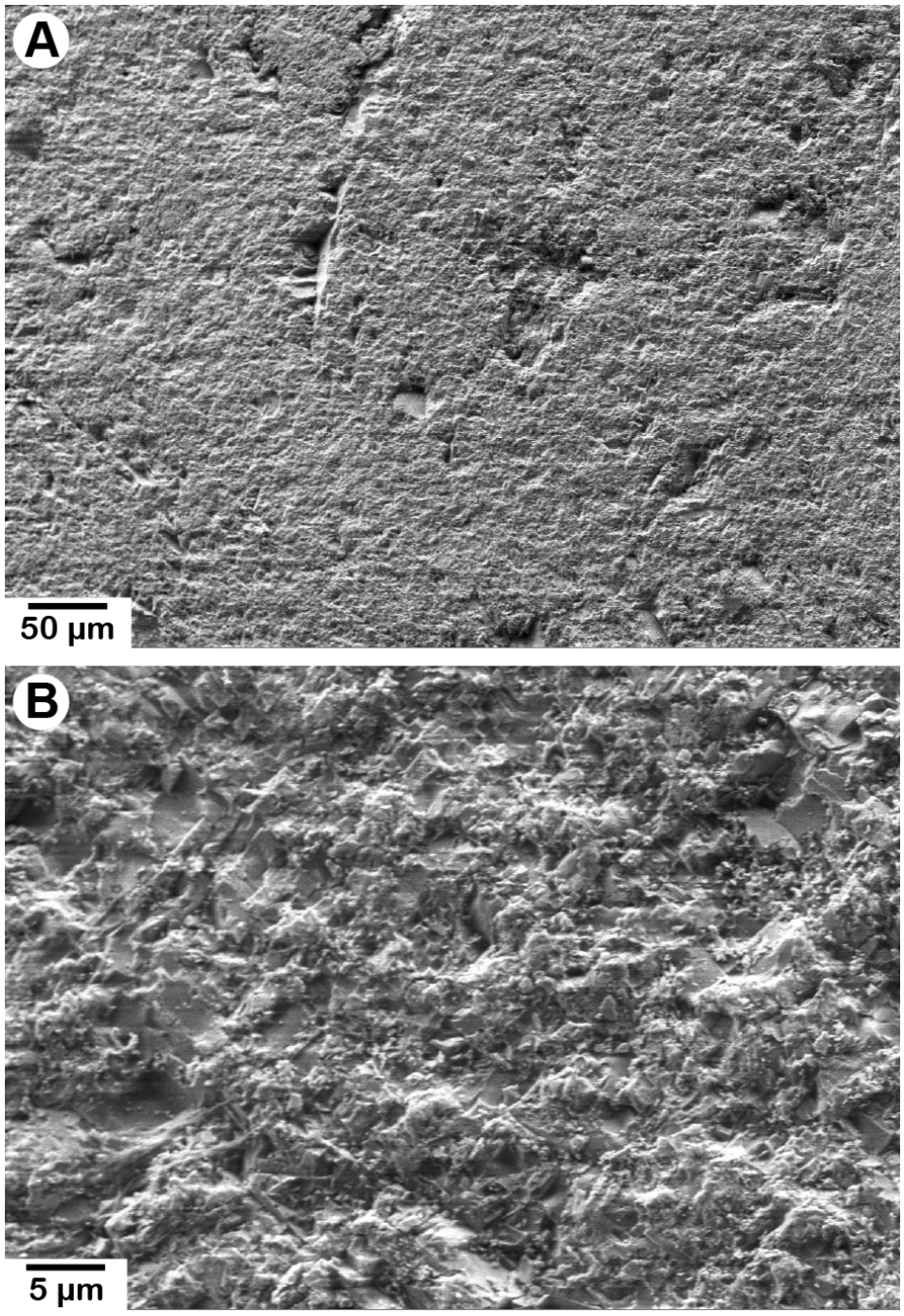

Figure 2. Secondary-electron images of the prepared starting sawcut surface of Westerly Granite. *A*, Slightly roughened surface with scattered deeper pits. *B*, Higher magnification view of the baseline topographic relief, probably developed on a feldspar grain given the two, nearly perpendicular, planar trends.

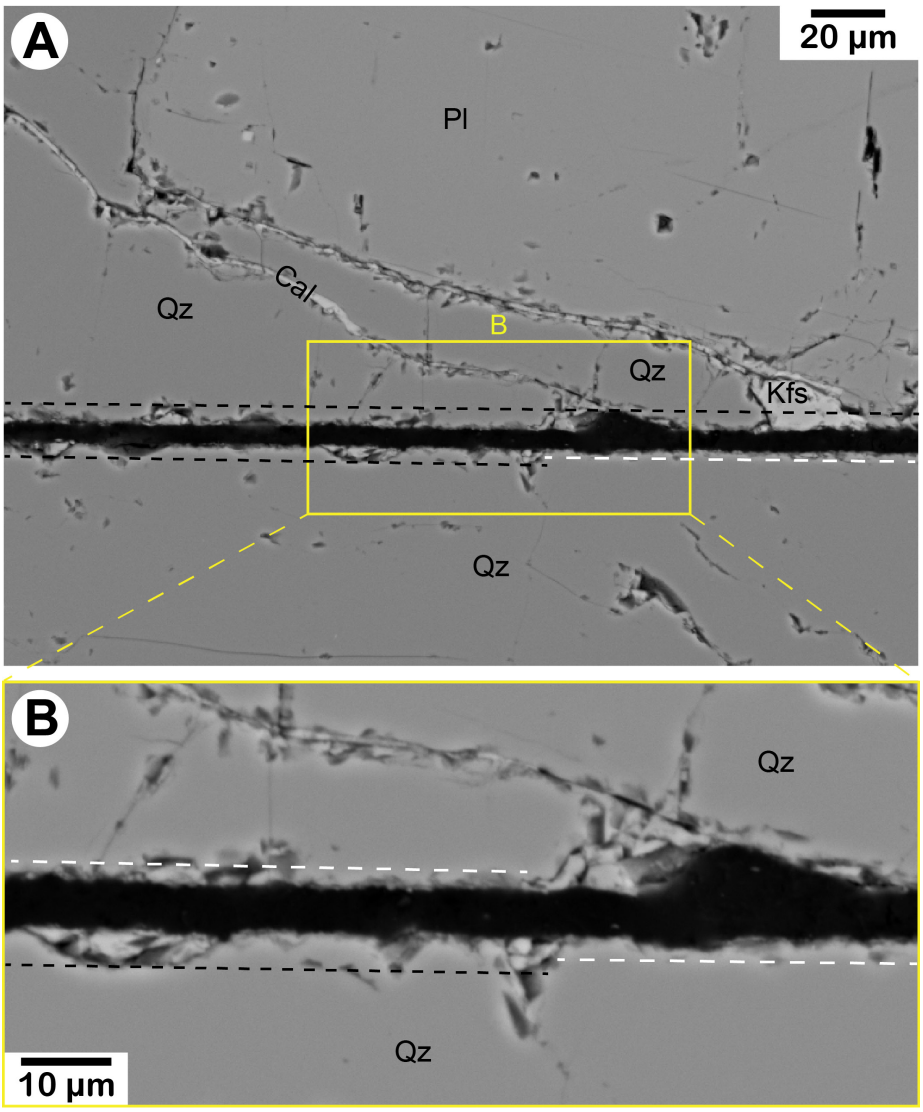

Figure 3. Backscattered-electron images of starting Westerly Granite sawcut surfaces in cross section showing a quartz-rich area at lower (*A*) and higher (*B*) magnification. White dashed lines denote the topography of the roughened surfaces seen in figure 2, and black dashed lines mark the approximate limit of extensive fracturing.

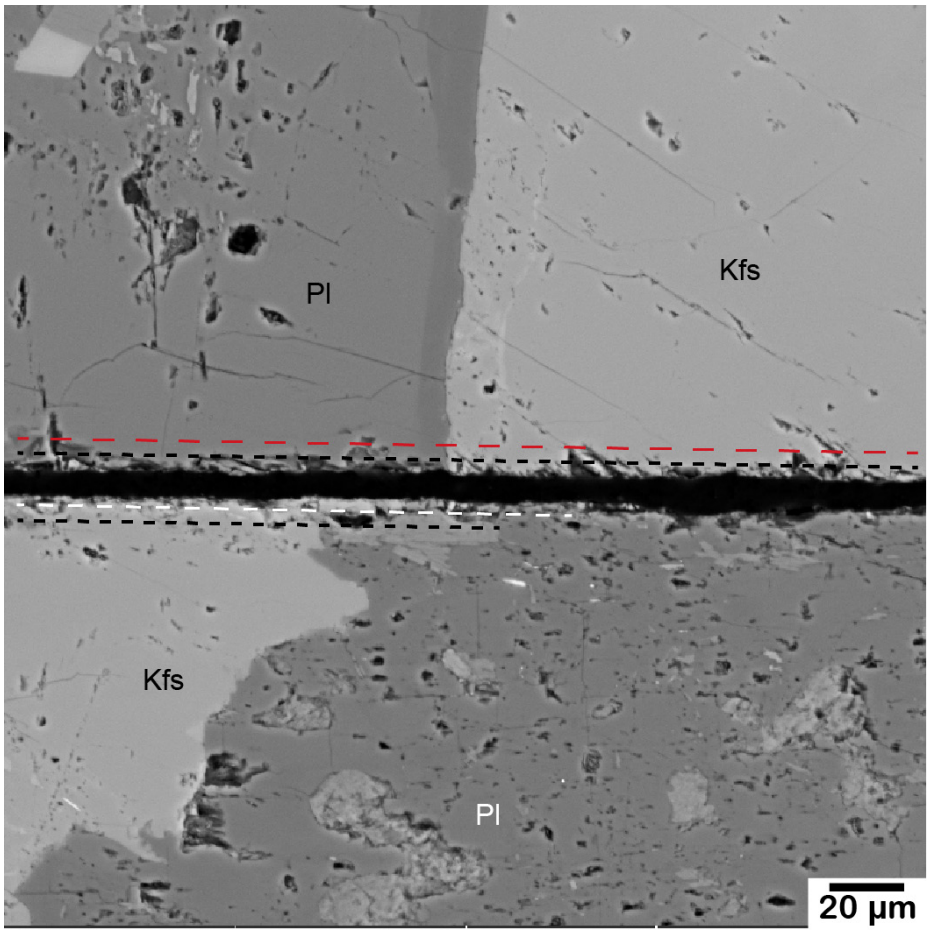

Figure 4. Backscattered-electron image of feldspar surface textures in the prepared starting materials. White dashed line denotes the topography of the roughened surfaces seen in figure 2 and black dashed lines mark the approximate limit of extensive fracturing. The extent of a few subparallel cleavage cracks that extend slightly farther (~10 µm) into the crystals is marked by the red dashed line.

Overview of Melt Textures

The two 400-MPa experiments (DL511 and DL513) featured in figures 5–7 were characterized by two stick-slip events, the first a partial stress drop (125–140 MPa) and the second a total (325–340 MPa) stress drop. Fault-parallel slip increases with increasing stress drop, and the stress drops of 325–340 MPa were accompanied by roughly 3 mm of offset along the sawcut (Lockner and others, 2010). The two halves of these samples were welded together along the sawcut and, when the confining pressure was lowered, the driving blocks separated along fractures and cleavage planes in the adjoining minerals rather than through the glass-filled shear band (fig. 5*B*). The shear band, a narrow, bright (relatively Fe-rich) band in BSE images, switches back and forth across the two sides, and the sides can be fitted back together. For example, a fragment of calcite from the crystal on the upper side in figure 5*B* remained stuck to the shear band on the lower sawcut (marked by the downward pointing arrow) when confining pressure was removed and the two driving blocks separated. Looking down on the sawcut surfaces (fig. 5*A*), the highest elevations are mineral fragments that became separated from the overlying driving block when it was removed. Glimpses of the shear texture below (striated areas

in the center) are seen in "windows" through the damaged rock. The fractured and fragmented minerals above the shear band in figure 5*A* are intermixed with vesicle-filled glass. In this report, the term "shear band" is used to denote the thin layer of quenched melt that lies along the plane of the sawcut and served as the principal slip surface during the experiments.

The striated shear band visible in figure 5*A* displays delicate glassy structures (fig. 6*A*) that quenched in substantial void spaces. Excellent preservation suggests that they must have formed at the end of the final stick-slip event. Minor brittle fracturing of the glass occurred during post-experiment handling. The shear band between the muscovite and plagioclase crystals in figure 6*B* contains a considerable amount of void space, or "vugs" after the usage of Kennedy and Spray (1992), crisscrossed by narrow bands that may correspond to the glassy features in figure 6*A*. A row of rounded pores (≤500 nanometers diameter) adjacent to the muscovite may be vesicles, and a similar layer of vesicles is visible below the stretched-out glass in figure 6*A* (at right).

Every phyllosilicate mineral (biotite, muscovite, and chlorite) noted along the sawcut in cross-sectional view adjoins large vugs crossed by threads of glass similar to those in figure 6*B*. Biotite is the most abundant phyllosilicate mineral in Westerly Granite, and the bright central layers of the shear band situated between quartzofeldspathic minerals (for example, fig. 5*B*) commonly are enriched in Fe, Mg, and Ti derived from partial melting of biotite.

Shear-band thickness (for example, fig. 7) generally varies between 4 and 7 μm. The topography of the sawcuts, however, causes the widths to vary locally. The width of the band of fractured granite adjoining the shear band on each side, measured in low-magnification images, averages ~57 μm but varies over nearly two orders of magnitude (3.5–220 μm).

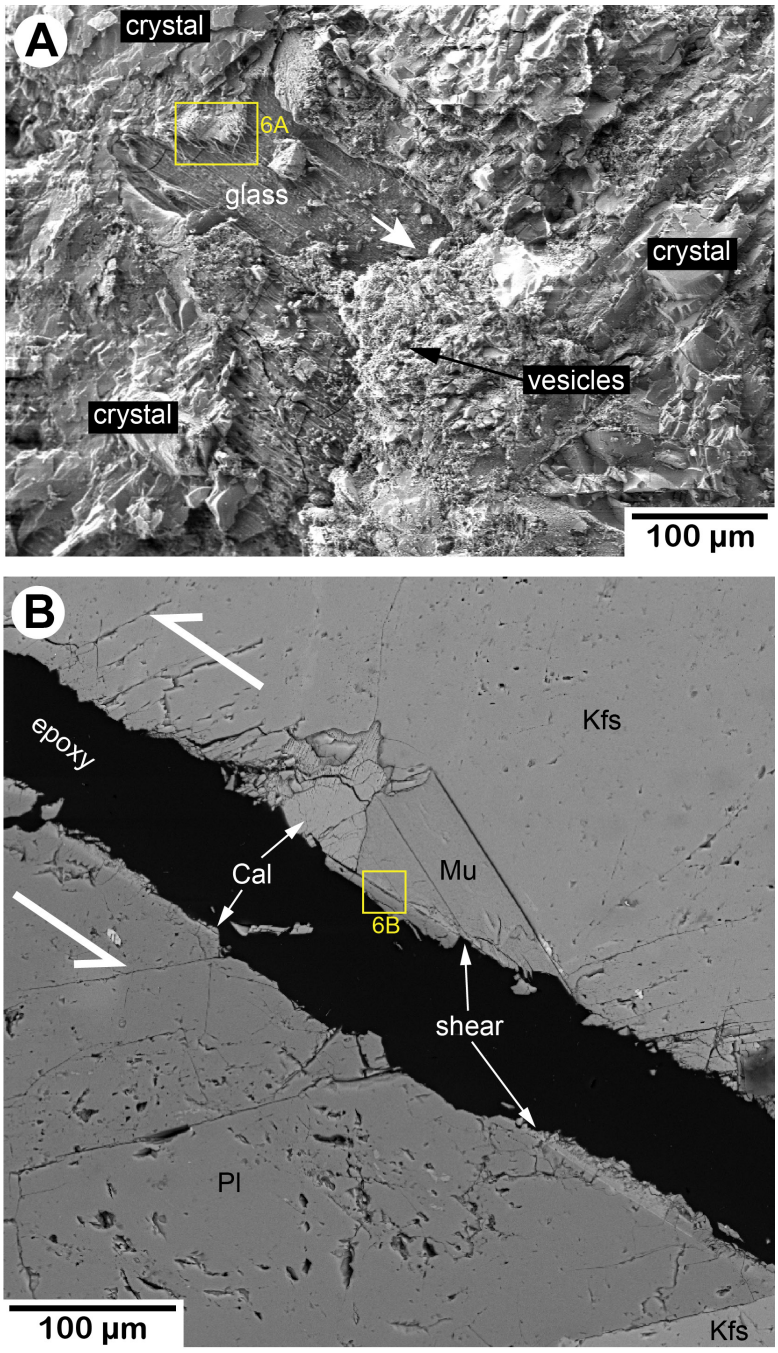

Figure 5. Images of samples sheared at 400-MPa confining pressure. Yellow boxes mark locations of images in figure 6. *A*, Secondary-electron image looking down on one of the driving blocks (also fig. 511-4*A*). Patches of the striated, glassy, sheared material are surrounded by a mixture of crystal fragments and vesicular glass detached from the overlying driving block. White arrow indicates the direction of motion of the driving block. *B*, Backscattered-electron image showing a ~5-µm-thick shear band (quenched melt) that is readily visible because of the brightness contrast (also presented subsequently as fig. 513-6*A*). Shear was left lateral, denoted by pair of large white arrows.

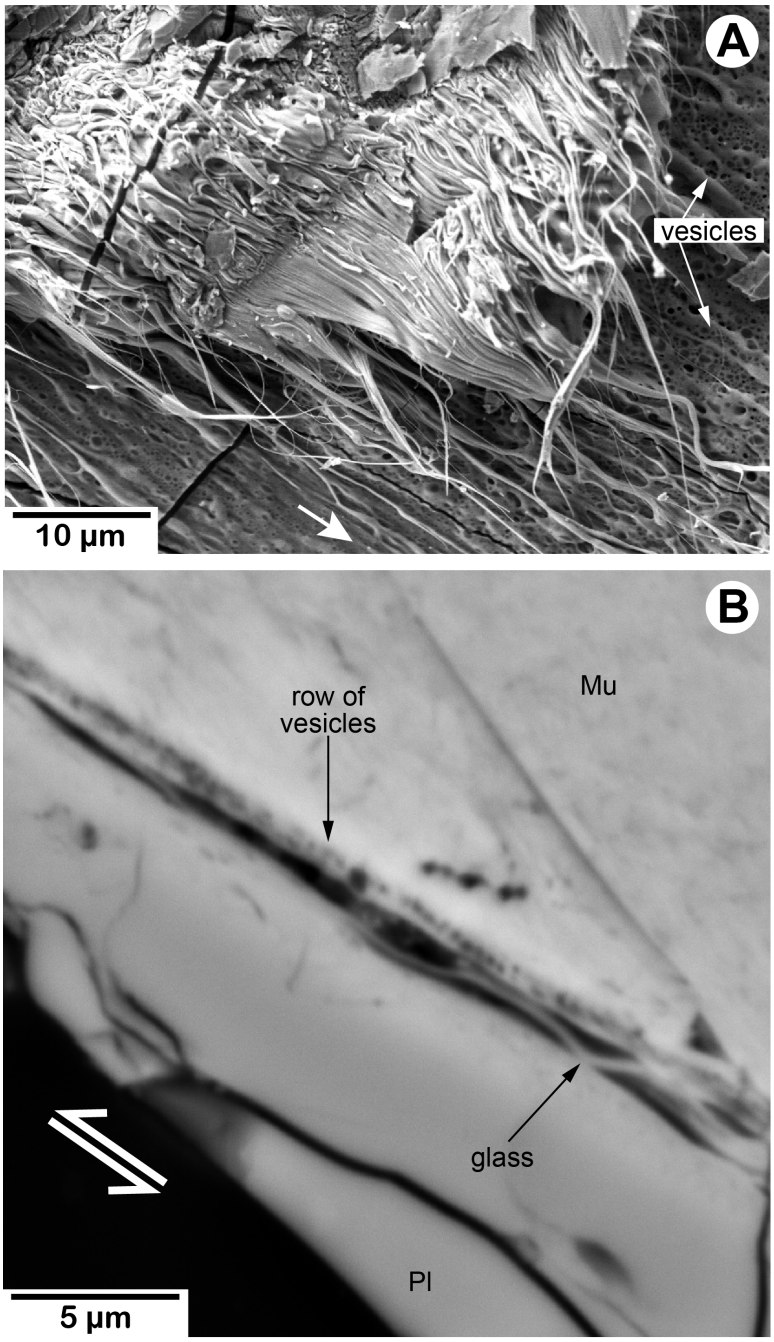

Figure 6. Higher magnification images of melt textures in figure 5. *A*, Secondary-electron image showing dramatic hairlike, glassy structures that quenched in substantial voids (also fig. 511-4*D*). Large white arrow indicates the direction of motion of the driving block. *B*, Backscattered-electron image showing wavy bands that crisscross the void space adjacent to a muscovite crystal, which may correspond to the glassy features in *A* (also fig. 513-6*D*). Shear was left lateral, denoted by pair of white arrows.

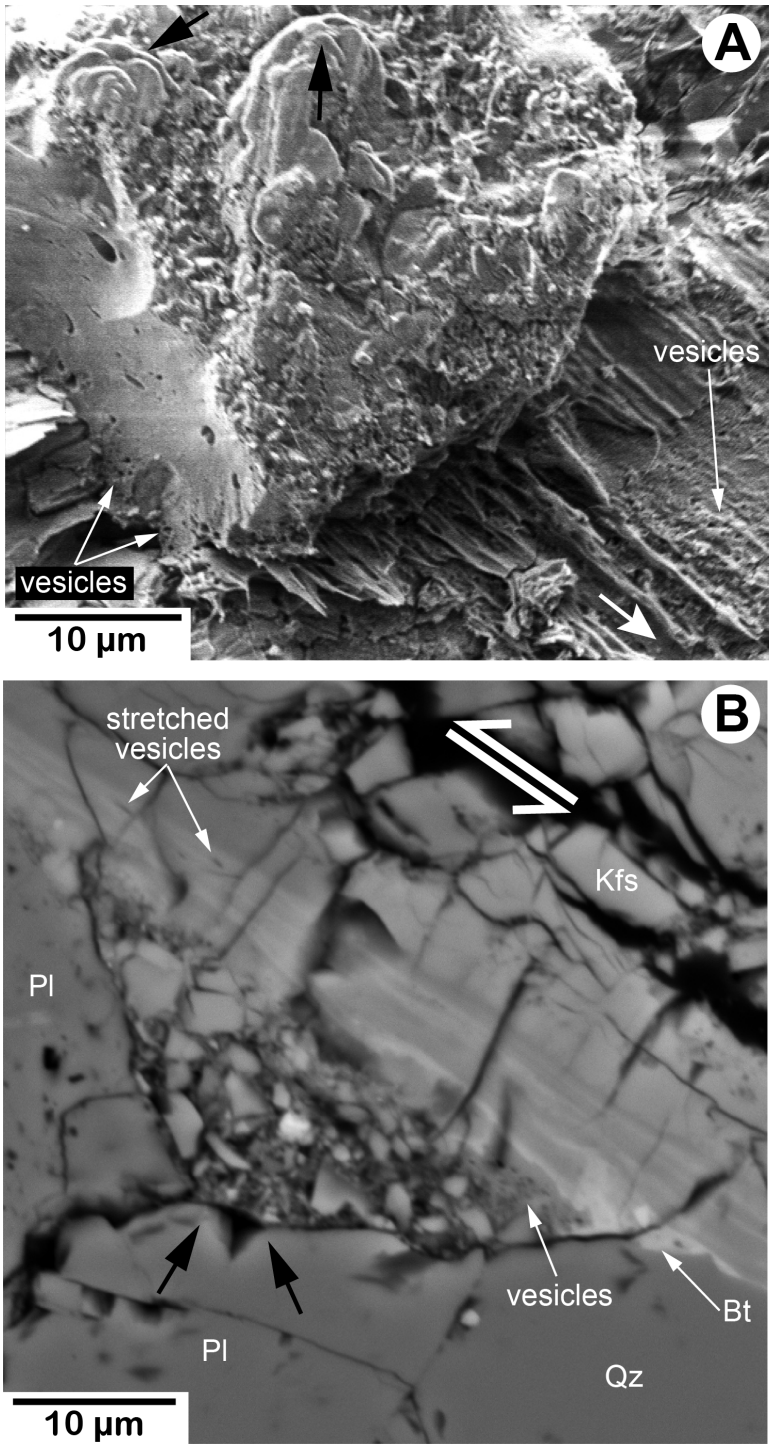

Figure 7. High-magnification images showing the distribution of vesicles within and adjacent to the shear band. Black arrows point to rounded mineral edges, located roughly 10 µm from the shear band. *A*, Secondary-electron image showing rare cross-sectional view of the shear band, which is exposed on the left side of the fragment above the sawcut (also fig. 511-11*B*). The center contains only a few stretched vesicles and the curved, scalloped face is suggestive of conchoidal fracturing. The base is more irregular and vesicle filled. On the lower right side, layers of striated glass grade downwards to a vesicle-rich base

that may correspond to the vesicle-rich band at the bottom of the left face. Large white arrow indicates the direction of motion of the driving block. *B*, Backscattered-electron image showing a texture that may be the approximate equivalent of that in *A*, although here the vesicle- and clast-filled lower area is of limited extent (also fig. 513-16*C*). The clasts probably represent gouge material, formed during initial shearing, that was trapped and consequently preserved in the depression. The shear band that seals the cavity consists of layers of varying composition that may correspond to the projecting layers of glass in *A*. Shear was left lateral, denoted by pair of large white arrows.

Discussion

Comparison to Other Studies (Lab and Field)

The melt textures generated at high confining pressures in these experiments correspond in many ways to those formed in high-speed friction tests conducted at low normal stresses. Most notably, Spray (1995, 2010) described striated coatings with stretched vesicles and "frozen melt strands," that correspond to features in figures 6*A* and 7*A*, in Westerly Granite tested in a frictional welding apparatus. Lin (2008) found similar hairlike strands of glass that formed as melt was ejected from the shearing surface and quenched in air during rotary-shear experiments. The general character of the samples examined in plan view (fig. 5*A*), in which considerable surface topography is created by aggregates of clasts that have been welded together and to the sawcut surface, was also described by Spray (1987). The flow structures seen in figures 5*A*, 6*A*, and 7 were also reported by Lin and Shimamoto (1998; also Lin, 2008). Spray (1992) described the formation of vapor bubbles at amphibole-melt boundaries that may correspond to figure 6*B*.

The examined 400-MPa samples lack two melt textures that are characteristic of both the high-speed friction experiments and natural pseudotachylytes: injection veins and a large proportion of clasts in the melt (for example, Sibson, 1975; Spray, 1987, 1993; Maddock, 1992; Lin and Shimamoto, 1998; Di Toro and Pennacchioni, 2004; Di Toro and others, 2006; Lin, 2008 and references therein). No melt-filled injection veins extending out from the main fault were seen in the samples, although some melt did migrate a few micrometers into the adjoining damaged wall rocks (for example, figs. 5*A*, 7). The lack of injection veins can be explained in terms of the different experimental conditions. The high-speed friction tests represent a single slip event encompassing several meters of displacement and lasting several seconds. The main frictional melting zones generated in those tests can reach 300–500-µm width (for example, Spray, 1987, 1993, 2010) and the accompanying injection veins can be as much as 50 µm wide (for example, Lin, 2008), despite the ejection of melt from the sides of the samples during shear. Natural pseudotachylytes can exceed 10-cm thickness (for example, Sibson, 1975) and ones ≤300 µm thick are considered to be "ultra-thin" (Griffith and others, 2008). In contrast, the total fault-parallel offset in the triaxial tests is on the order of millimeters, and the 400-MPa experiments comprised multiple stick-slip events. The minimal duration and displacement in the triaxial tests yielded only a ~5-µm-thick melt layer that did not fill all the available pore space in the adjoining damage zone, thus minimizing the potential for forcible injection of melt into tension fractures.

The overall paucity of clasts in the glass generated in these two experiments may reflect the two-stage slip history. No evidence was found for more than one episode of melting in those samples. This suggests that during the first stick-slip event (a partial stress drop), finely comminuted gouge was generated, similar to that found in lower confining pressure experiments (Lockner and others, 2010). As a result, few large clasts were present in the shear band when

melt was generated during the second stick-slip event. In addition, the very short duration and small displacement minimized the incorporation of fragmented minerals from the damage zone into the shear band.

The laminar or layered character of the shear bands, best seen in figure 7, is consistent with flow banding in the melt. In igneous rocks flow banding is considered to result from frictional forces developed between the magma and a solid rock surface. Applied to these experiments, the melt closest to the wall rocks slows down relative to that in the center, leading to laminar flow and the development of heterogeneities in composition and vesicle and clast content across the width of the shear band.

Another notable feature of these high-pressure experiments is that the glassy textures are similar to those seen in volcanic rocks, in particular the delicate glass hairs and the lava-like textures. Such structures form by quenching of magma erupted onto the Earth's surface or under water, not at several kilometers depth in the Earth's crust. Vesicles form by exsolution of a vapor phase from melts at low lithostatic pressures. For example, vesicles in pseudotachylytes produced by landsliding were estimated to form at ~20 MPa (Masch and others, 1985), and the depth of vesiculation in fault-generated pseudotachylytes in the Outer Hebrides Thrust, Scotland, was estimated to be ~1.6 km (41 MPa; Maddock and others, 1987). The presence of these glassy textures in the run products of high-speed friction tests is consistent with the low-stress conditions of those experiments. But how do they form at 400 MPa?

The most dramatic glassy textures are developed in the vugs adjacent to the phyllosilicate minerals (figs. 5*B*, 6*B*). Biotite and muscovite contain 3–5 weight percent H_2O and chlorite contains ~12 weight percent H_2O. "Flash" heating of these minerals created pockets of water-rich melt, that seemingly were forcibly ejected from their points of origin to flow along the sawcut. This process presumably occurred in a single pulse that largely but not completely drained the fault surface adjacent to the micas and chlorite (for example, fig. 6). As it flowed, some melt migrated into high-porosity areas of fractured and fragmented crystals along the sawcut, where a vapor-rich phase exsolved from the hydrous melts. The vesicle content of the glass, as viewed in cross section, appears to decrease with increasing distance from hydrous minerals along the sawcut.

Temperature Estimates

The chemistry of both natural (for example, Bossière, 1991; Maddock, 1992; Spray, 1993; Jiang and others, 2015) and laboratory (for example, Spray, 1987, 1993, 2010; Lin and Shimamoto, 1998; Lin, 2008) pseudotachylytes indicates that melting accompanying shear occurs as a nonequilibrium process, in which lower melting-point, typically hydrous minerals are the first to melt. Melt compositions are characteristically more basic (in other words, lower SiO_2 content) than the wall rocks, and are enriched in Fe with or without Mg from the preferred melting of hydrous mafic minerals such as biotite and amphibole.

All of the phyllosilicate minerals in Westerly Granite—biotite, muscovite, and chlorite—were preferentially melted along the sawcut, indicating temperatures of frictional heating in excess of ~700 °C (for example, Spray, 2010). Estimating an upper limit for the melt temperature is complicated by (1) the presence of highly comminuted fault gouge, which will melt at lower temperatures than larger grains, and (2) possible temperature variations across the sawcut surface. Tsutsumi and Shimamoto (1994; reported in Lin and Shimamoto, 1998) measured temperatures ≥1,169 °C at the fault surface during a high-speed friction experiment on granite, such that sodic plagioclase and orthoclase could readily melt. The welding of feldspar fragments

along the sawcut (for example, fig. 7*B*) is consistent with temperatures at or near their melting points (~1,100–1,200 °C for orthoclase and Na-rich plagioclase; from fig. 5 of Spray, 2010). The rounding of quartz clasts found locally in the shear band also indicates the possibility of some partial melting of quartz at T >1,600 °C, although other rounding mechanisms are possible (Sibson, 1975). Lockner and others (2010) estimated temperatures ≥1,500 °C at the fault surface for the 400-MPa stick-slip events characterized by total stress drops.

References

Bossière, G., 1991, Petrology of pseudotachylytes from the Alpine Fault of New Zealand: Tectonophysics, v. 196, p. 173–193.

Di Toro, G., and Pennacchioni, G., 2004, Superheated friction-induced melts in zoned pseudotachylytes within the Adamello tonalites (Italian Southern Alps): Journal of Structural Geology, v. 26, p. 1783–1801.

Di Toro, G., Hirose, T., Nielsen, S., Pennacchioni, G., and Shimamoto, T., 2006, Natural and experimental evidence of melt lubrication of faults during earthquakes: Science, v. 311, no. 5761, p. 647–649.

Griffith, W.A., Di Toro, G., Pennacchioni, G., and Pollard, D.D., 2008, Thin pseudotachylytes in faults of the Mt. Abbot quadrangle, Sierra Nevada—Physical constraints for small seismic slip events: Journal of Structural Geology, v. 30, p. 1086–1094.

Jiang, H., Lee, C.-T.A., Morgan, J.K., and Ross, C.H., 2015, Geochemistry and thermodynamics of an earthquake—A case study of pseudotachylites within mylonitic granitoid: Earth and Planetary Science Letters, v. 430, p. 235–248, doi:10.1016/j.epsl.2015.08.027.

Kennedy, L.A., and Spray, J.G., 1992, Frictional melting of sedimentary rock during high-speed diamond drilling—an analytical SEM and TEM investigation: Tectonophysics, v. 204, p. 323–337.

Lin, A., 2008, Fossil Earthquakes—The Formation and Preservation of Pseudotachylytes, Lecture Notes in Earth Sciences: New York, Springer, 348 p.

Lin, A., and Shimamoto, T., 1998, Selective melting processes as inferred from experimentally generated pseudotachylytes: Journal of Asian Earth Sciences, v. 16, no. 5–6, 533–543.

Lockner, D.A., Moore, D.E., Beeler, N.M., and Kilgore, B.D., 2010, Surface melt produced on faults during laboratory stick-slip experiments [abs.]: American Geophysical Union, Fall Meeting 2010 Abstracts, abstract no. T23A–2245, available at http://abstractsearch.agu.org/meetings/2010/FM/T23A-2245.html.

Maddock, R.H., 1992, Effects of lithology, cataclasis and melting on the composition of fault-generated pseudotachylytes in Lewisian gneiss, Scotland: Tectonophysics, v. 204, p. 261–278.

Maddock, R.H., Grocott, J., and Van Nes, M., 1987, Vesicles, amygdales and similar structures in fault-generated pseudotachylytes: Lithos, v. 20, p. 419–432.

Masch, L., Wenk, H.R., and Preuss, E., 1985, Electron microscopy study of hyalomylonites—evidence for frictional melting in landslides: Tectonophysics, v. 115, p. 131–160.

Moore, D.E., 1993, Microcrack populations associated with a propagating shear fracture in granite: U.S. Geological Survey Open-File Report 93–245, 88 pp.

Sibson, R.H., 1975, Generation of pseudotachylyte by ancient seismic faulting: Geophysical Journal of the Royal Astronomical Society, v. 43, p. 775–794.

Spray, J.G., 1987, Artificial generation of pseudotachylyte using friction welding apparatus—simulation of melting on a fault plane: Journal of Structural Geology, v. 9, p. 49–60.

Spray, J.G., 1992, A physical basis for the frictional melting of some rock-forming minerals: Tectonophysics, v. 204, p. 205–221.
Spray, J.G., 1993, Viscosity determinations of some frictionally generated silicate melts—Implications for fault zone rheology at high strain rates: Journal of Geophysical Research, v. 98, no. B5, p. 8053–8068.
Spray, J.G., 1995, Pseudotachylyte controversy—Fact or friction?: Geology, v. 23 no. 12, p. 1119–1122.
Spray, J.G., 2010, Frictional melting processes in planetary materials—From hypervelocity impact to earthquakes: Annual Review of Earth and Planetary Sciences, v. 38, p. 221–254.
Tsutsumi, A., and Shimamoto, T., 1994, An attempt to measure the temperature of frictional melts of rocks produced during rapid fault motion: Structural Geology Journal of Tectonic Research Group of Japan, v. 39, p. 103–114. [In Japanese, English abstract.]
Whitney, D.L., and Evans, B.W., 2010, Abbreviations for names of rock-forming minerals: American Mineralogist, v. 95, p. 185–187, doi:10.2138/am.2010.3371.

Image Gallery

DL513—400 MPa

This experiment consisted of two stick-slip events, the first a partial stress drop (140 megapascals [MPa]) and the second a total stress drop (~325 MPa). The examined sample is a polished half cylinder that was sliced parallel to the cylinder axis and perpendicular to the plane of the sawcut (fig. 513-1). Backscattered-electron (BSE) images (20 kilovolt [kV]) show cross sections of the shear bands. This cross-sectional orientation is good for determination of shear-band thickness, flow processes within the shear bands revealed by compositional variations, and the nature of the transition to the adjoining damage zone. Shear is left lateral in all images of this sample. The cylinder axis was oriented to be roughly horizontal during scanning electron microscope (SEM) examination, as illustrated below (fig. 513-1), and the images were taken moving progressively from the upper left termination of the sawcut part way to the lower right corner.

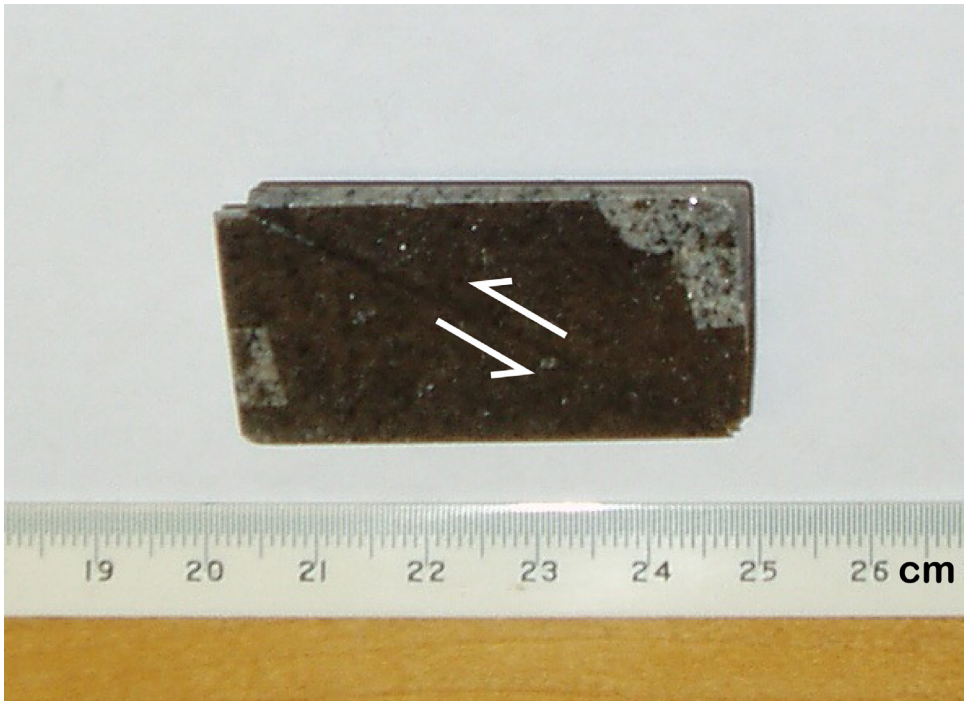

Figure 513-1. Photograph showing half cylinder of sample DL513, sliced perpendicular to the sawcut plane. The pair of white arrows indicates the offset directions of the driving blocks. The black color on the surface is the carbon coating used in the scanning electron microscope.

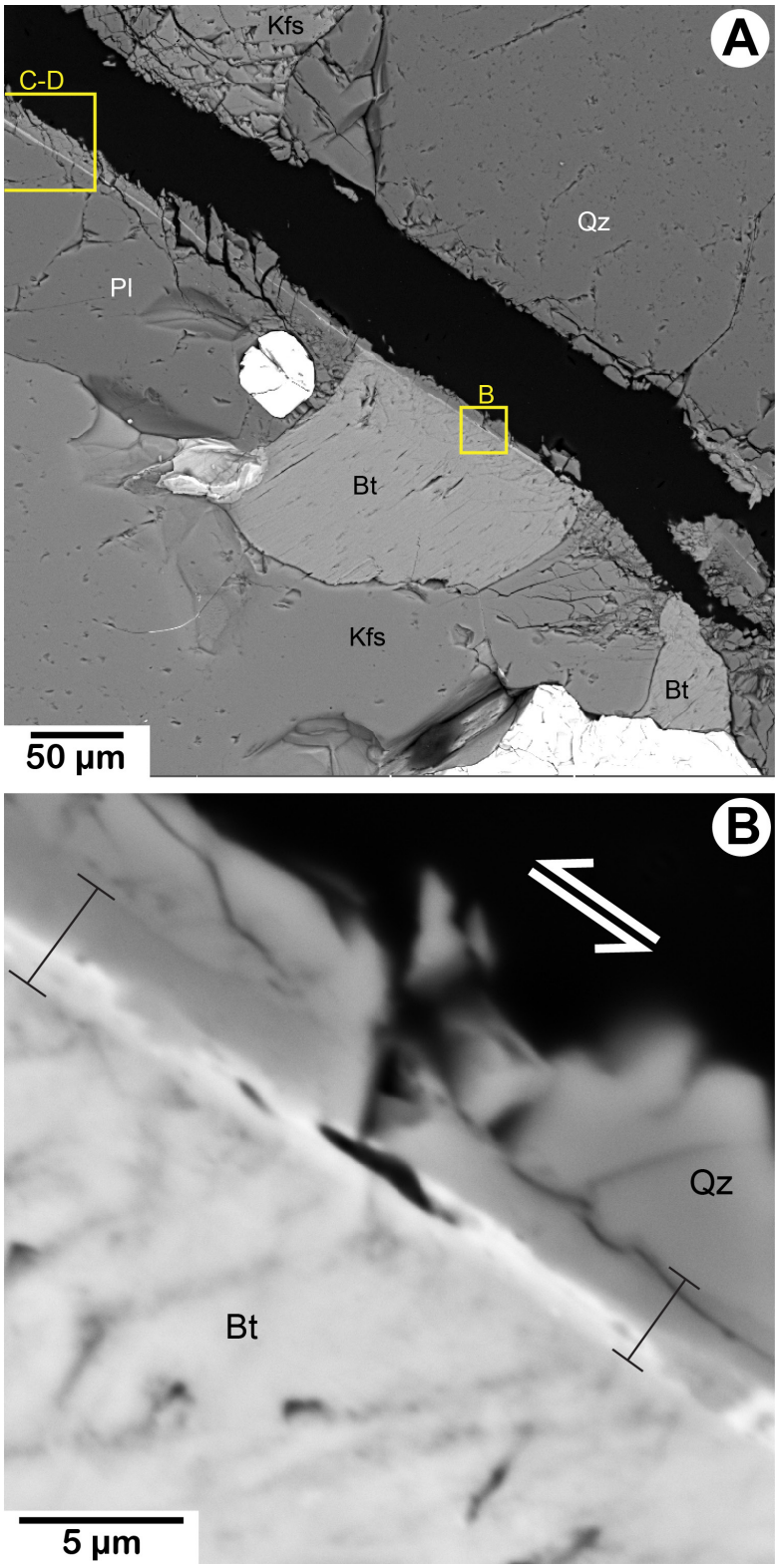

Figure 513-2. Backscattered-electron images highlighting the different degrees of fracturing of the minerals lining the sawcut surface. Shear was left lateral, denoted by pairs of white arrows. Black bars in *B* and *D* demarcate the shear band. *A*, Low-magnification view shows locations of *B*–*D*. At this location, K-feldspar crystals are more highly damaged than quartz or plagioclase. *B*, Close-up of the compositionally zoned, glass-filled shear band of variable thickness. The upper, darker layer appears to be slightly darker than the overlying quartz, whereas parts of the bright lower layer are substantially brighter than the biotite, suggesting the presence of a smeared-out opaque mineral. The bright lower layer also contains some irregularly shaped darker splotches, possibly derived from the upper layer, and a few elongate voids. The bright band contains Ca and Na in addition to components of biotite (K, Fe, Ti, and Mg), indicating some plagioclase content. Because nearly all of the minerals are silicates, the contribution of quartz to the melt generally could not be estimated.

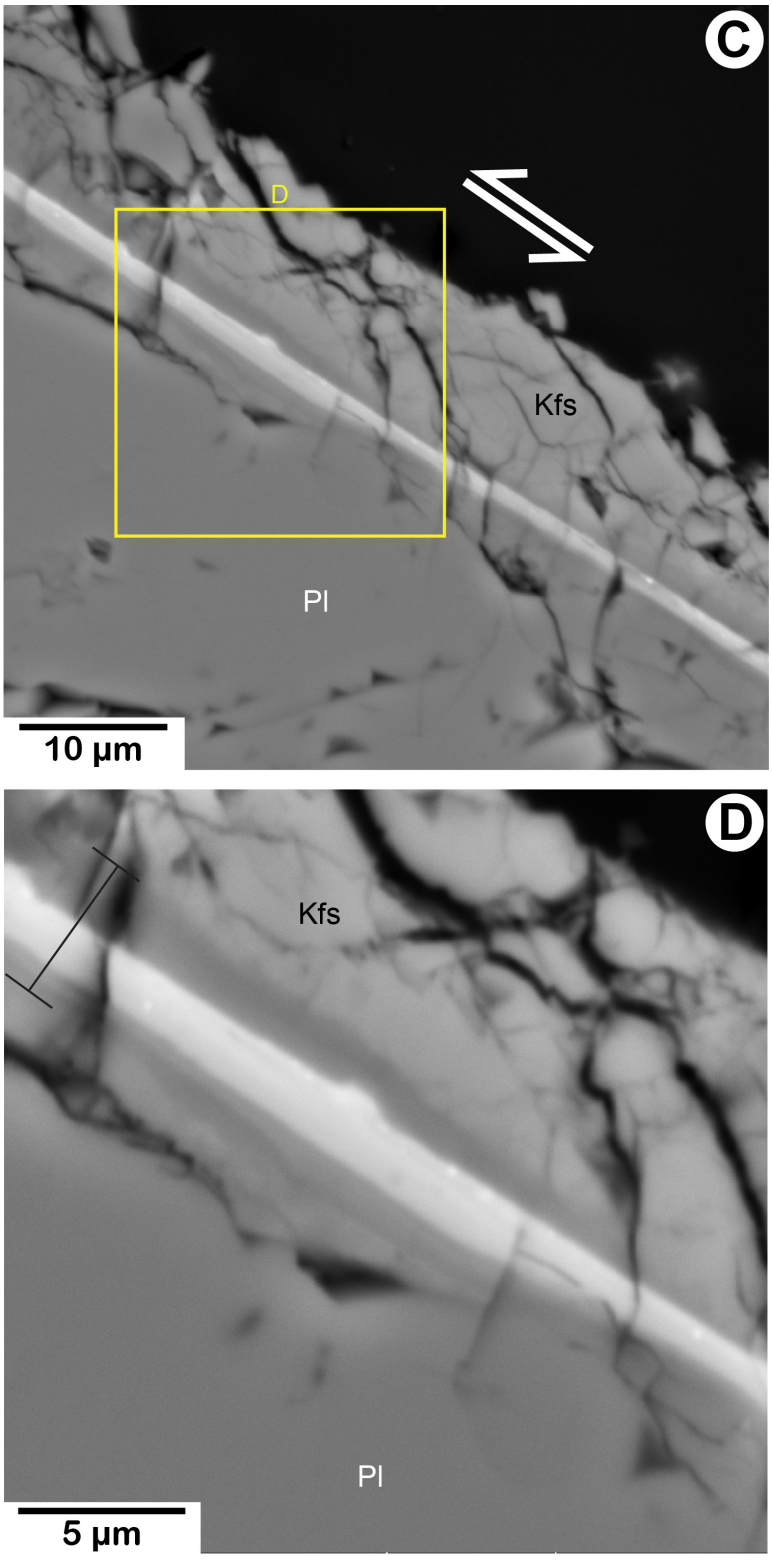

Figure 513-2.—Continued. *C*, Lower and *D*, higher magnification images of the shear band between K-feldspar and plagioclase. The central zone of the shear band is substantially brighter than either feldspar, and it is enriched in Fe and Ti derived from biotite and (or) opaque minerals. Even brighter dots, flecks, and smears are present in the upper part of the bright band. The bright layer is sandwiched between darker layers of varying thickness. The individual bright and dark layers are, themselves, layered. One to two darker layers are present in the bright central band, along with some slightly brighter bands of varying width in the dark band below.

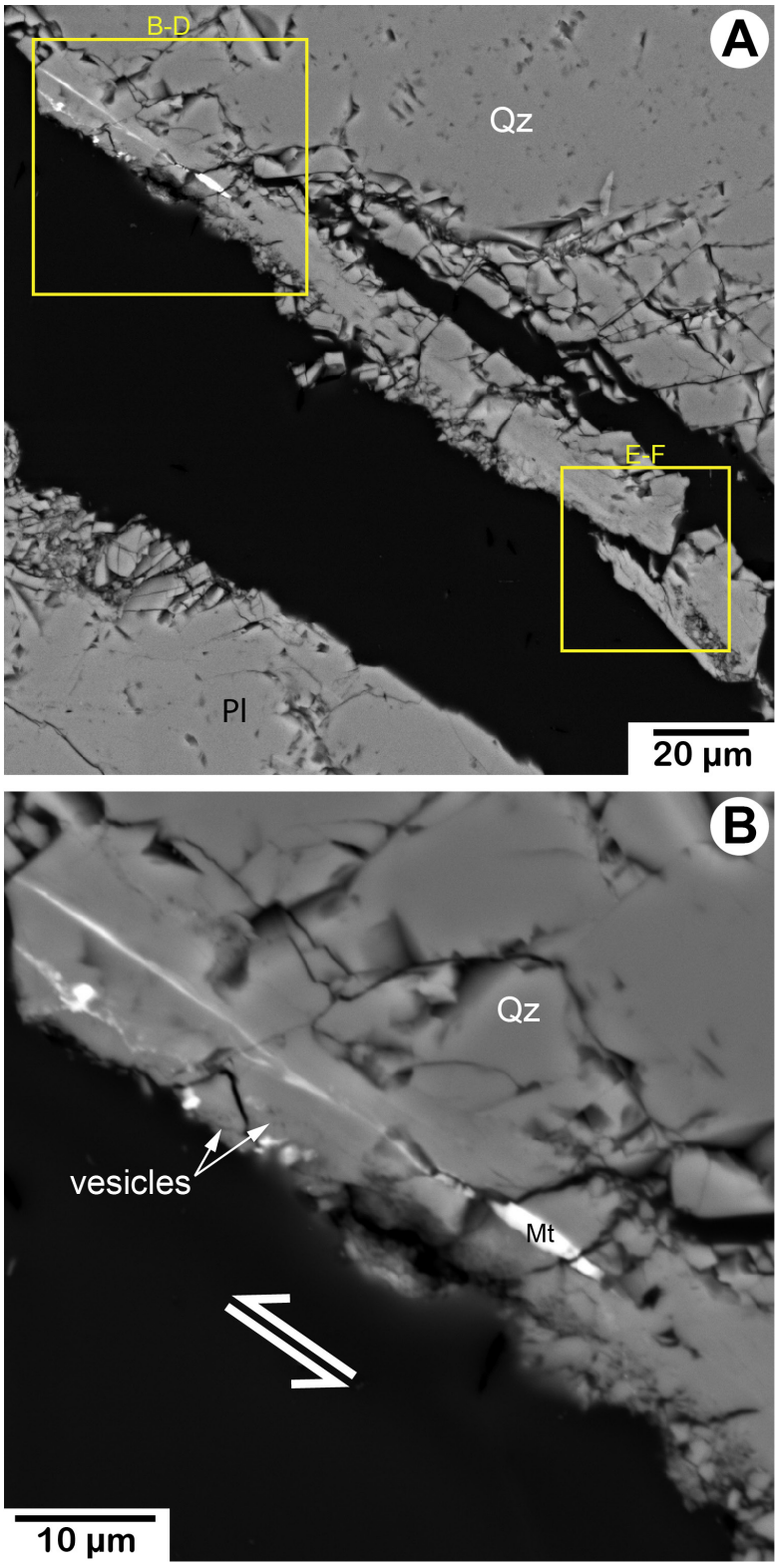

Figure 513-3. Backscattered-electron images illustrating the contrast between the solid, glass-filled shear band and the heavily fractured quartz and plagioclase crystals on either side. Shear was left lateral, denoted by pairs of white arrows. *A*, Low-magnification view shows locations of *B*–*F*. *B*, The bright streak in the middle of the shear band is magnetite. The more irregular bright magnetite band below it is at or near the lower boundary of the shear band, where it forms a wavy band. The shear boundaries are obscure in several places in this image.

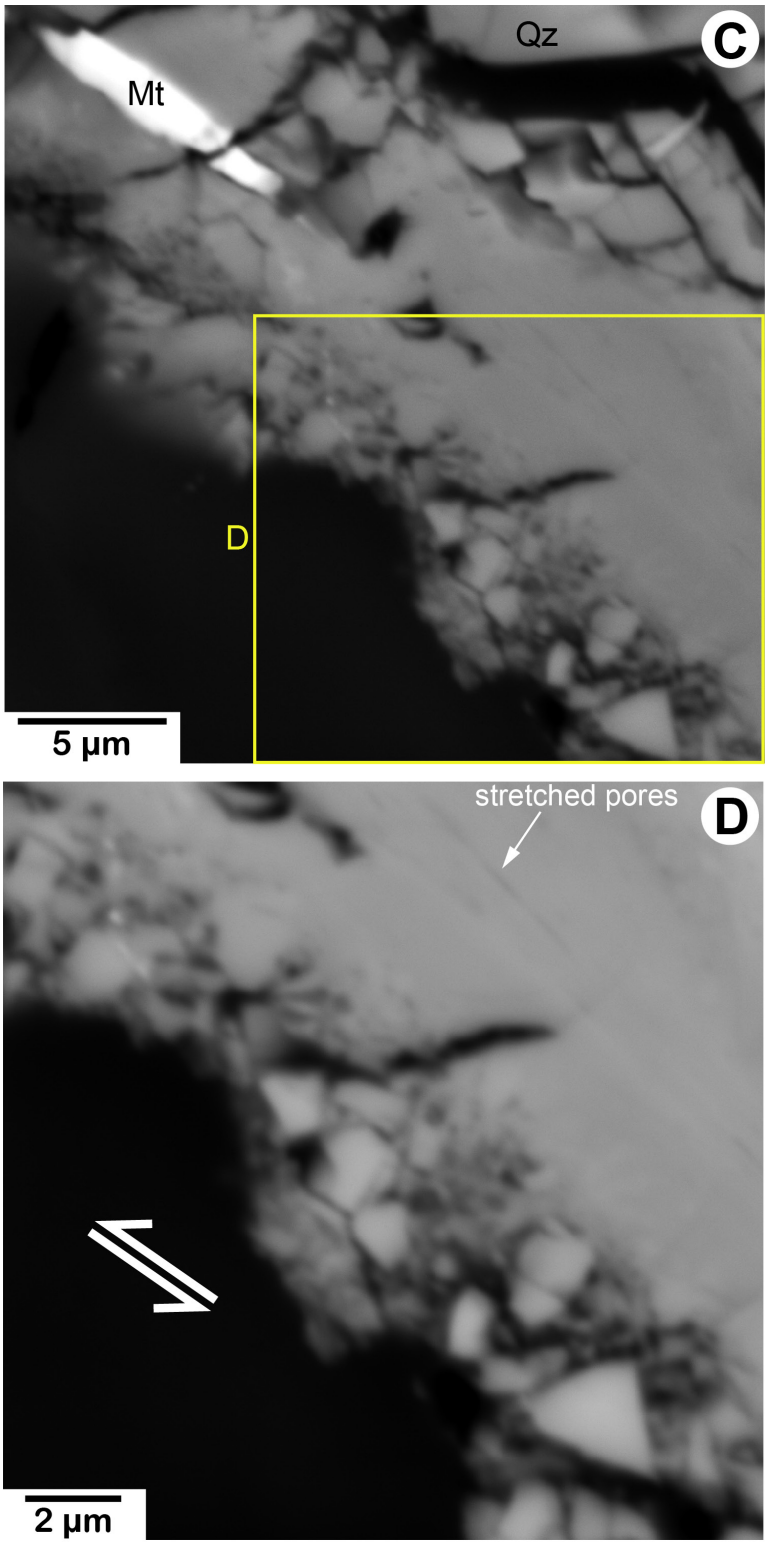

Figure 513-3.—Continued. *C*, *D*, Progressively higher magnification images of the lower right corner of *B*. The shear band contains elements indicative of plagioclase, K-feldspar, and possibly biotite. There is possible flow banding in the shear band, indicated by slightly darker lines parallel to the shear direction that may be stretched-out vesicles. The grains and (or) clasts below the shear band are relatively angular; the largest one is ~3.5 µm long. As viewed in *D*, they appear to be held together by vesicle-bearing glass. Faint clast outlines can be discerned at the base of the solid layer above the vesicles.

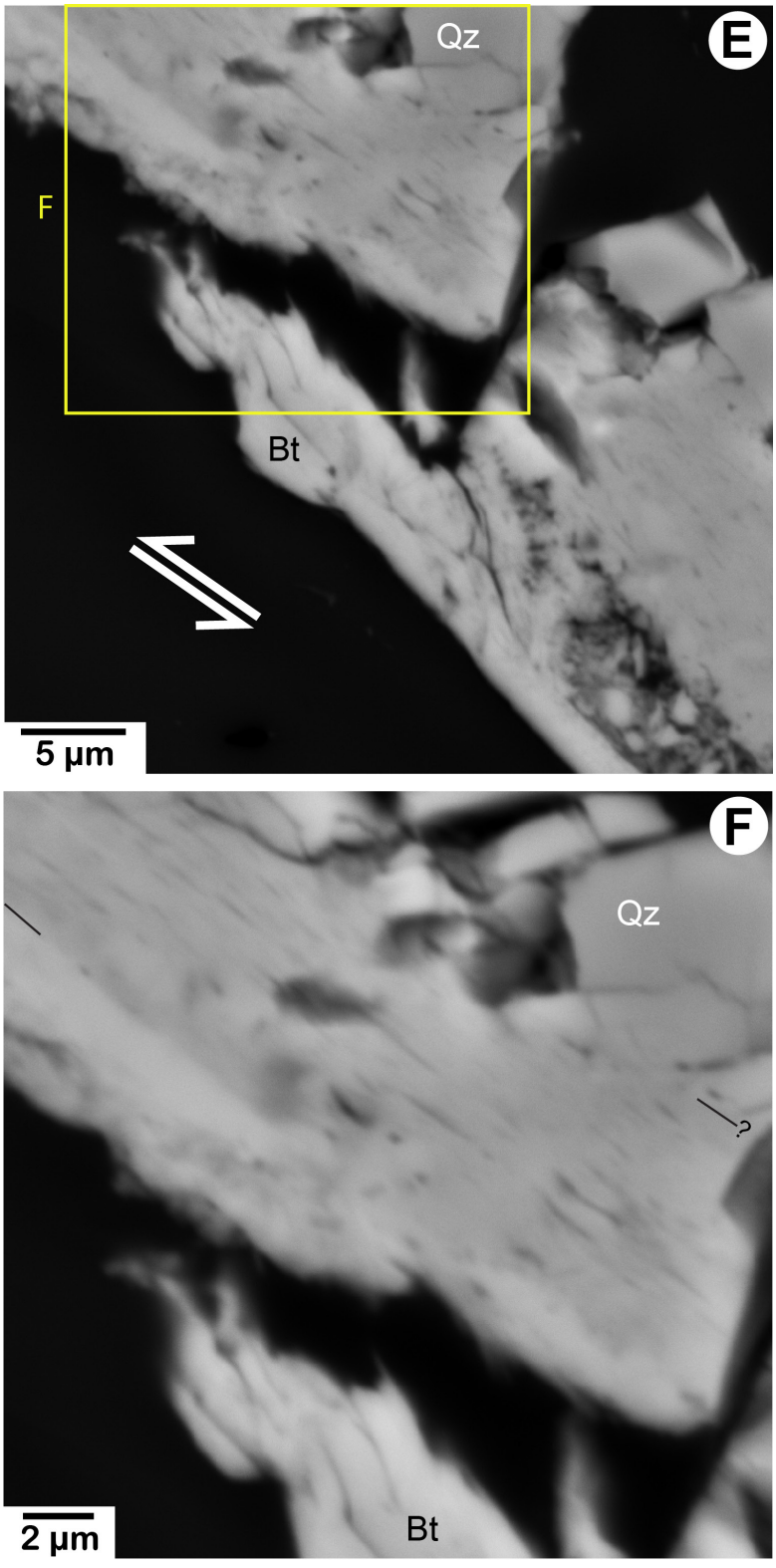

Figure 513-3.—Continued. *E*, Although biotite is below the shear band and quartz above it at this location, the composition near the middle of the shear band seems to be largely derived from plagioclase (Na and CA) and K-feldspar (K), without any Fe, Ti, or Mg from biotite. A lens filled with mineral grains similar to those in *C* and *D* is between the biotite and the shear band at lower right, and the shear band contains numerous stretched vesicles. *F*, Closer view of the stretched vesicles; the greatest elongation appears to be in the middle of the shear band. The biotite is brighter than the overlying shear band, and the boundary is considered to coincide with the change in brightness. The boundary of the shear band with the overlying quartz is vague and probably irregular. Black lines indicate the possible position of the shear boundary at the lower left and upper right sides.

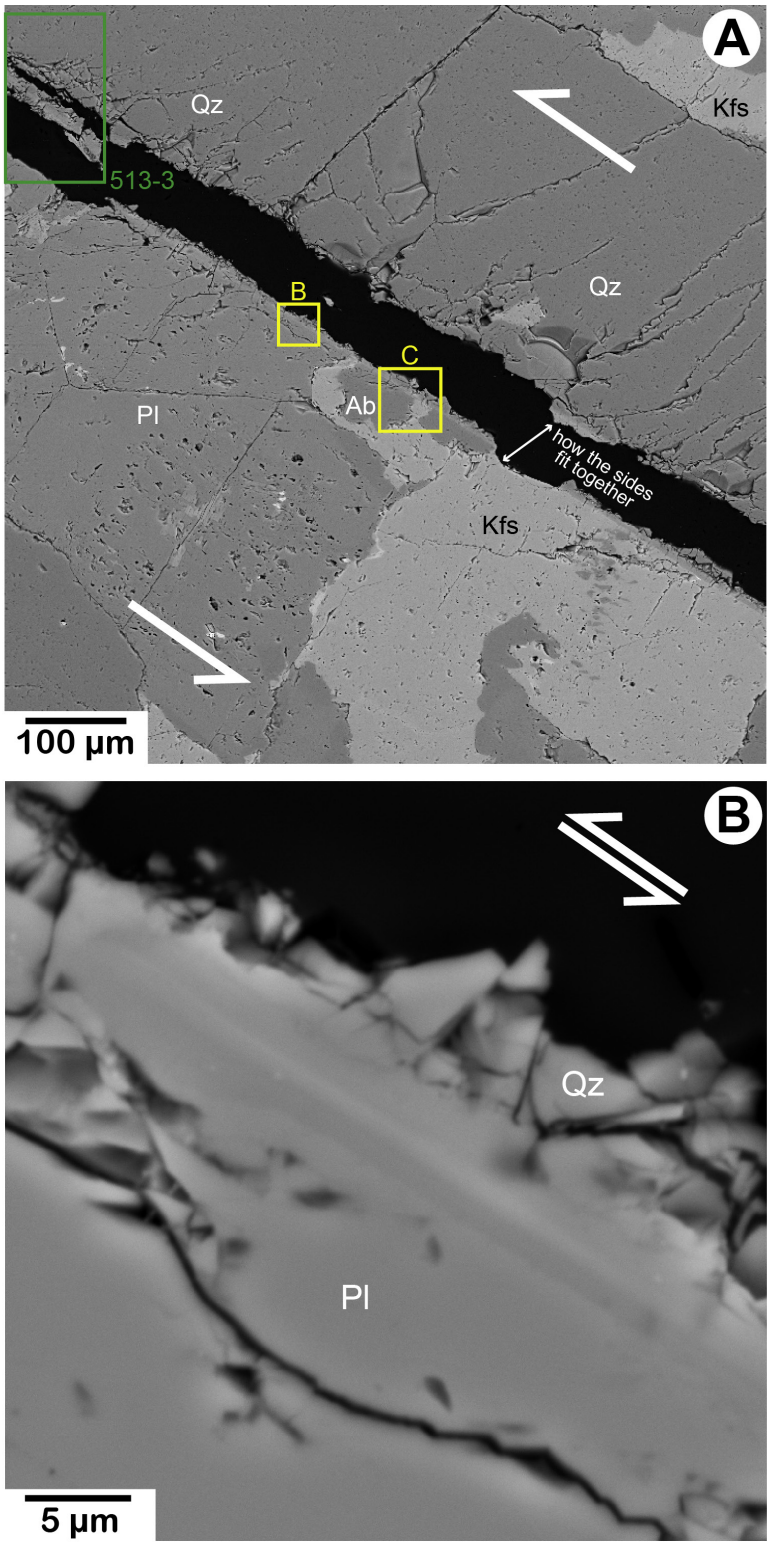

Figure 513-4. Backscattered-electron images showing compositional zoning in the shear band. Shear was left lateral, denoted by pairs of white arrows. *A*, Low-magnification view shows locations of *B* and *C*; part of figure 513-3*A* is visible in the upper left corner. *B*, Zoned, dense shear band between quartz and plagioclase. The relatively bright, central layer of the shear band contains some K, probably from K-feldspar; it is between slightly darker layers. The outlines of quartz fragments above the shear band gradually lose definition with increasing proximity to the shear band. *C*, The narrow bright layer in the shear band terminates above the small K-feldspar crystal, which may be the source of K in that layer. The direction of migration of material from K-feldspar is consistent with left-lateral shear. The darker layers in the shear band may be quartz rich with some contribution from feldspars. Shear-band thickness is relatively well defined on the left side (~4.8–5.3 µm). The width appears to narrow by about 50 percent in the middle, where a few clasts directly overlie the bright band.

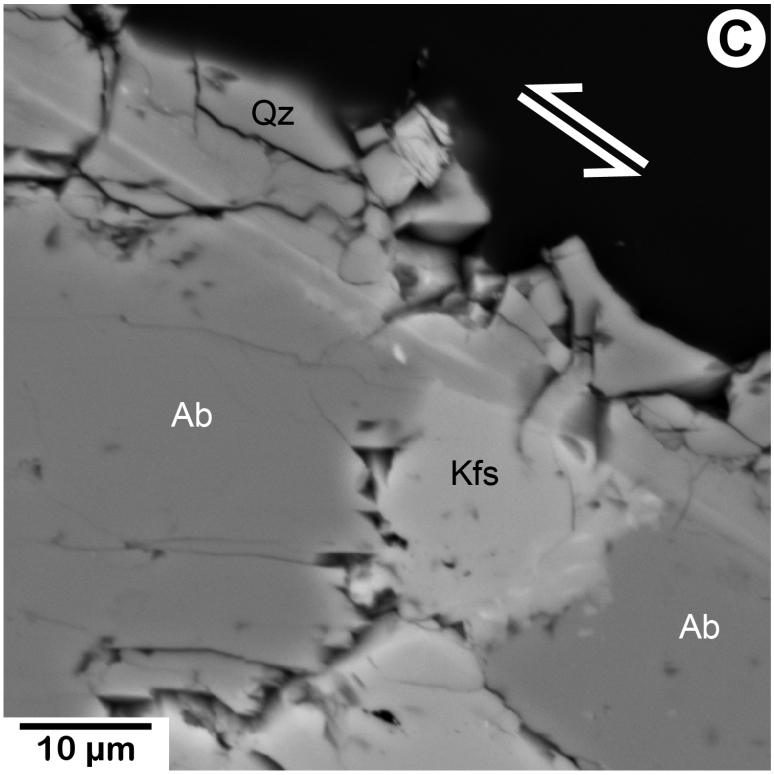

Figure 513-4.—Continued.

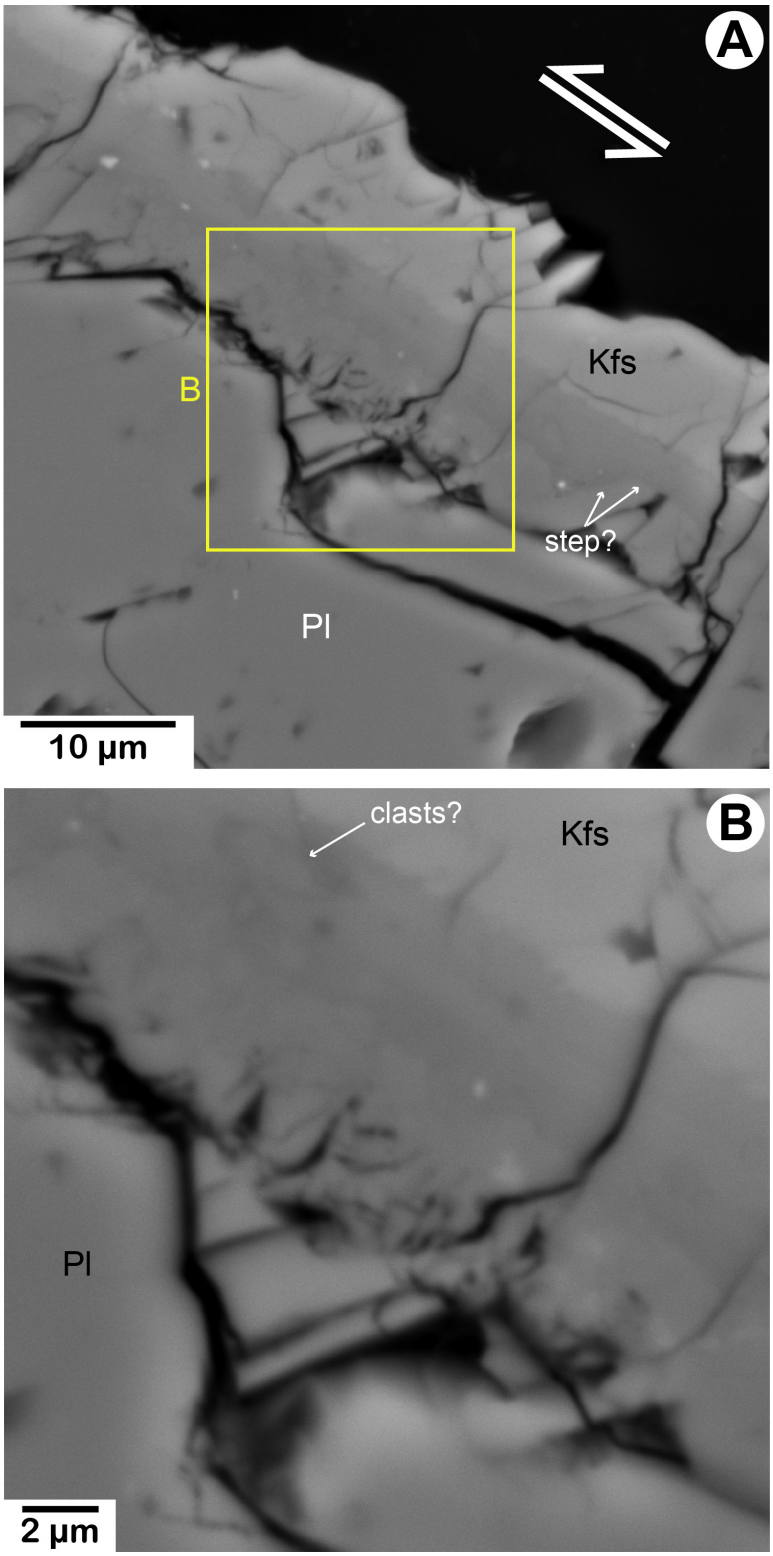

Figure 513-5. Backscattered-electron images showing fracturing and welding of plagioclase adjacent to the shear band. Shear was left lateral, denoted by pair of white arrows. *A*, Low-magnification view shows location of *B*. The composition of the shear band at this location, situated between plagioclase and K-feldspar crystals, appears to be a mixture of the two minerals with perhaps some quartz (a somewhat higher Si peak than expected for the feldspar mixture alone). The shear-band thickness varies from ~5.1 µm at upper left, where it's relatively well defined, to as little as 2.75 µm at lower right, at a step in the plagioclase (marked by arrows). The shear band shows faint compositional layering, consisting of darker and lighter bands. *B*, Closer view of the disturbed area in the plagioclase below the shear band. Plagioclase fragments have been welded together, and the boundaries between the fragments and the base of the shear band are difficult to discern. Faint outlines of angular clasts are visible within the shear band.

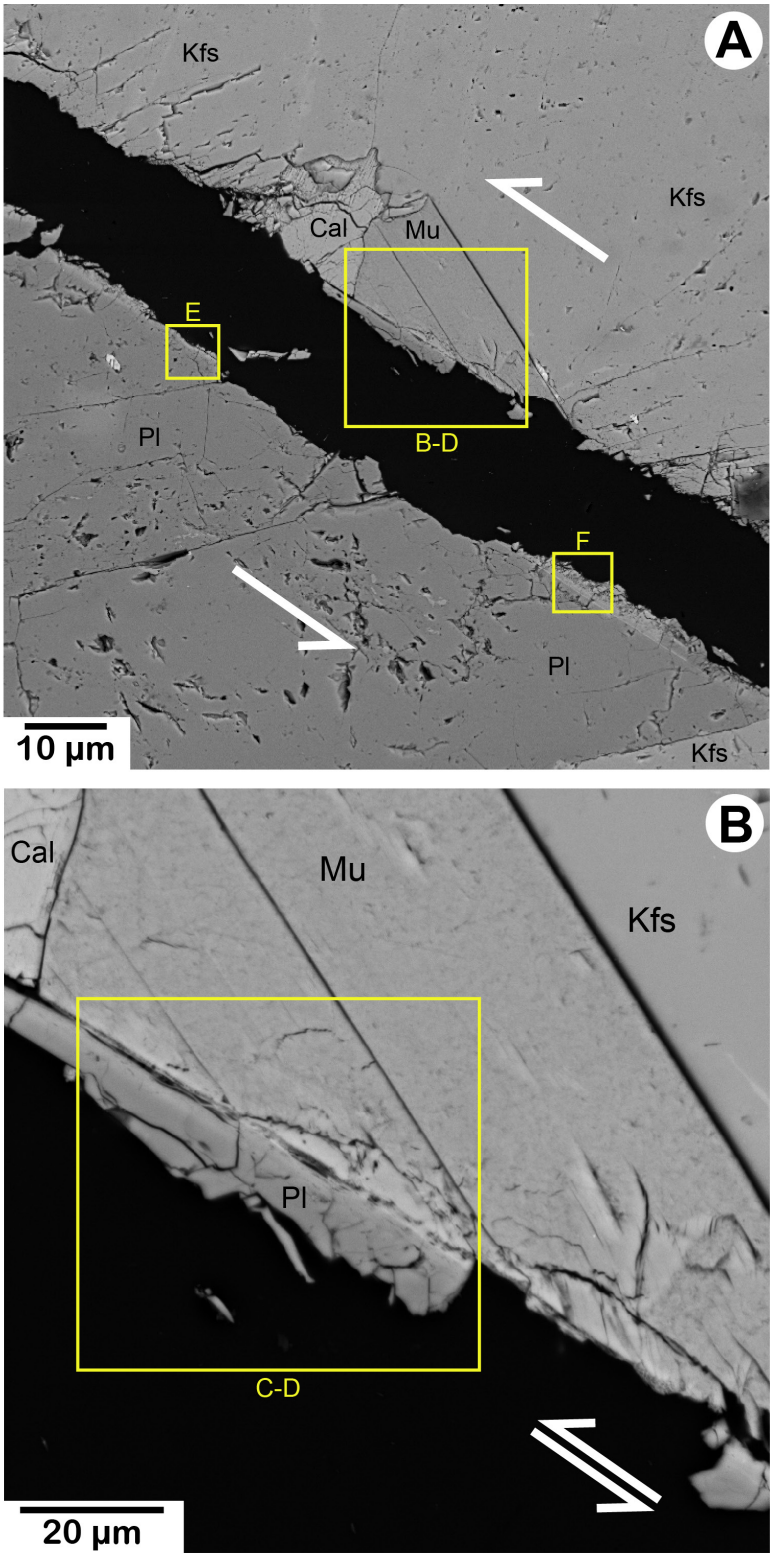

Figure 513-6. Backscattered-electron images showing the concentration of voids in the shear band adjacent to muscovite and calcite crystals. Shear was left lateral, denoted by pairs of white arrows. *A*, Low-magnification view shows locations of *B*–*F*. *B*, Void-rich band lines the sawcut adjacent to a muscovite crystal, and it continues alongside the adjoining calcite crystal.

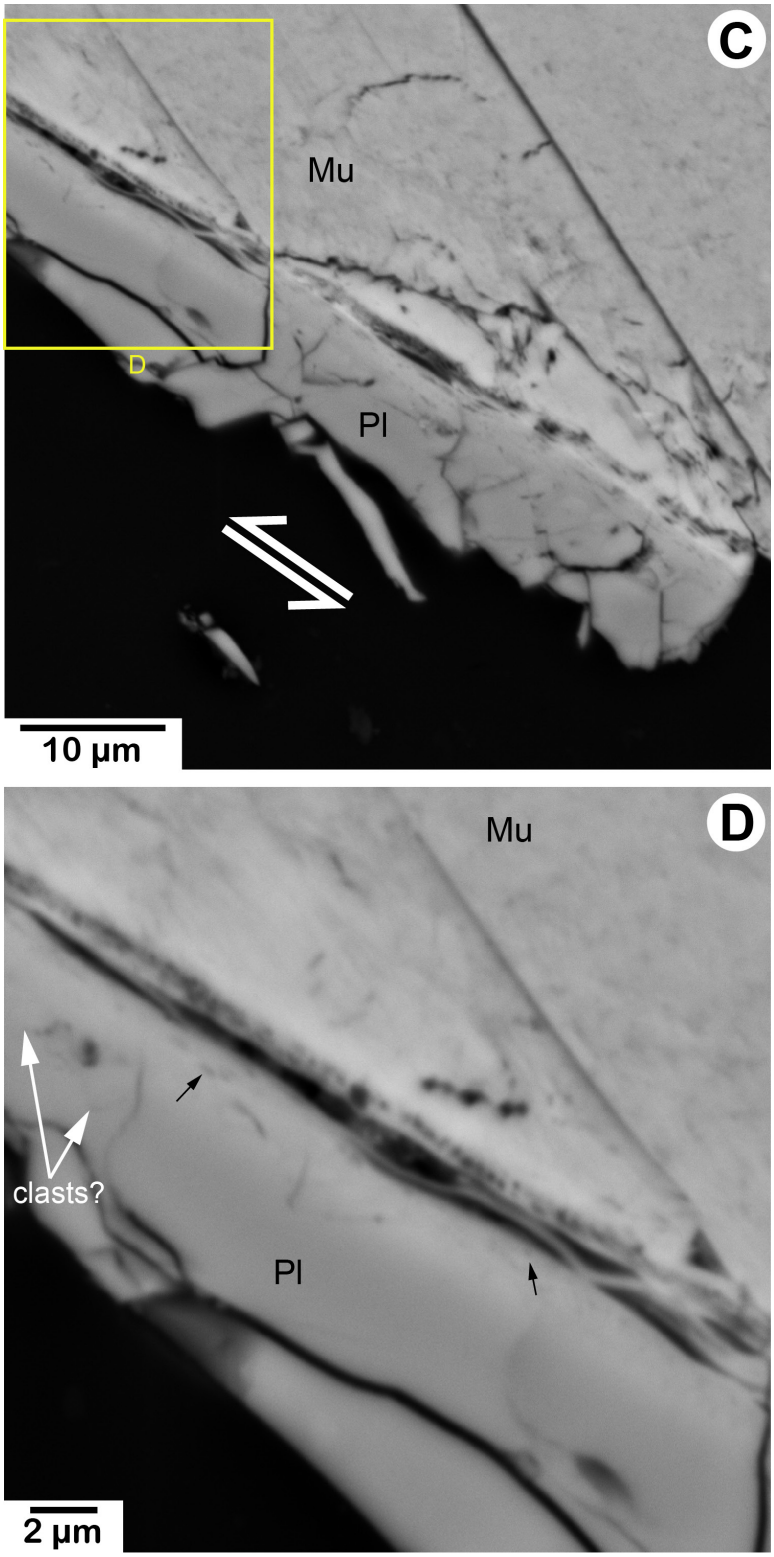

Figure 513-6.—Continued. *C*, *D*, The voids, seen at higher magnifications in these images, are as much as ~1.25 µm wide, and they contain wavy bands of glass. A line of vesicles (≤500-nm diameter) marks the shear band-muscovite boundary. The base of the line of pores, adjacent to the void, is straight and well defined, whereas the upper surface fades into the muscovite. The ~2-µm-thick bright layer between the voids and the plagioclase beneath contains numerous rounded-to-stretched vesicles, indicated by black arrows. Fragments of plagioclase are welded to the base of the shear band.

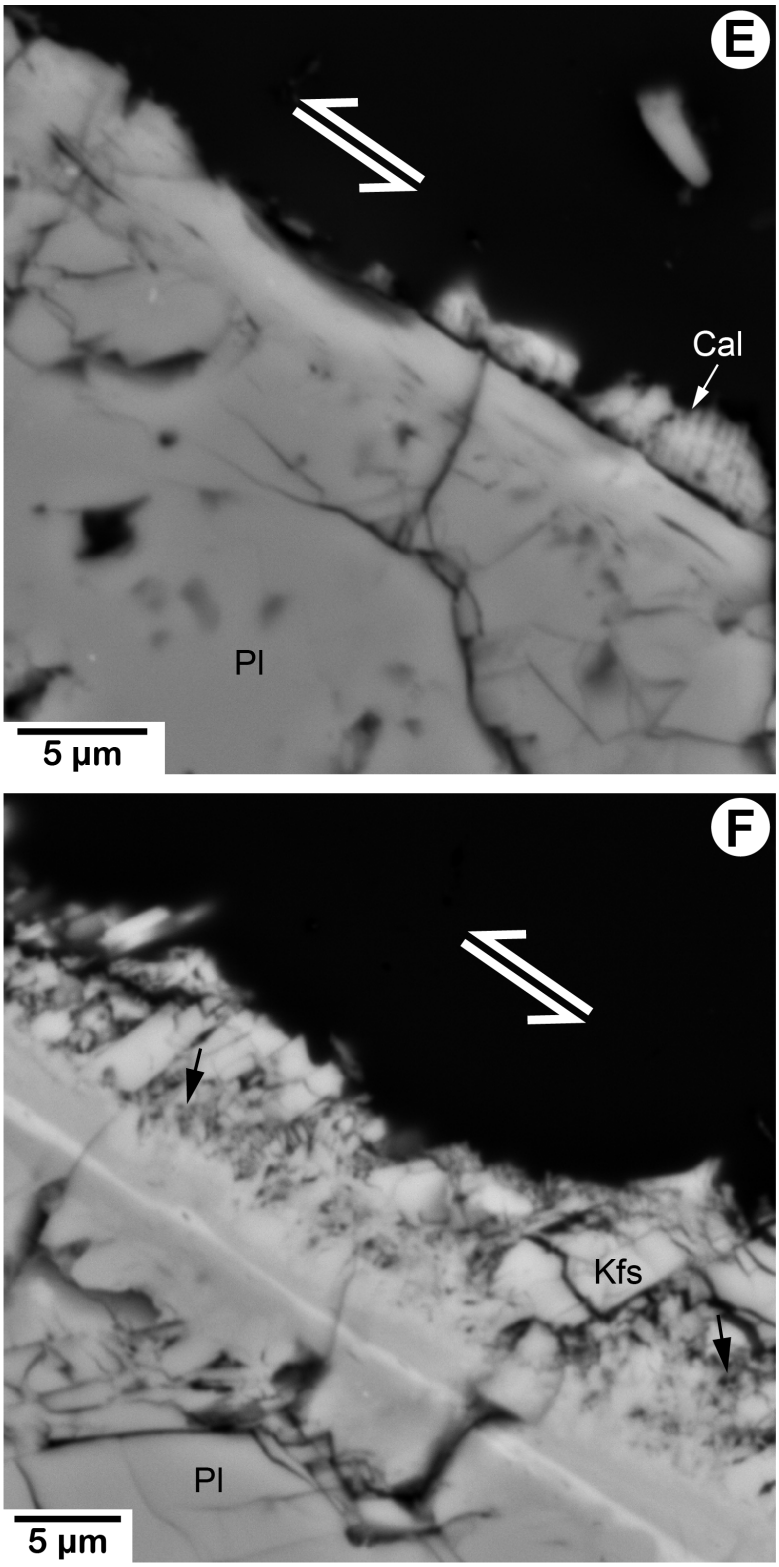

Figure 513-6.—Continued. *E*, Continuation of the void-rich band adjacent to the calcite, on the other driving block. The calcite fragments above the shear band at right are separated from it by voids and pores. There are several stretched vesicles in the shear band. *F*, Dense, zoned shear band consisting of a very bright central layer of varying thickness and darker outer bands. Fragments of K-feldspar above and plagioclase below are welded to the outer edge of the shear band. Vesicle-rich glass migrated ≥5 µm into the zone of fine-grained K-feldspar pieces; black arrows point to a few of the vesicle-bearing glass fillings.

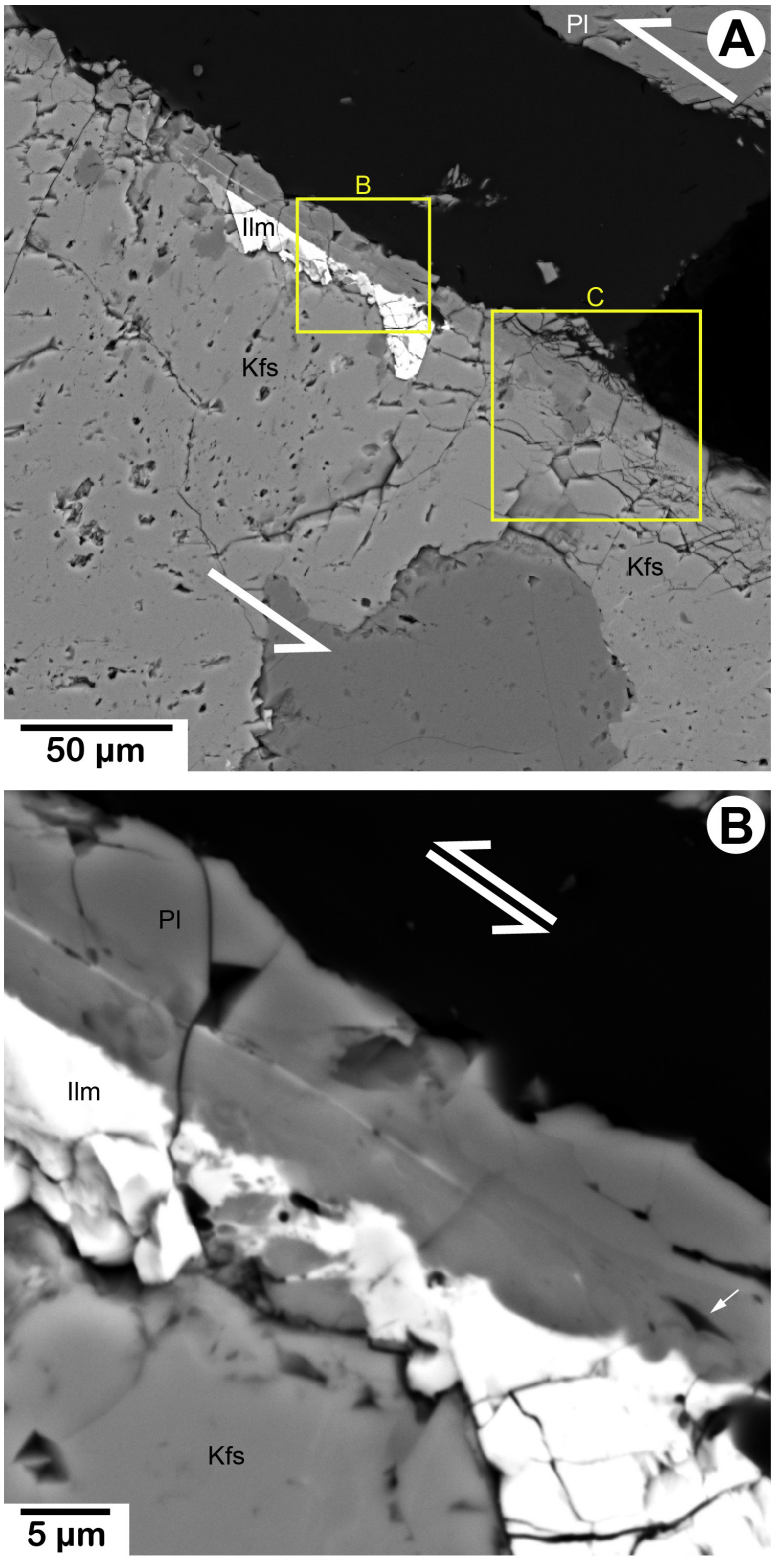

Figure 513-7. Backscattered-electron images showing compositional zoning in the shear band. Shear was left lateral, denoted by pairs of white arrows. *A*, Low-magnification view shows locations of *B* and *C*. The shear boundaries are well defined in this view, particularly above the ilmenite, but they are less distinct at higher magnifications. *B*, The upper surface of the ilmenite crystal is irregular, with a few bright wisps extending towards or into the shear band. Dark bands flank the discontinuous, bright layer in the shear band. The upper layer is slightly darker than the plagioclase above it, and the shear band appears to widen at lower right, above a ~4-µm-long, cuspate void (marked by a small white arrow). The scalloped lower edge of this void may be caused by the two clasts situated directly below it that are slightly brighter than the surrounding matrix. *C*, Faintly zoned shear band between plagioclase and K-feldspar; the composition of the shear band is largely a mixture of the two feldspars, but with traces of Fe. Both the upper and lower boundaries of the shear band are indistinct at this location, but the thickness is estimated to vary between ~7 and 9.5 µm. A 2–3-µm-wide zone in the center of the shear band appears to contain a number of small pores. Fragments of feldspar on either side of the shear band are welded together, and matrix areas contain numerous rounded pores, suggestive of vesicle-rich glass.

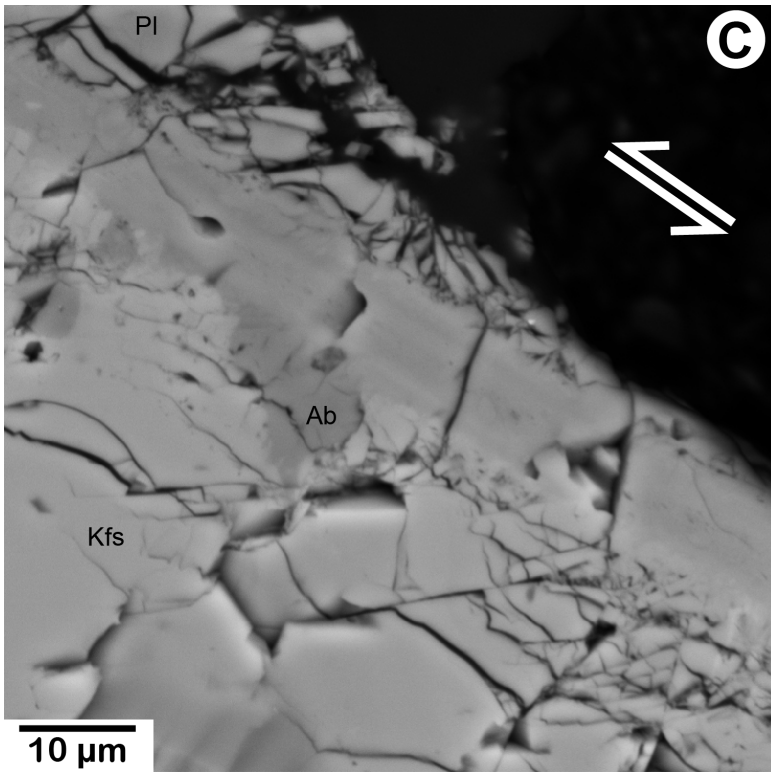

Figure 513-7.—Continued.

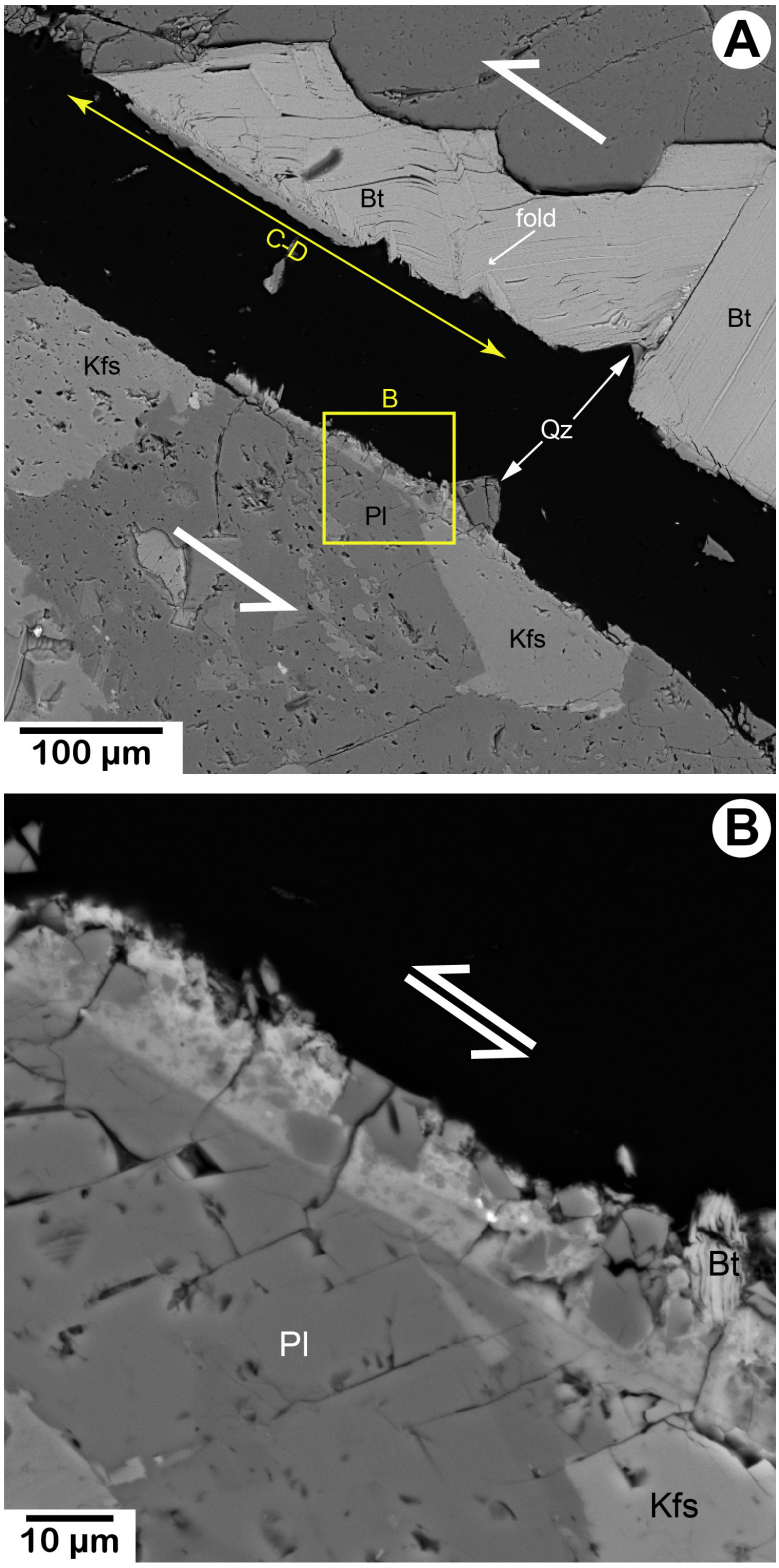

Figure 513-8. Backscattered-electron images showing voids and clasts in the shear band adjacent to biotite. Shear was left lateral, denoted by pairs of white arrows. *A*, Low-magnification view shows locations of *B–D*; also shows melt textures adjacent to a cluster of biotite crystals at the upper sawcut surface, opposite feldspars. *B,* The debris in a ~130-µm-long, unusually clast-rich shear segment may have been trapped between barriers on the upper sawcut shown in *A*. Fold hinge forms the barrier on the left side, and a small, triangular quartz crystal was wedged between biotites on the right. Shear-band thickness decreases by about 50 percent to the left and right of this patch. The matrix of the shear band is brighter overall on the biotite side, and it contains some biotite fragments. The numerous dark clasts may be quartz.

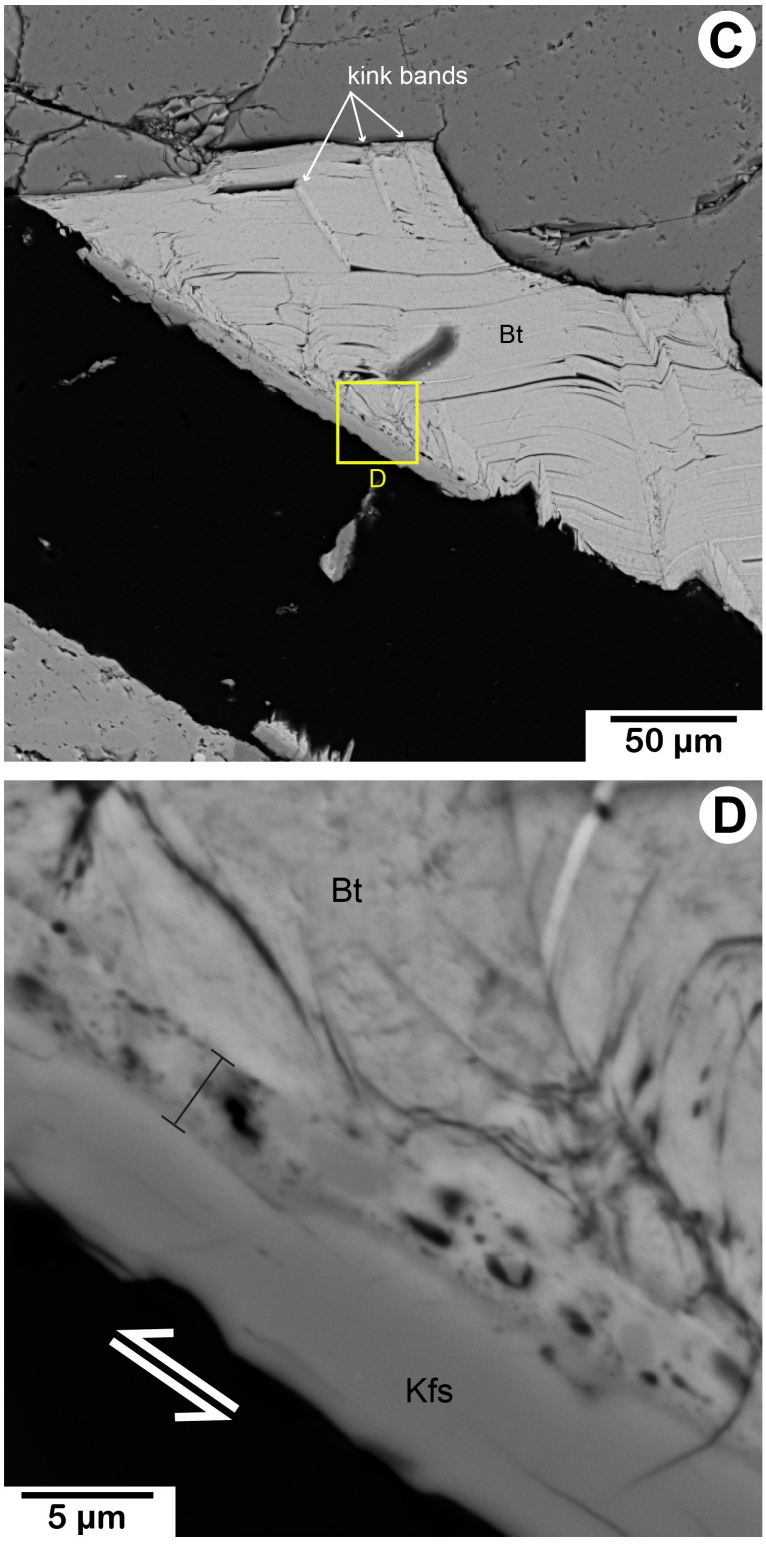

Figure 513-8.—Continued. *C,* Closer view of the leftmost biotite crystal in *A*, whose folded and kinked (001) cleavage is consistent with left-lateral shear. The shear band adjacent to it is void-rich in this view. *D*, The shear band is relatively narrow (~4.2 µm wide) and its boundaries are generally well defined (indicated by the black bar) except for disrupted areas such as beneath the fold hinge at right. Somewhat rounded, darker and brighter patches in the shear band may be clasts with vague boundaries. The K-feldspar beneath the shear band is oriented such that one of the cleavages is subparallel to the sawcut, and there are faint traces of the second cleavage at large angles to it. The shear boundary steps down to the left at two places, consistent with the cleavage orientations.

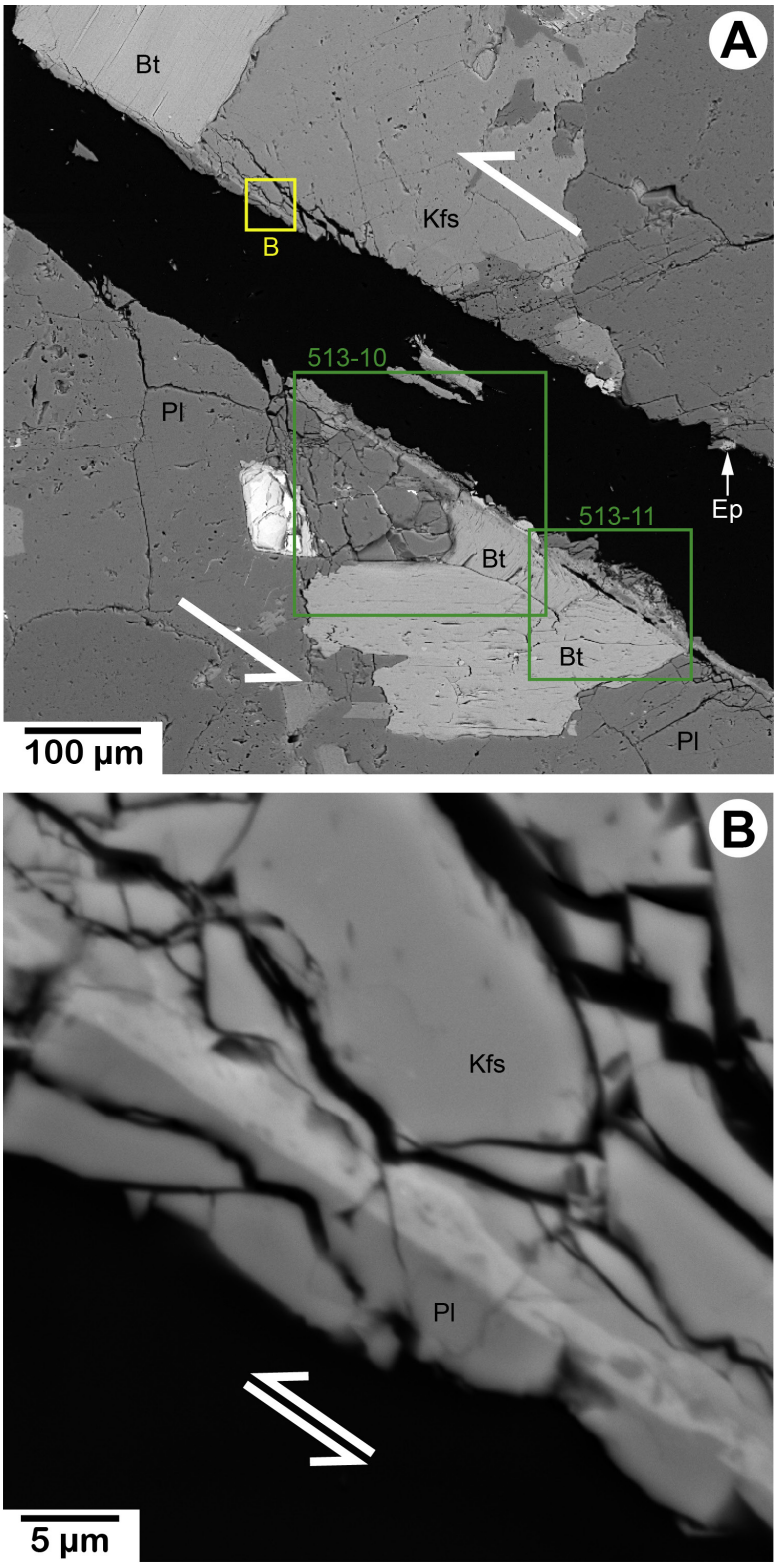

Figure 513-9. Backscattered-electron images showing shear-band textures at a location near several biotite crystals. Shear was left lateral, denoted by pairs of white arrows. *A*, Low-magnification view shows location of *B*; also shows transition from the biotites of figure 513-8, at left, to the group below the shear band that is featured in figures 513-10 and 11. *B*, Bright, biotite-rich (Fe, Ti, K, Mg) shear band with an irregular upper boundary against a highly fractured K-feldspar. The shear band contains several small clasts, possibly derived from the feldspars on either side.

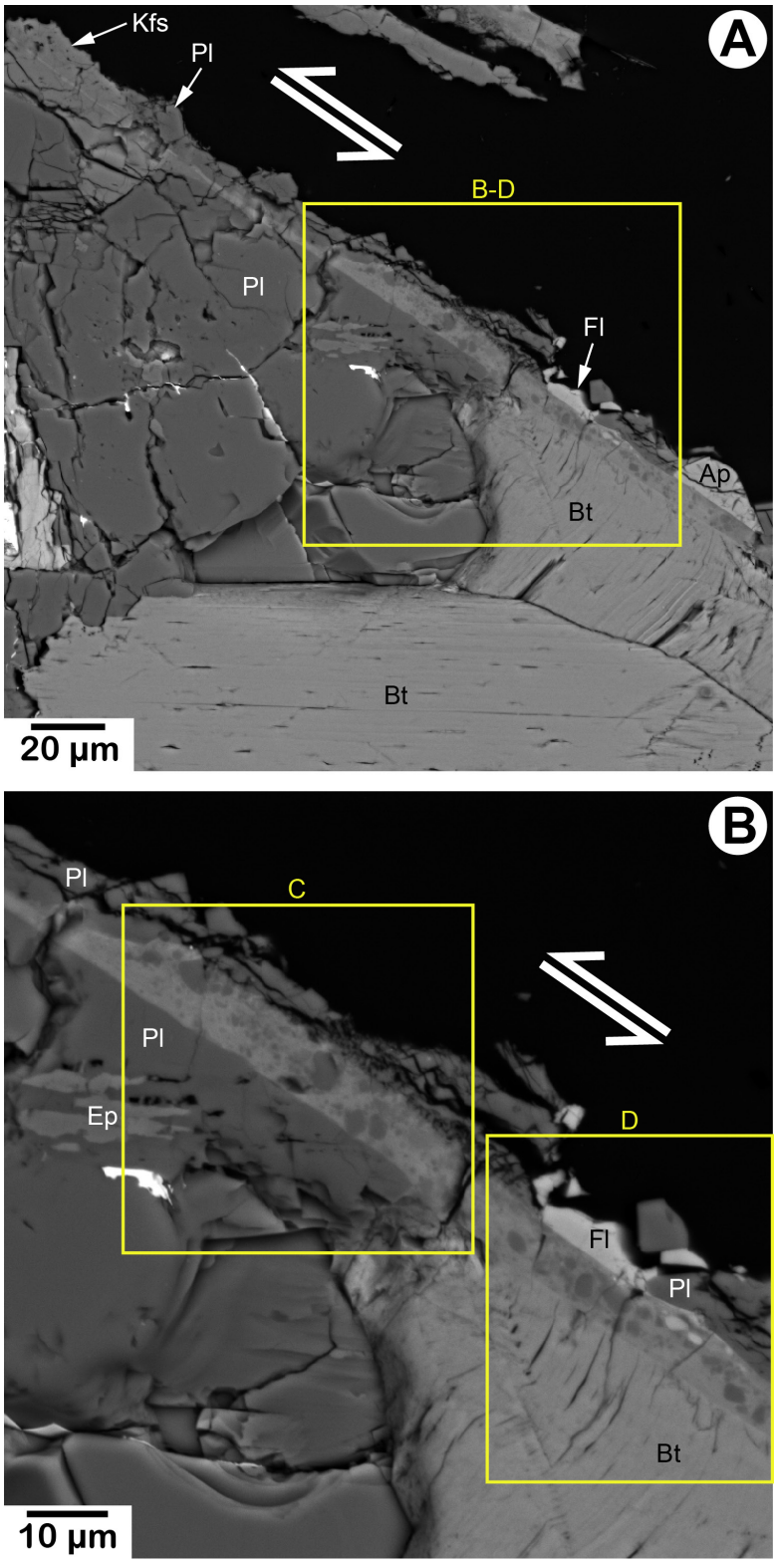

Figure 513-10. Backscattered-electron images showing clast-rich shear band. Shear was left lateral, denoted by pairs of white arrows. *A*, Low-magnification view shows location of *B*–*D*. Also shows clast-rich shear band with well-defined boundaries above and extending to the left of the lower biotites in figure 513-9. The flat base of an apatite crystal at the far right side marks the upper sawcut position. The shear band narrows considerably from right to left. *B*, A closer view of the clast-rich area in the middle of *A*. Trail of bright material extends along the top of the shear band to the right of a small fluorite (see also *D*). Bulk shear-band composition of a relatively bright area with small clasts is biotite rich, with at least some plagioclase (Na, Ca) component.

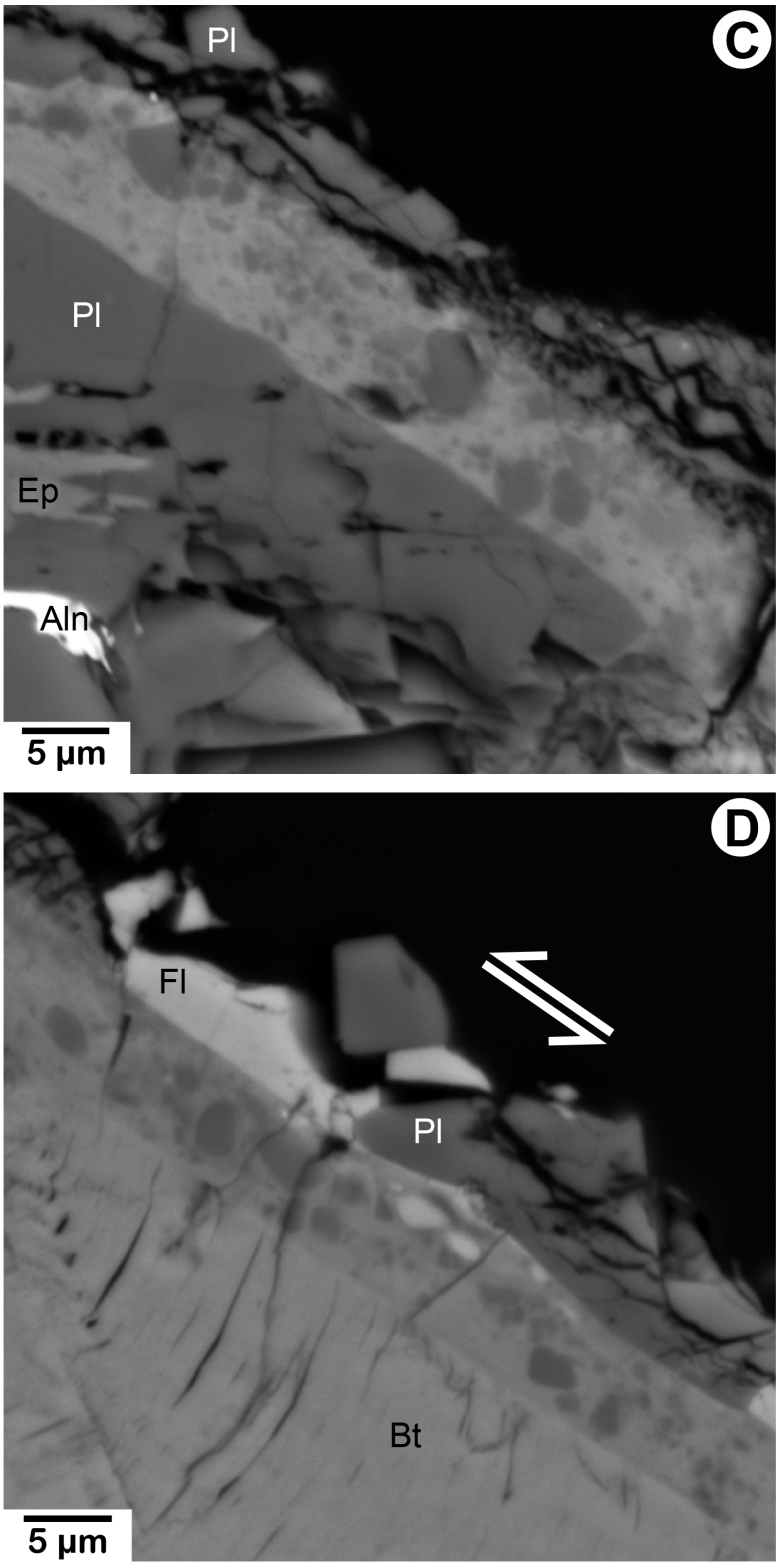

Figure 513-10.—Continued. *C*, Left- and *D*, right-hand sides of the shear band imaged in *B*. Small fragments of plagioclase are attached to the top of the shear band at lower right in *C*, separated by rounded pores ≤0.5 µm in diameter. Shear-band thickness in *C* and *D* is 5.7–7.4 µm, and the largest clast diameters are roughly half the shear-band thickness.

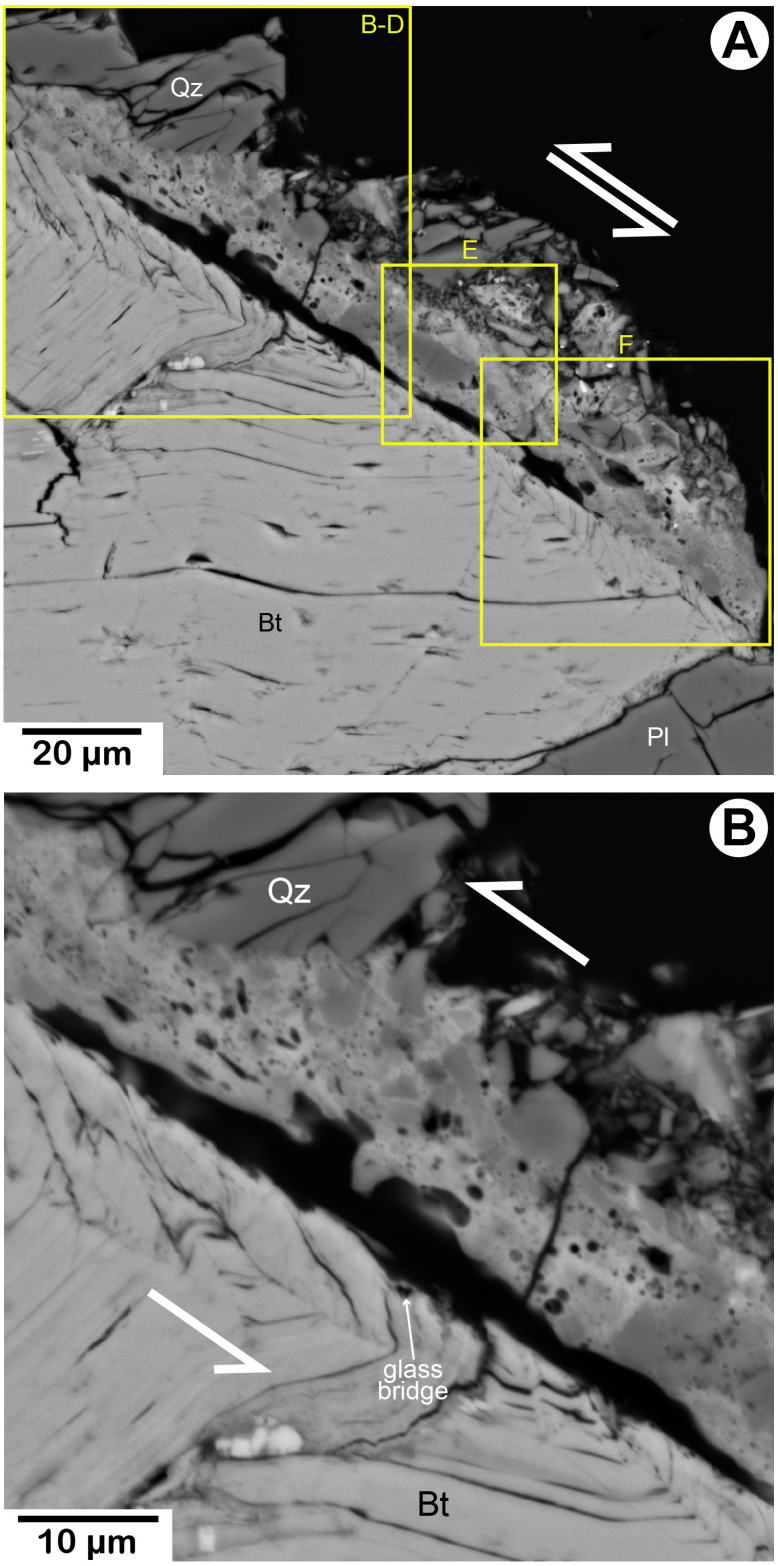

Figure 513-11. Backscattered-electron images showing melt textures adjacent to biotite. Shear was left lateral, denoted by pairs of white arrows. *A*, Low-magnification view shows locations of *B*–*F*; also shows chaotic zone above the biotite on the right-hand side of figure 513-9. Wide, elongate voids adjoin the biotite over most of its length on the sawcut. *B*, The left half of the biotite in *A* is folded at the sawcut, and it is overlain by a wide, elongate void with an irregular perimeter. Subrounded crystal fragments in the highly damaged area above the biotite are surrounded by vesicle-rich glass of varying chemistry.

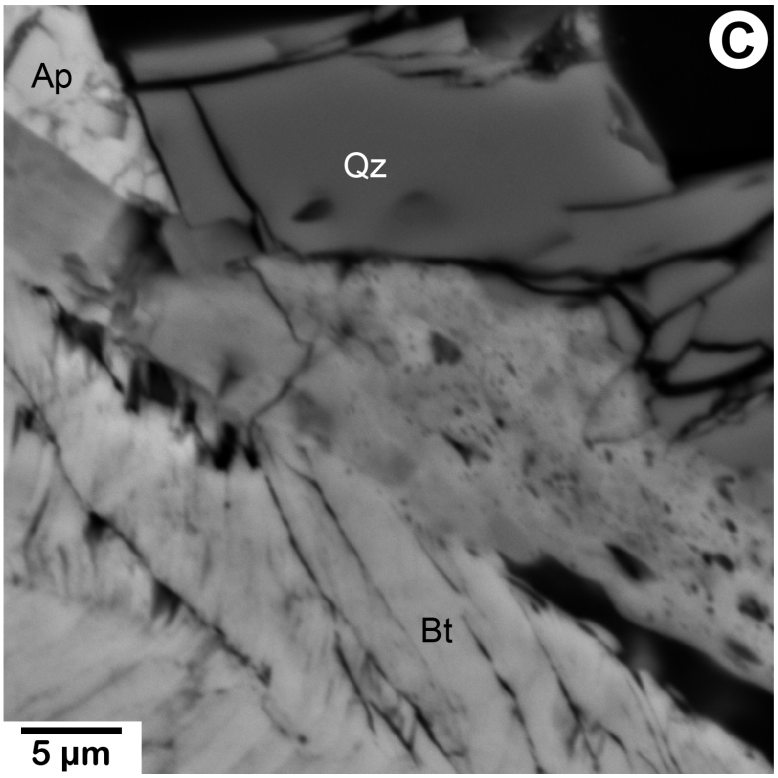

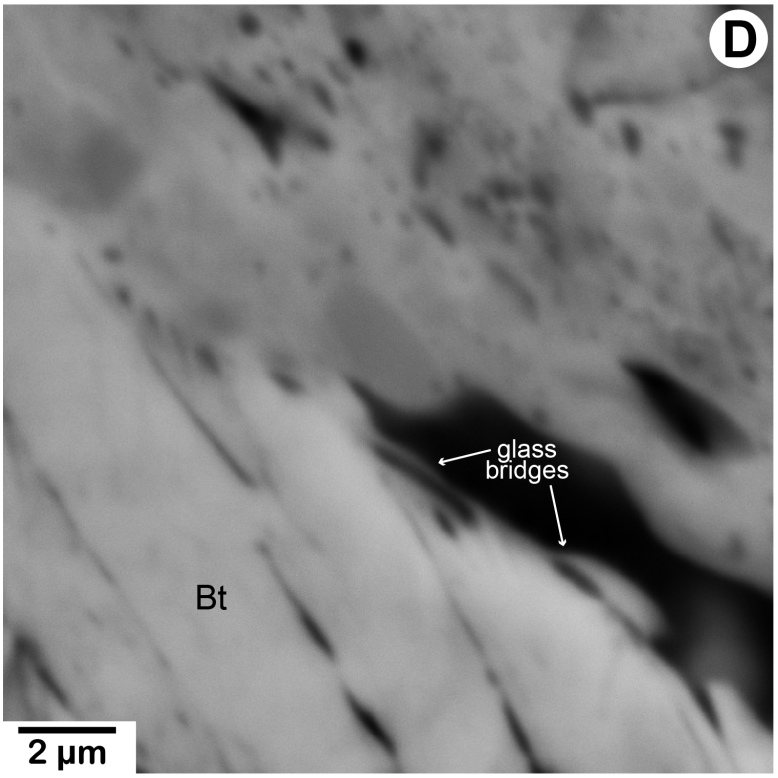

Figure 513-11.—Continued. *C*, *D*, Progressively higher magnification images of the left edge of the large void. Glass bridges are present around the perimeter, which has a scalloped outline. The bright matrix of the clast-rich area contains traces of phosphorus from nearby apatite, in addition to elements from biotite and plagioclase.

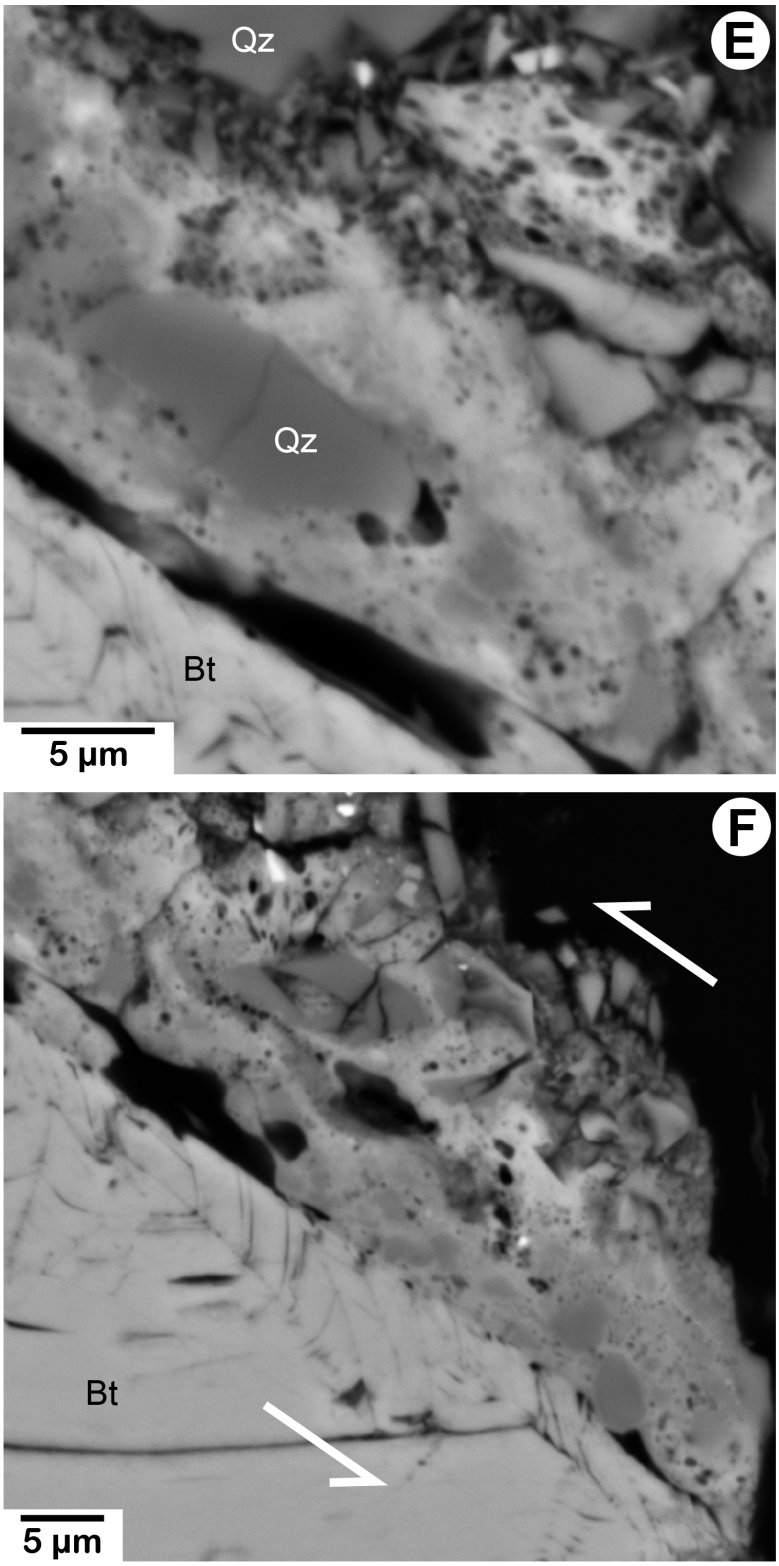

Figure 513-11.—Continued. *E*, *F*, Closer views of the right side of *A*. The perimeter of the large quartz clast in *E* is indistinct in places, and several vesicles are present along it. Strands of glass are attached to the bottom of the long void adjacent to the biotite below. Melt, quenched to vesicle-filled glass, may have migrated more than 20 µm from the sawcut in places.

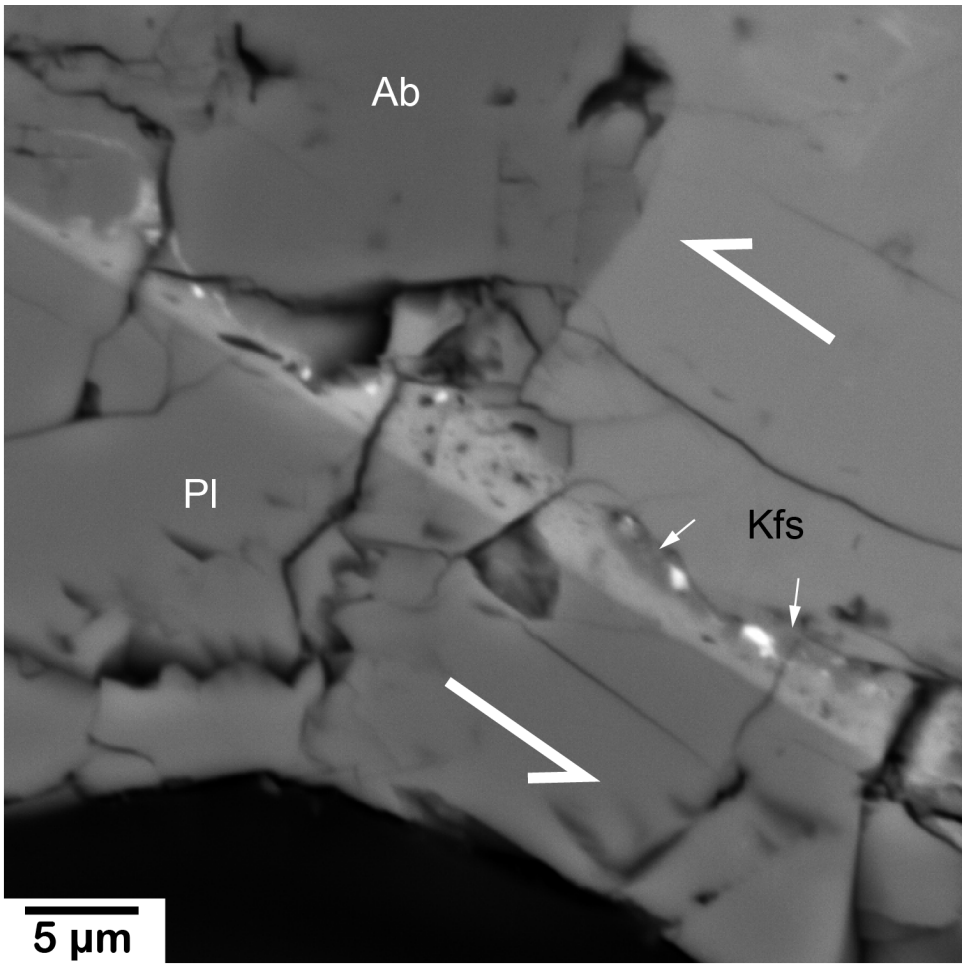

Figure 513-12. Backscattered-electron (BSE) image showing bright shear band of varying composition that has a straight lower boundary and a very irregular upper boundary. The main bright part of the shear band is enriched in elements from biotite (Fe, Ti, Mg). A few darker patches of glass (marked by small white arrows) and flecks of an opaque mineral (very bright in BSE image) are concentrated along the upper shear boundary. Several rounded to elongate voids are present. Shear was left lateral, denoted by pair of large white arrows.

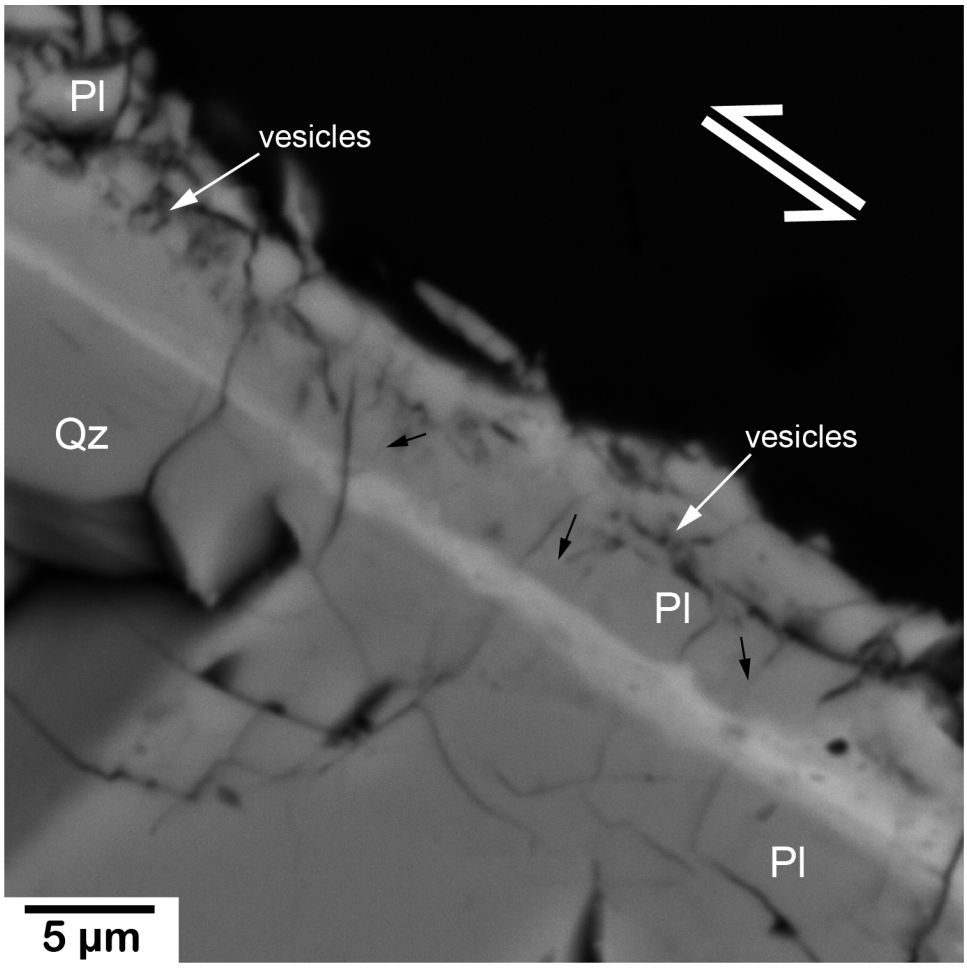

Figure 513-13. Backscattered-electron image showing bright shear band, rich in elements derived from biotite, of varying thickness and with poorly defined boundaries. An approximately 3-µm-wide band of plagioclase above the bright layer consists of angular fragments that have been welded to the shear band and to each other; a few examples are marked by black arrows. Beyond this band, vesicle-rich glass fills the spaces between more widely spaced fragments. Shear was left lateral, denoted by pair of white arrows.

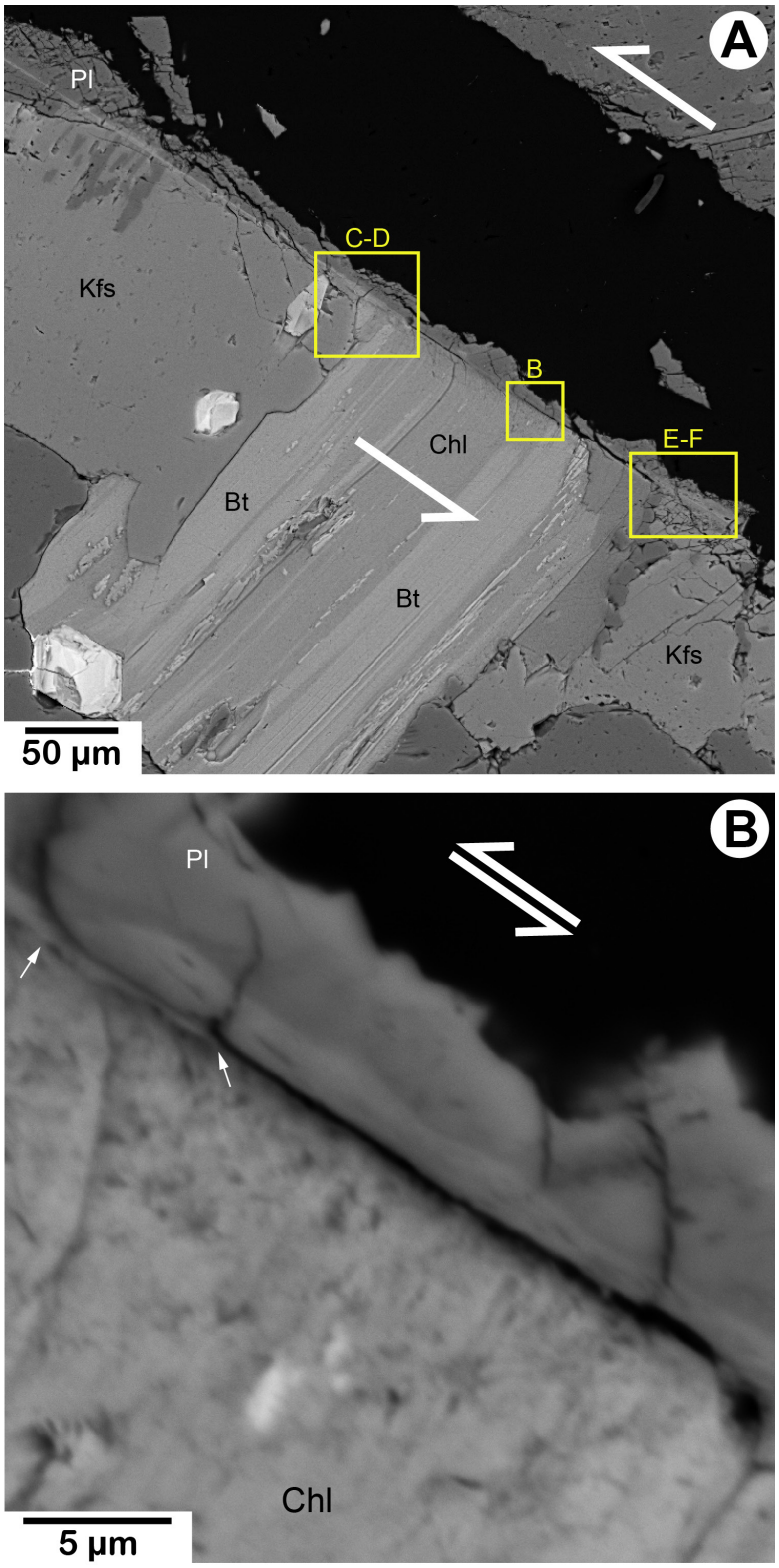

Figure 513-14. Backscattered-electron images showing shear-band textures adjacent to biotite and chlorite crystals. Shear was left lateral, denoted by pairs of white arrows. *A*, Low-magnification view shows locations of *B*–*F*. The shear band above a partly chloritized biotite is largely void space, but it forms a solid, bright band between K-feldspar and plagioclase on either side. *B*, Complex shear band between chlorite and plagioclase. An elongate void, ~0.45 µm wide on average, separates the two sides over much of the imaged length. A glass bridge (between the two small white arrows) fills most of the opening on the far left side; this feature may correspond to the hairlike glassy structures seen in views looking down on the sawcuts. Above the void, the brighter part of the shear band contains some elongate vesicles, the majority of which are oriented at a small angle to the plane of the sawcut. A darker layer of varying width adjoins the plagioclase; the width may vary with the topography of the plagioclase crystal on the sawcut. Chlorite located within ~6 µm of the shear band has a fragmented, porous appearance.

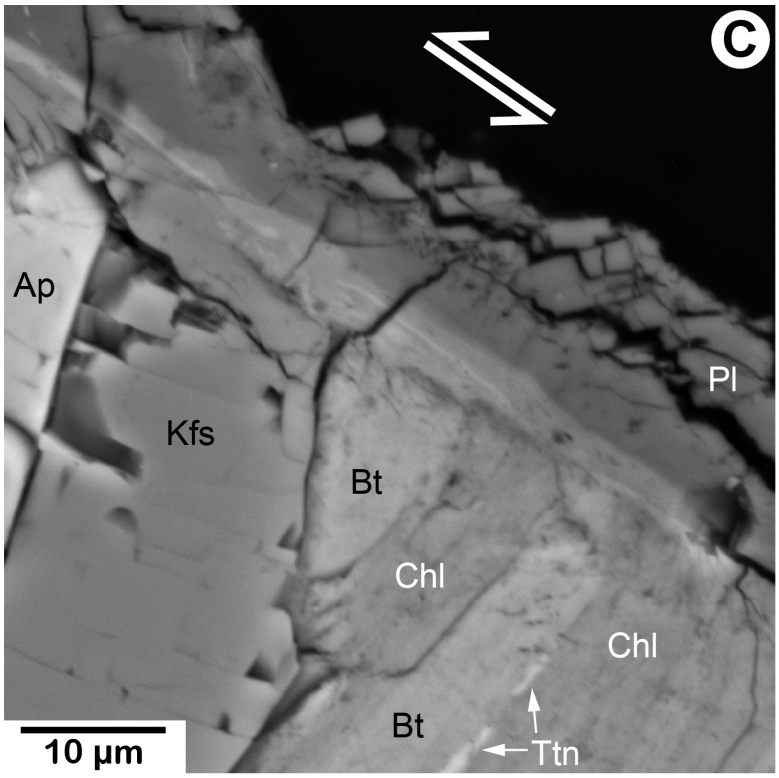

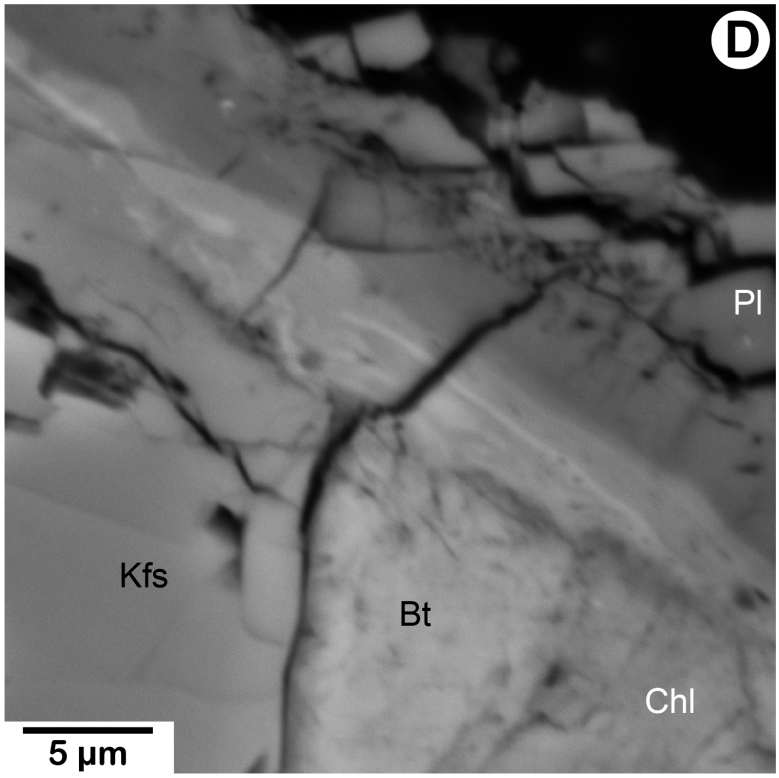

Figure 513-14.—Continued. *C*, *D*, The large voids terminate at either end of the partly chloritized biotite, although vesicles and small voids are still present in the shear band. The shear band is very heterogeneous compositionally, with numerous bright streaks apparently incorporated from the biotite. Shear boundaries are poorly defined and shear-band thickness varies. Vesicle-rich zones are present in the heavily fractured plagioclase above, and in a thin dark layer, beneath the shear band, best seen in *D*.

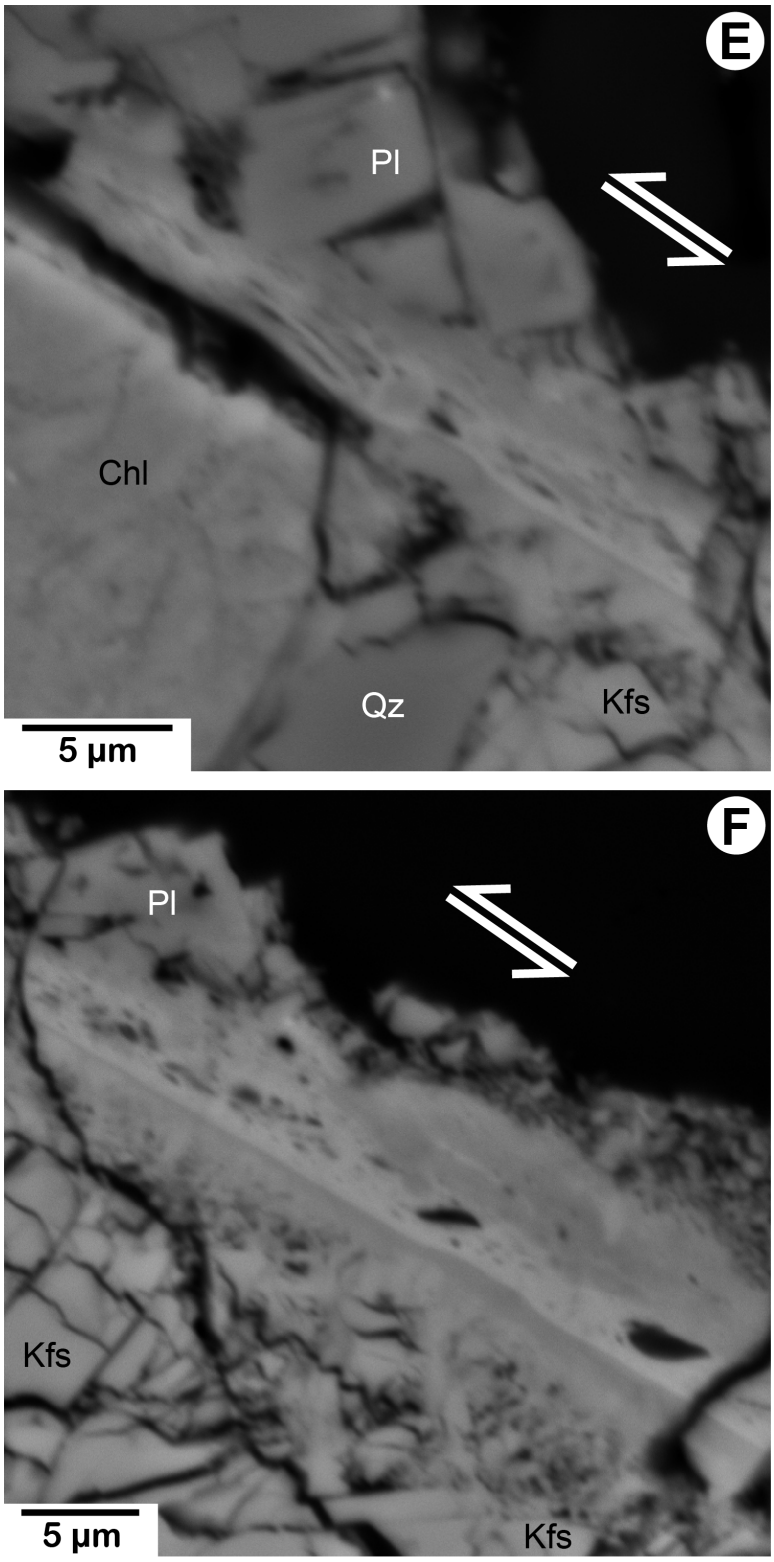

Figure 513-14.—Continued. *E*, *F*, Adjoining images taken at the far right side of the phyllosilicate minerals on the sawcut. The very elongate void seen in *B* terminates at the edge of the chlorite (*E*), but many stretched (*E*) to rounded (*F*) vesicles are concentrated in the brighter parts of the shear band. Shear-band thickness and composition are quite variable, and the boundaries with the highly damaged feldspars are indistinct, particularly the upper boundary with the plagioclase.

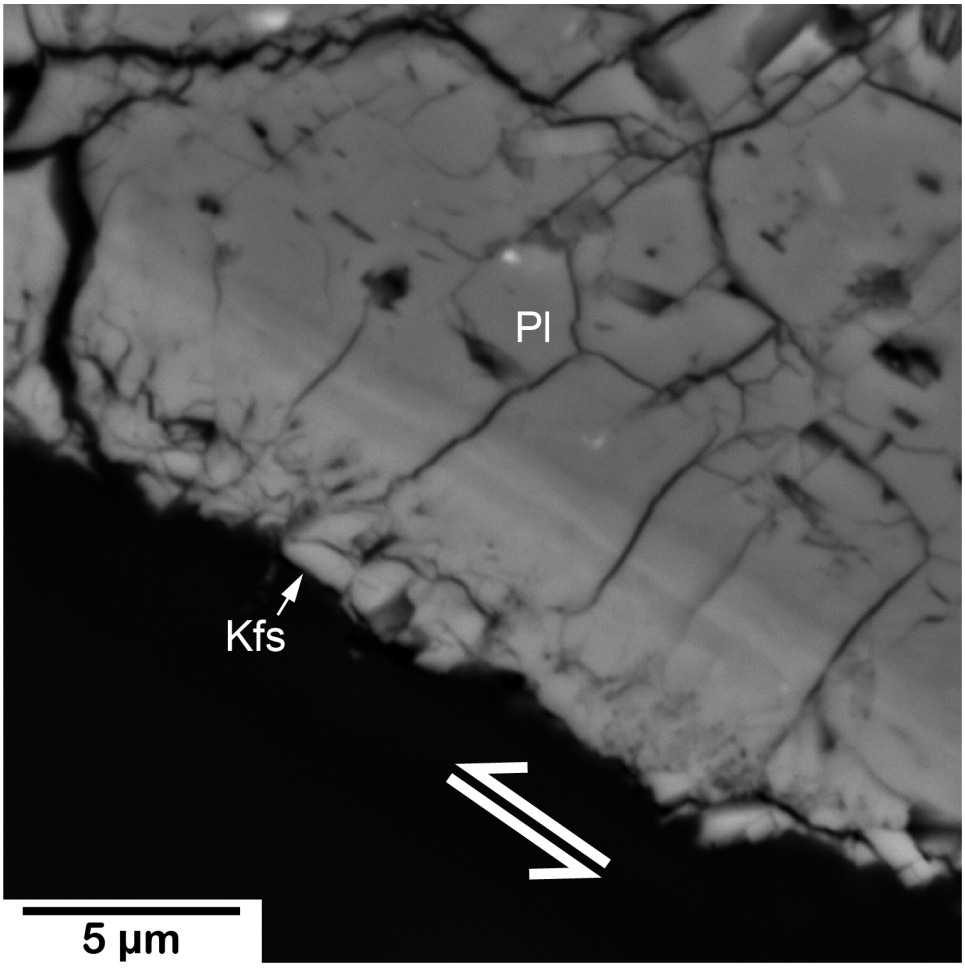

Figure 513-15. Backscattered-electron image showing shear band developed between plagioclase and a very broken-up K-feldspar. Quenched melt (darker, vesicle-filled) may have welded together the K-feldspar fragments closest to the shear band. The shear band contains K (without the Fe, Ti, and Mg characteristic of biotite) and some Ca and Na, suggesting derivation largely from feldspars. The shear band is compositionally layered: a thin, central, bright band is sandwiched between slightly darker ones, and an even darker layer adjoins the slightly brighter plagioclase. Shear was left lateral, denoted by pair of white arrows.

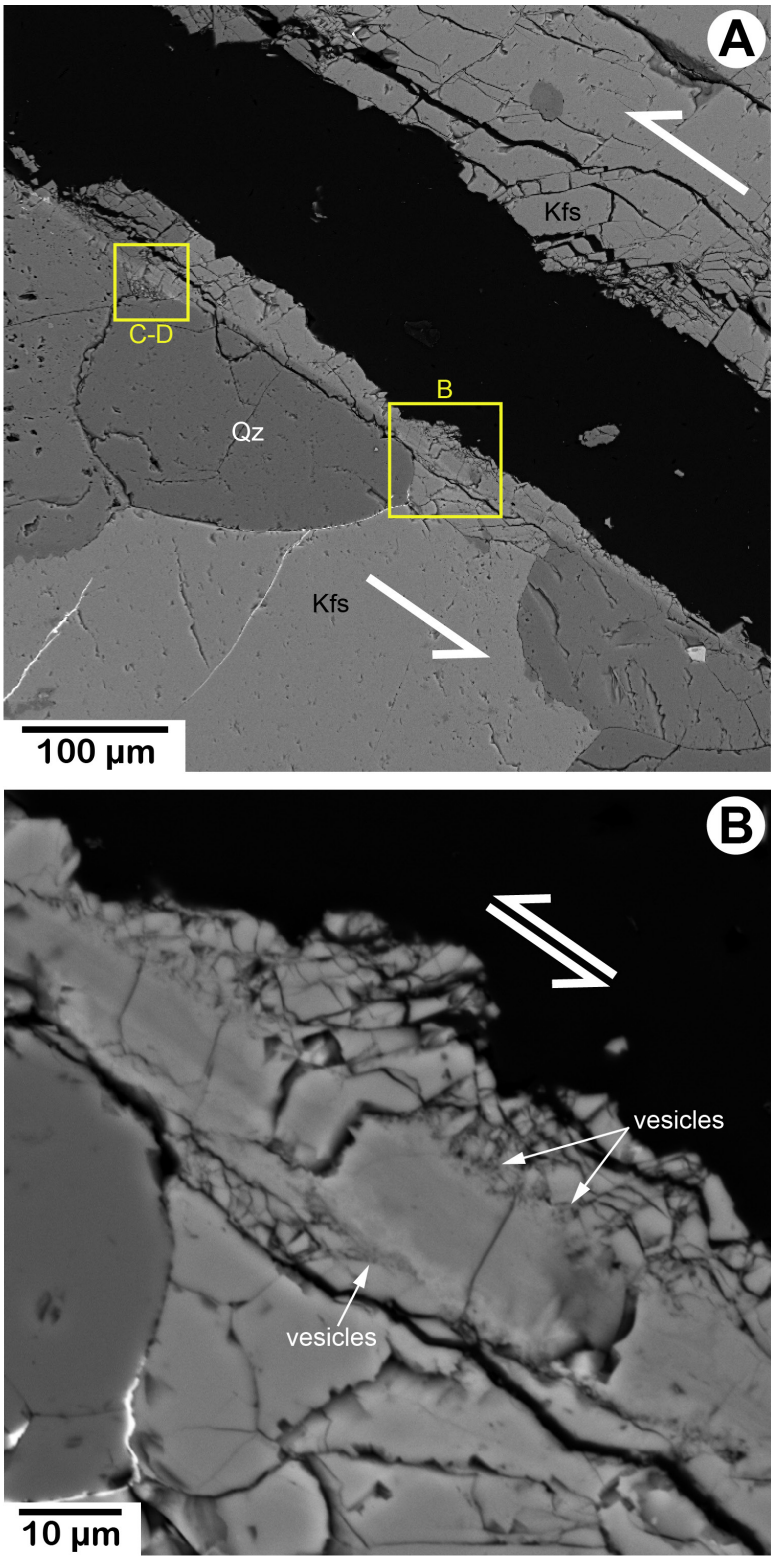

Figure 513-16. Backscattered-electron images showing textures at edges of quartz crystal. Shear was left lateral, denoted by pairs of white arrows. *A*, Low-magnification view shows locations of *B* and *C-D* at right and left edges of the crystal, respectively. *B*, Zoned shear band on the right side of the quartz. At this location the center of the shear band is relatively dark, whereas the upper and lower layers have similar brightness to the adjoining K-feldspars and may be enriched in K. Melt penetrated a few microns into the damaged areas above and below the shear band, and the shear boundaries are not well delineated.

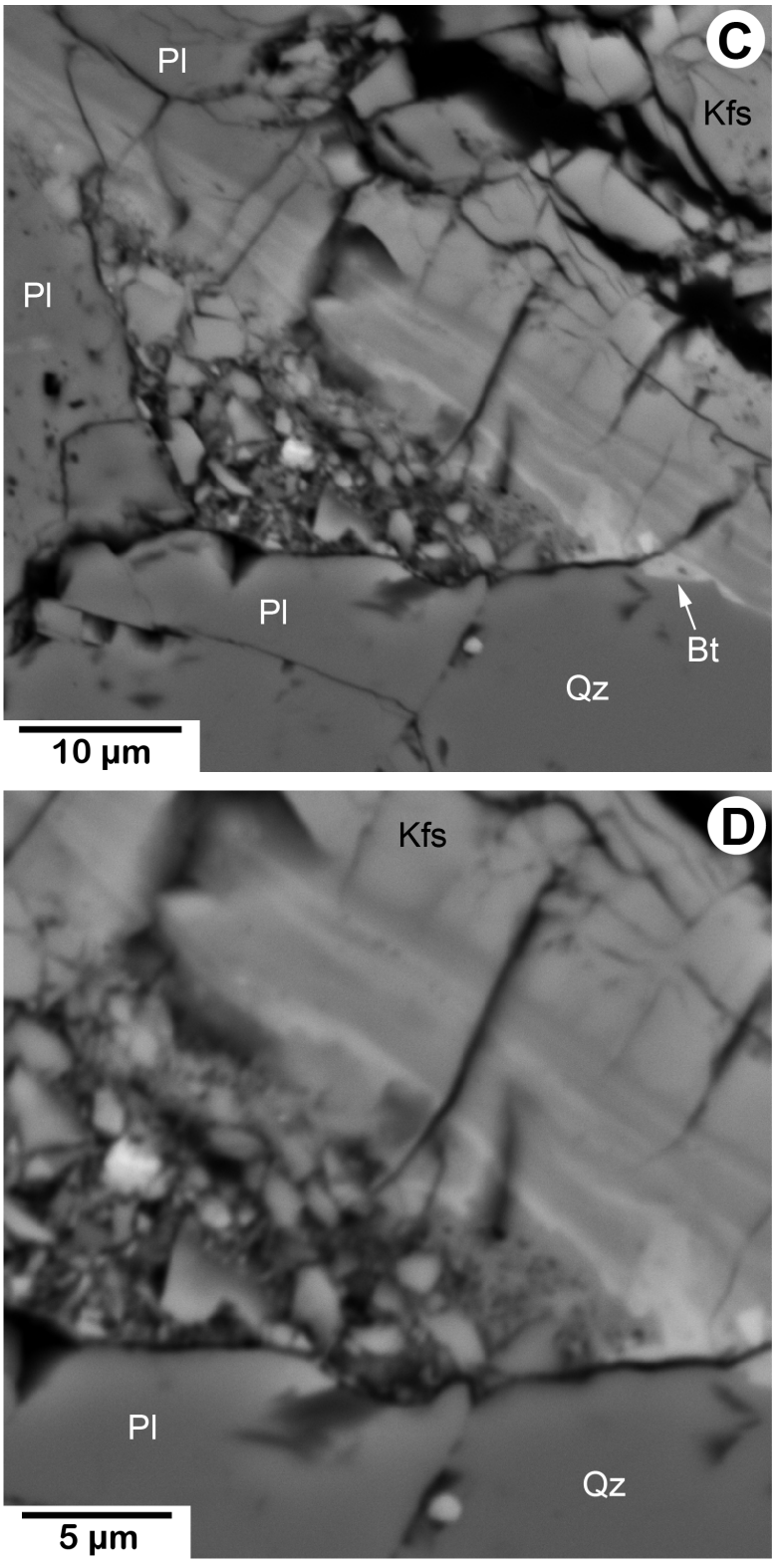

Figure 513-16.—Continued. *C, D*, Topographic low along the sawcut at the plagioclase-quartz boundary is filled with debris that was trapped in place by quenched melt. Vesicle-rich glassy matrix in the depression is concentrated into a zone of varying width adjacent to the shear band, and considerable porosity remains at the bottom of the depression. A tiny biotite crystal on the sawcut, at the edge of the quartz, has been smeared out into the shear band, giving it a streaky appearance. The streakiness suggests laminar flow during shear. The shear band also contains a few stretched vesicles.

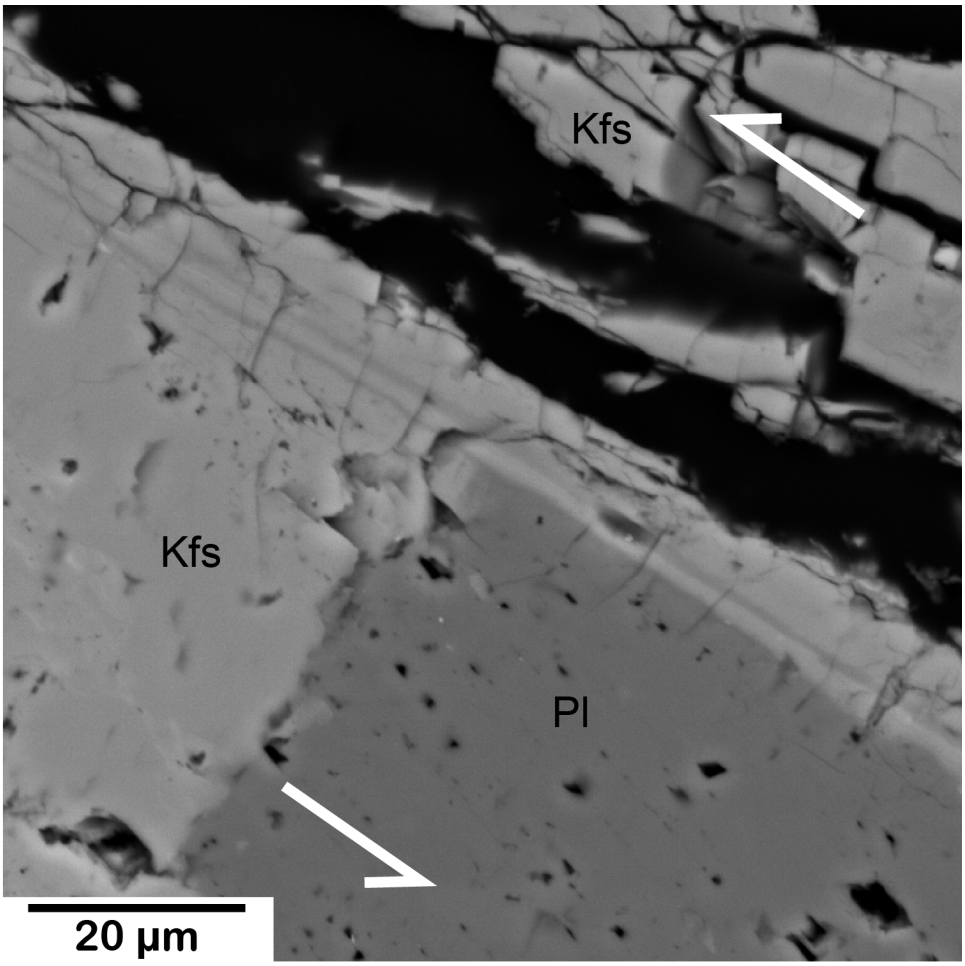

Figure 513-17. Backscattered-electron image showing compositionally layered, dense, relatively well-defined shear band between feldspars. The thickness of the dark-bright-dark layers on the left side of the shear band, between the K-feldspars, is 3.3 µm. The bright middle layer is itself layered; this is best seen above the K-feldspar at left. The set of short, nearly perpendicular cracks localized along the shear band are unloading cracks. Such cracks are commonly observed along the length of the sawcut. Shear was left lateral, denoted by pair of white arrows.

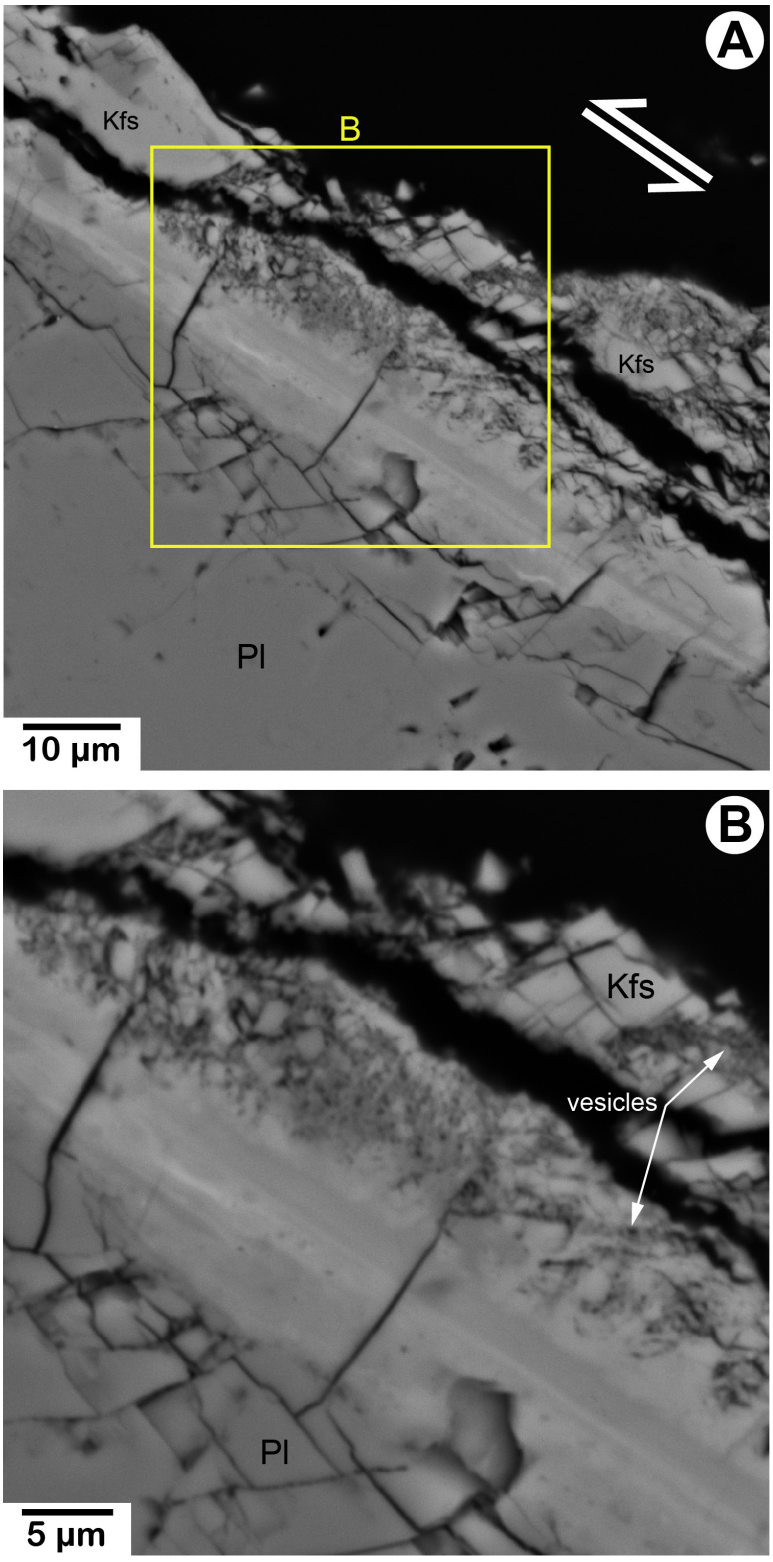

Figure 513-18. Backscattered-electron images showing compositionally layered shear band. *A*, Lower magnification view shows location of *B*. Variably wide and compositionally layered shear band between a plagioclase and a highly broken-up K-feldspar contains a biotite component. Shear was left lateral, denoted by pair of white arrows. *B*, Vesicles are concentrated in the brighter, central layer of the shear band, which probably has the highest concentration of biotite at this location. Vesicle-rich glass extends as much as ~20 µm into the overlying damage zone, whereas only minor amounts of melt penetrated the less fragmented plagioclase.

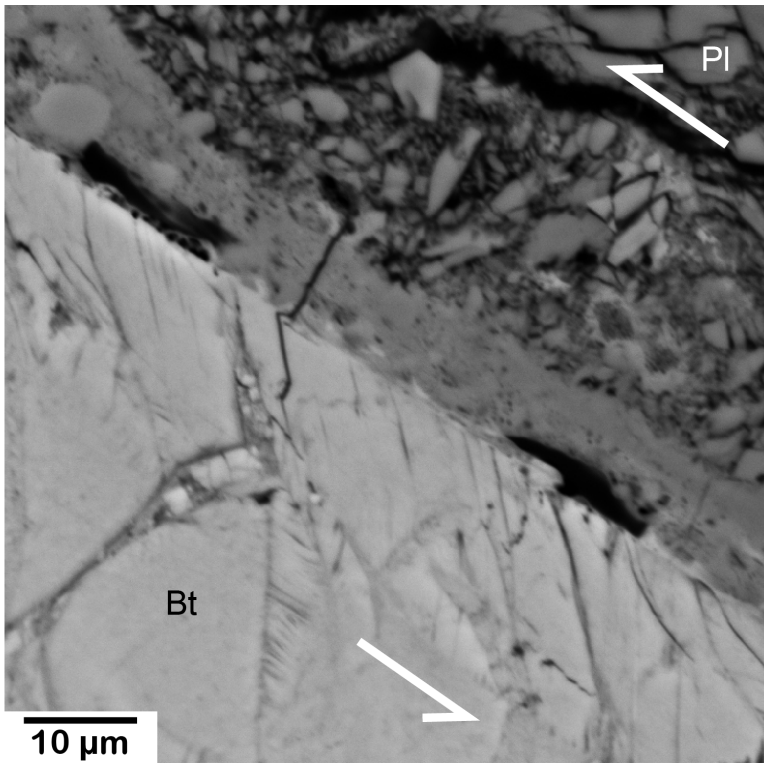

Figure 513-19. Backscattered-electron image of a well-defined, clast-rich, and very porous shear band above a kinked biotite. The lower sawcut surface along the biotite is very straight, as is commonly observed with the phyllosilicates. The upper boundary of the shear band is also remarkably well defined, given that it adjoins a debris-filled area beneath a plagioclase crystal that contains clasts of a number of different minerals. The large void directly above the biotite on the left stops abruptly at a large, moderately rounded clast, and the shear band is deflected upwards around the clast. Delicate glassy structures formed around the perimeters of both of the large voids. Wisps of bright material concentrated at the base of the shear band are probably derived from the biotite. Overall, however, the shear band is relatively dark, similar to the plagioclase. Shear was left lateral, denoted by pair of white arrows.

DL511—400 MPa

This stick-slip experiment had one partial stress drop (~125 MPa) followed by one total stress drop (340 MPa). The two driving blocks of this sample were separated along the sawcuts, and two pieces were taken from the same driving block (fig. 511-1) were examined with secondary-electron (SE) imaging techniques (5 kV). The larger piece (511d, right) shows approximately half the sawcut at the narrower end of the driving block (see fig. 1). The small chip (511c, left) came from the wider end. The approximate locations of figures 511-2 through 511-8 on 511c are circled; however, the positions of figures 511-9 through 511-12 on 511d were not noted.

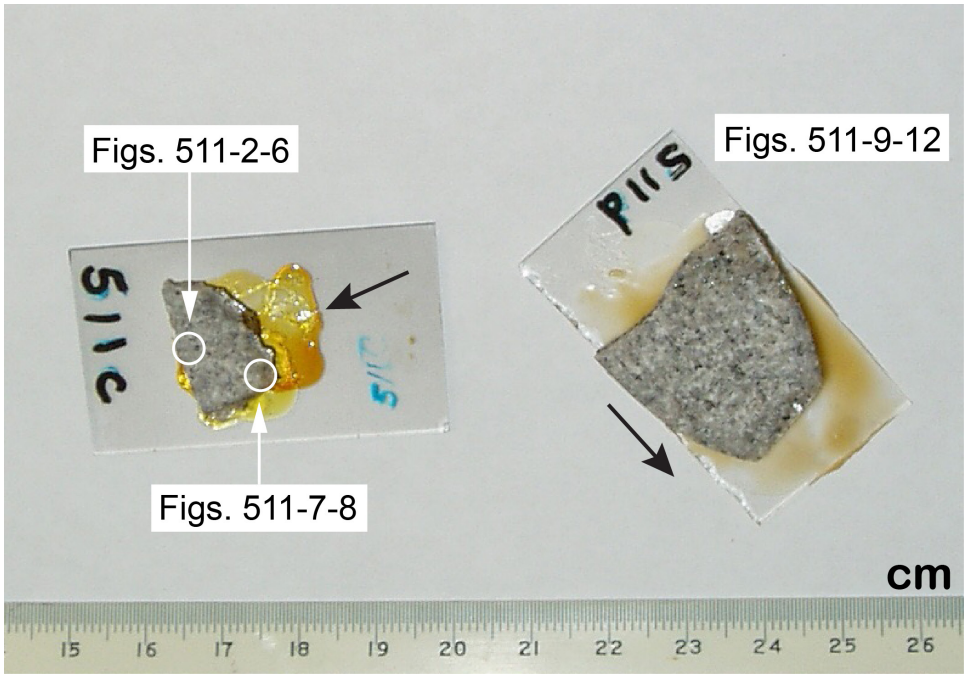

Figure 511-1. Photograph showing two pieces of sample DL511 (511c, d), derived from the same driving block, that were examined in this study. Black arrows indicate the slip direction of the pieces.

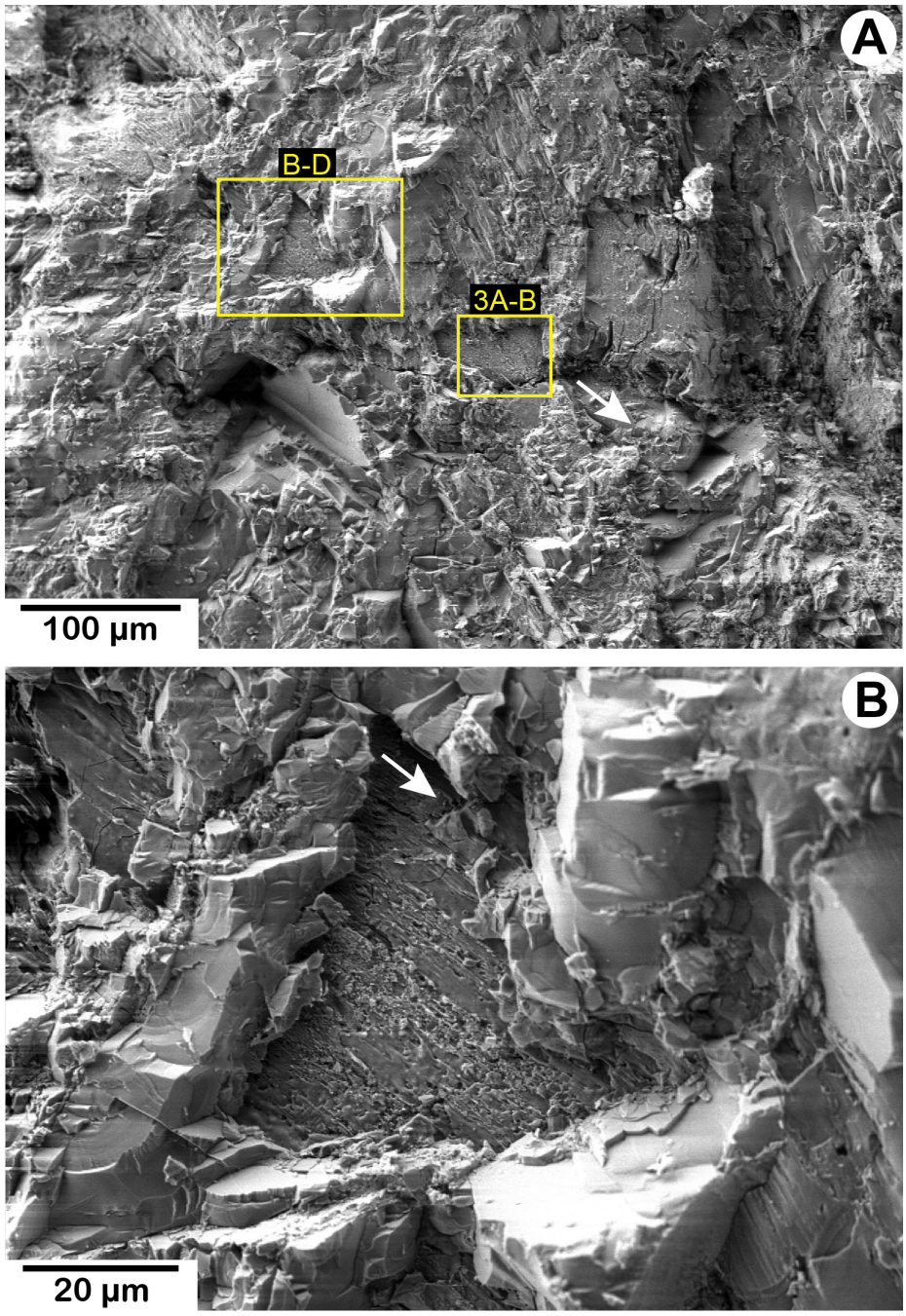

Figure 511-2. Secondary-electron images looking down on one of the granite driving blocks. White arrows show shear direction of driving block. *A*, Low-magnification view shows locations of "windows" through the damaged rock that expose the sawcut surface where melting occurred, featured in *B–D* and figure 511-3. *B*, The glassy, sawcut surface exposed in the center of the image is rich in clasts and rounded vesicles. Possible second exposure of this surface at the upper left corner has a nearly 20-µm-long stretched vesicle.

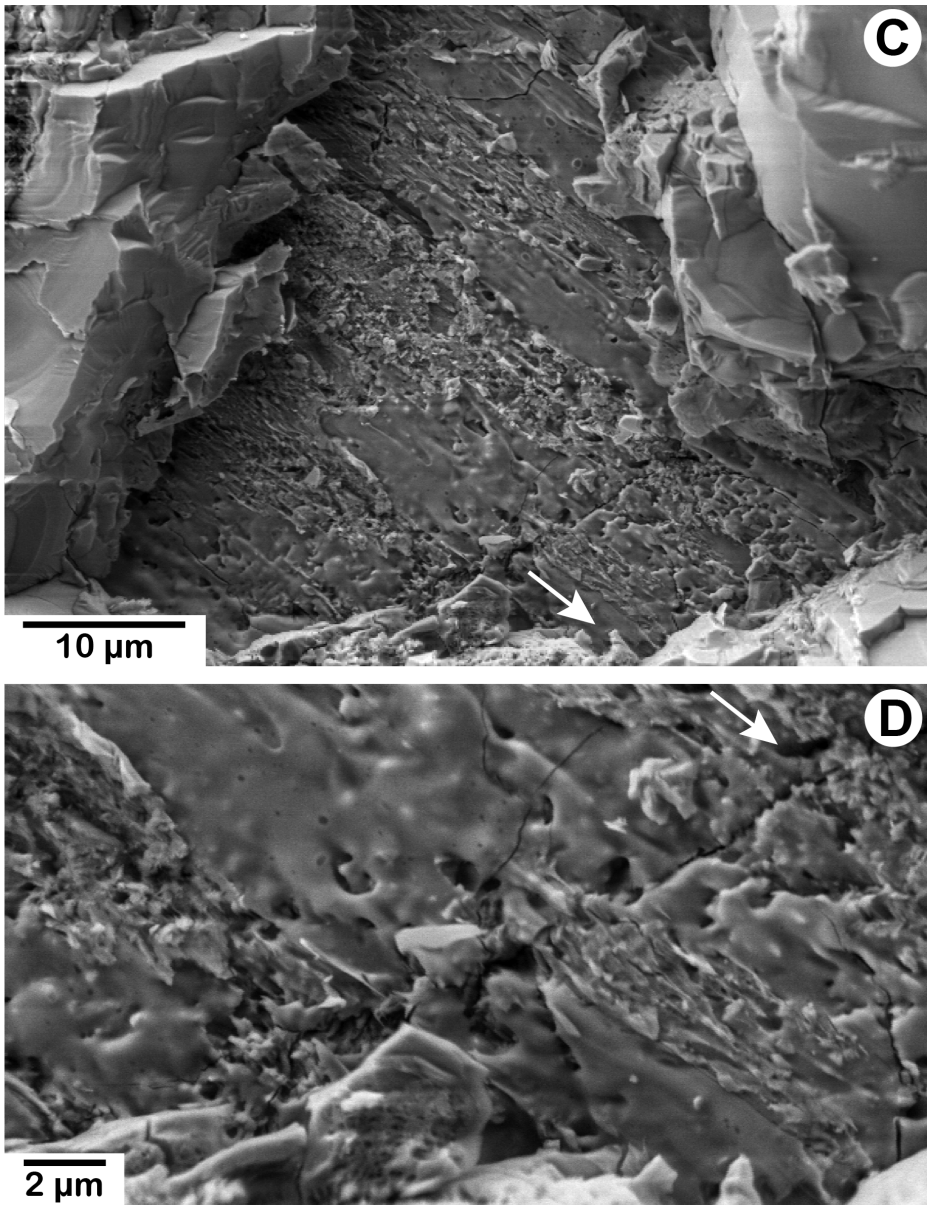

Figure 511-2.—Continued. *C*, *D*, Progressively higher magnification views of the glassy planar surface in *B*. Much of it appears viscous, very clast-rich, and porous, with many linear ridges and stretched vesicles aligned in the shearing direction. Approximately half the surface is coated with a thin layer of smooth glass containing only a few tiny, rounded pores.

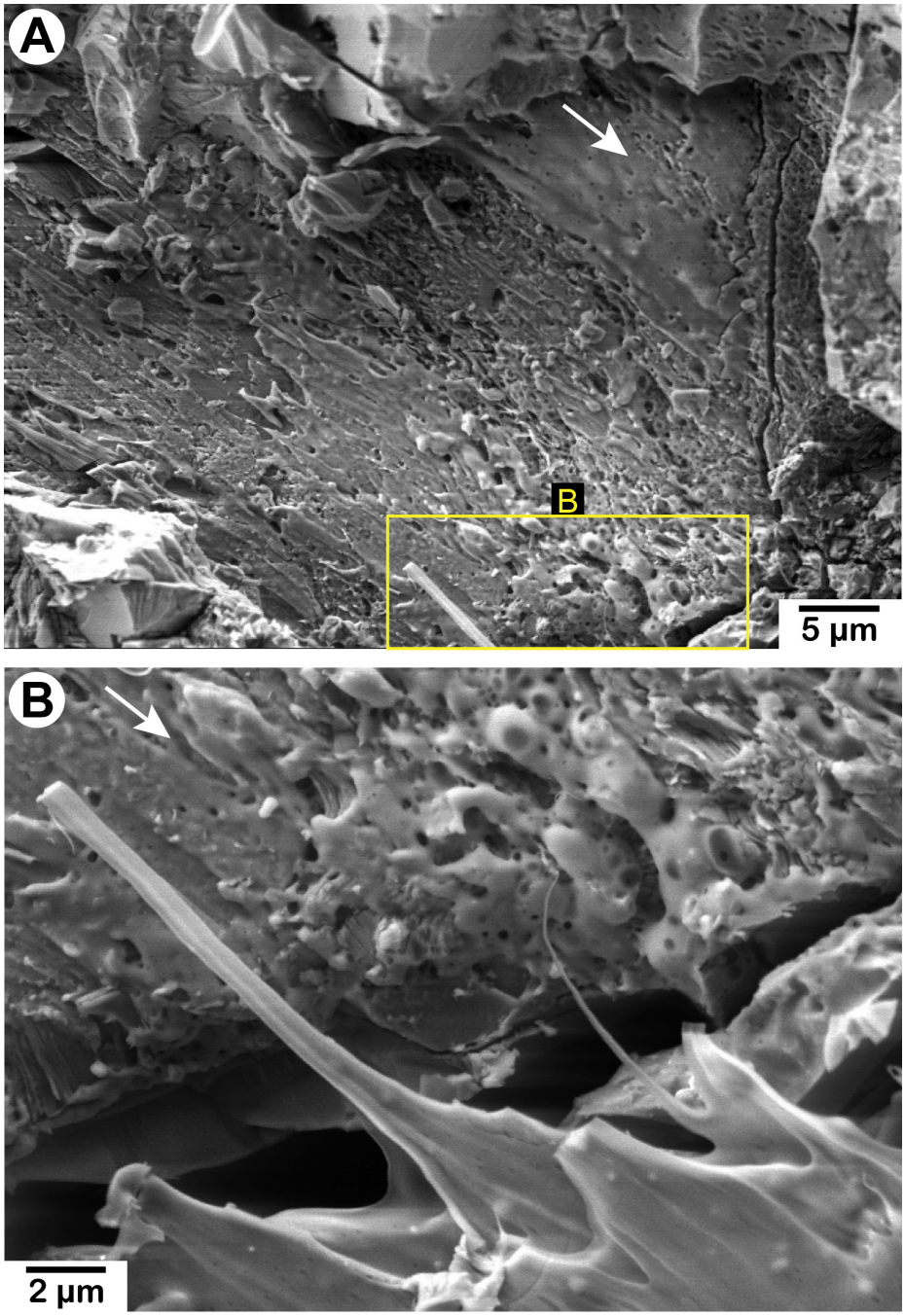

Figure 511-3. Secondary-electron images showing close-up views of the "window" in the center of figure 511-2*A*. White arrows show shear direction of driving block. *A*, The glassy surface is very similar to the one in figure 511-2*C*. *B*, Filaments of glass with very delicate, wispy terminations extend above a fracture. The glass on the side below the fracture is thinly layered; glass filaments project from a middle layer. The hairlike structures in this and subsequent images correspond to the glass bridges seen in cross-sectional views (DL513). The fracture wall reveals a layered character below the surface on the other side, but the lowermost layers may be the (001) cleavage of a phyllosilicate mineral.

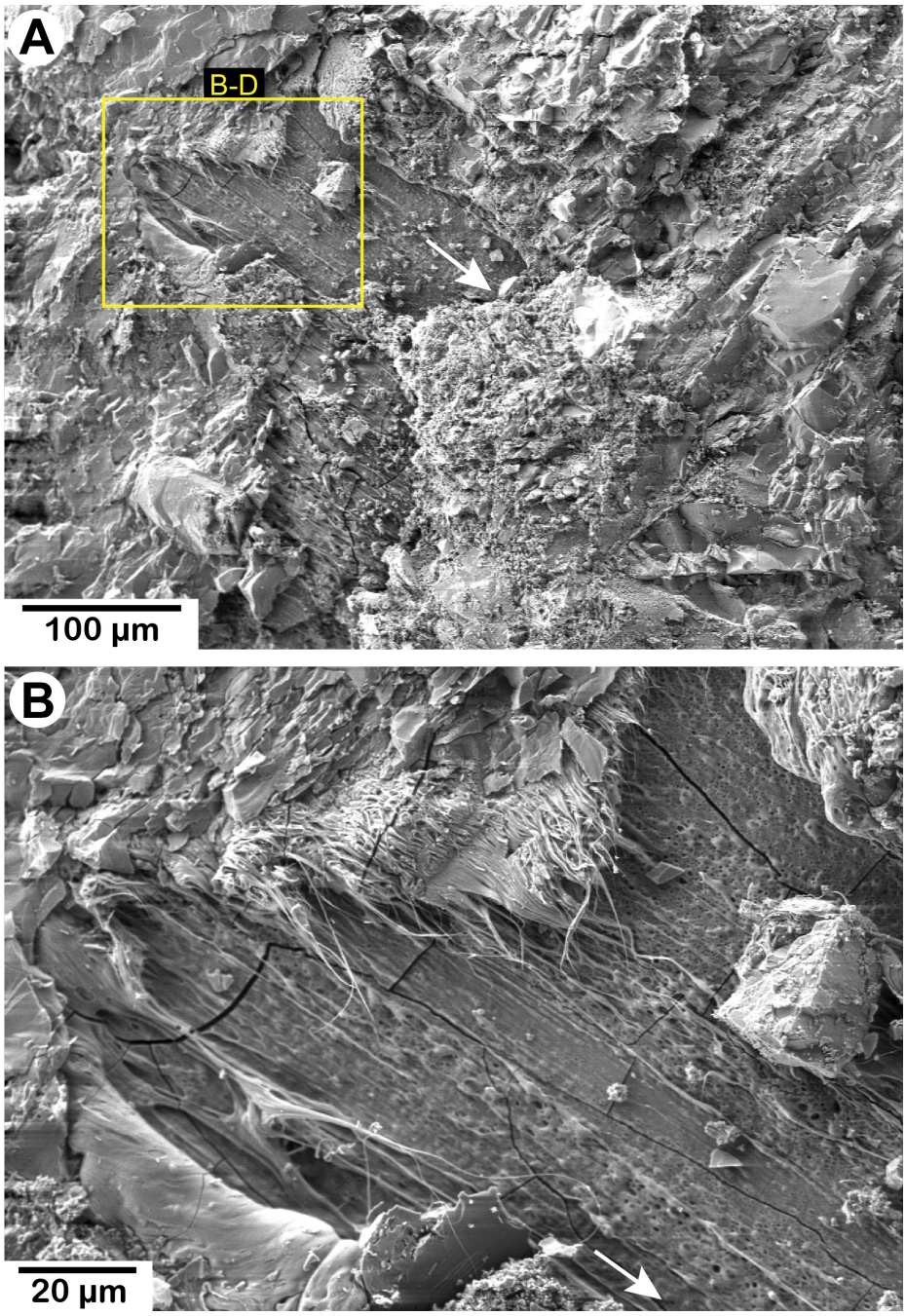

Figure 511-4. Secondary-electron images showing progressively higher magnification views of the shear band exposed in a "window" through the overlying damage zone. White arrows show shear direction of driving block. *A*, Low-magnification view shows location of *B–D*. The mineral in the upper left corner, topographically overlying the striated glassy surface, has a layered appearance suggestive of a phyllosilicate mineral. Patches of vesicle-rich glass are scattered over the crystal surfaces, in particular on the topographic high near the center of the image. *B*, Closer view of glassy textures along the shear band. The glass is fractured in several places.

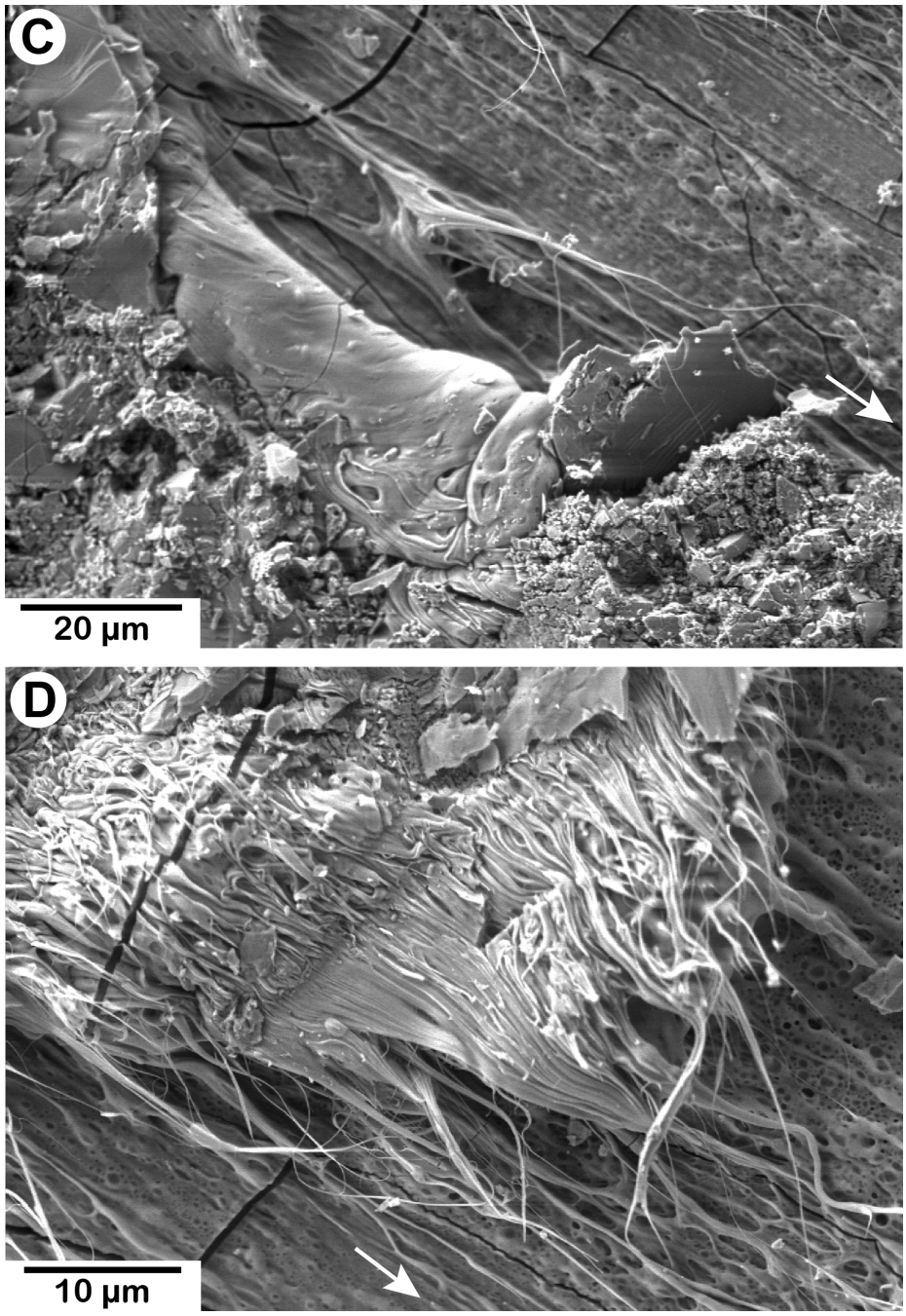

Figure 511-4.—Continued. *C*, Ropy lava texture adjacent to the striated glassy layer. *D*, Close-up of the delicate but intertwined, hairlike structures stretched out over the planar, glassy surface. Vesicles are concentrated on the right side of the lower surface.

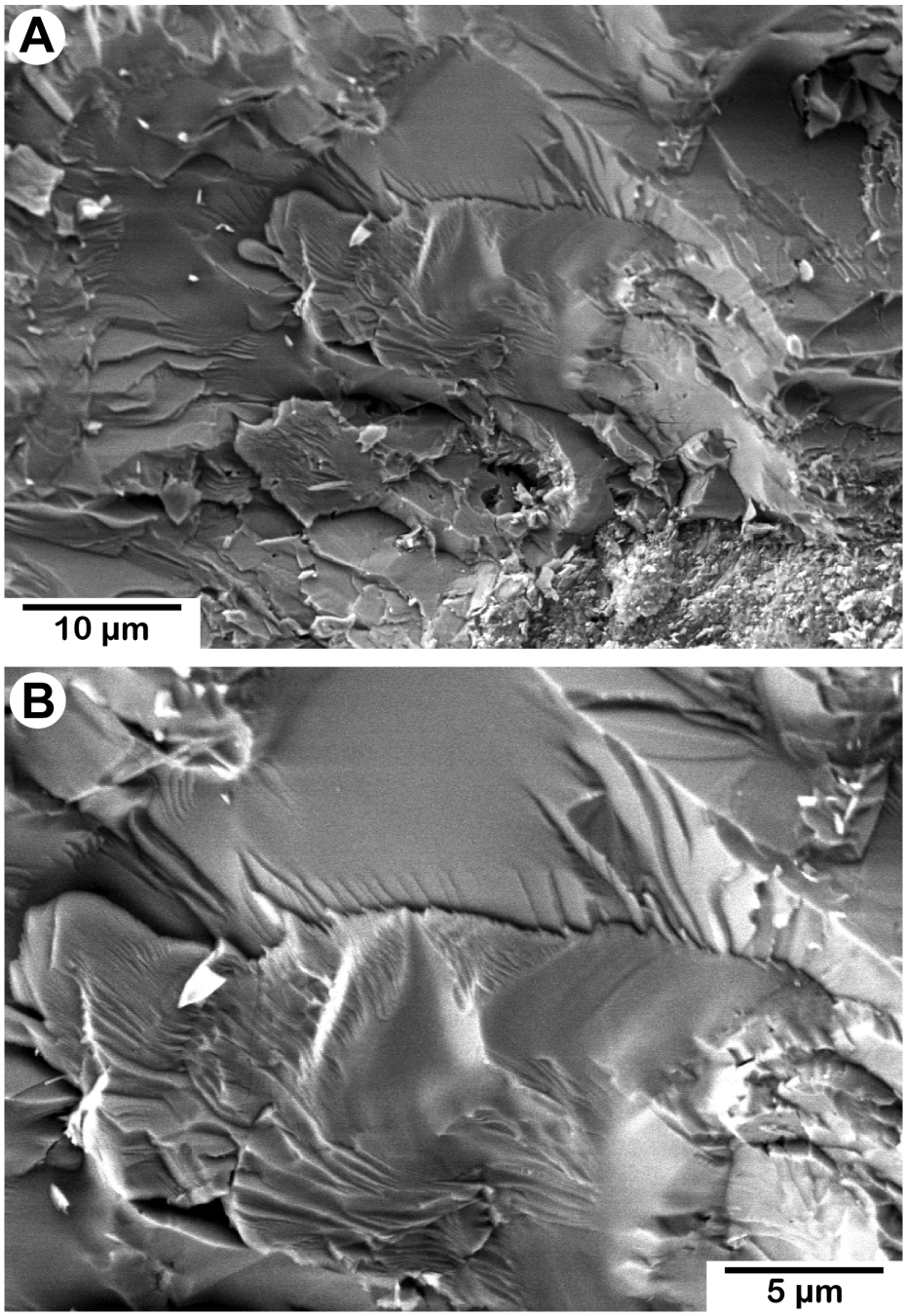

Figure 511-5. Secondary-electron images showing unusual fracture patterns in a probable quartz crystal. *A*, Crystal is adjacent to an area of vesicle- and clast-rich glass at lower right. *B*, Enlargement of the central part of *A*.

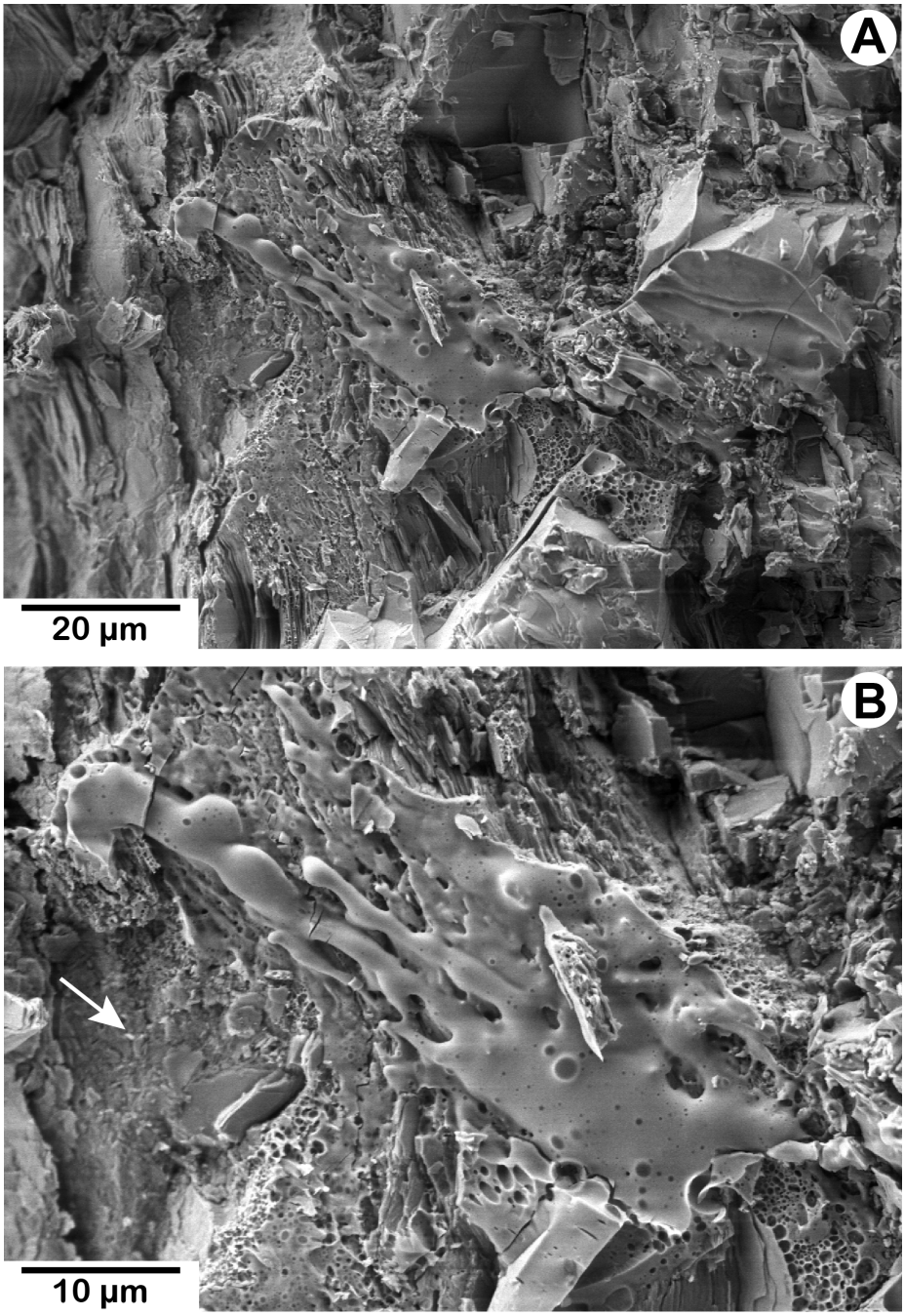

Figure 511-6. Secondary-electron images of a thin smear of smooth glass atop patches of very vesicle-rich glass at lower (*A*) and higher (*B*) magnification. White arrow shows shear direction of driving block. Lumpy fingers of the glass are aligned parallel to the shearing direction. The mineral on the left side of both images, topographically below the glassy surface, has a steeply dipping layered structure consistent with a phyllosilicate. The smooth glass texture suggests crystallization in a void space, typically associated with the phyllosilicates, and the texture may correspond to textures in figures 511-2*C* and *D* and 511-3*A*. Some of the vesicle-rich glass filled pores in the damaged wall rock.

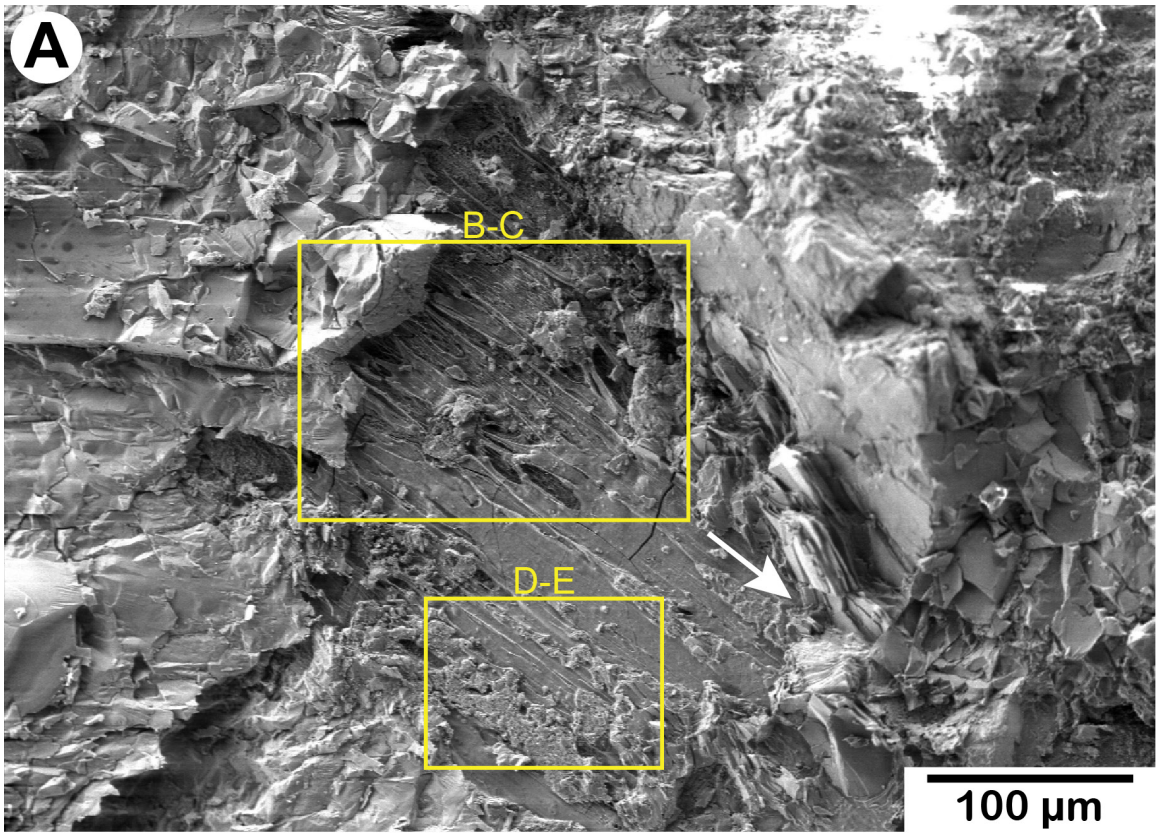

Figure 511-7. Secondary-electron images of a striated, glassy, planar surface surrounded by crystal fragments and patches of glass. White arrows show shear direction of driving block. *A*, Low-magnification view shows locations of *B*–*E*.

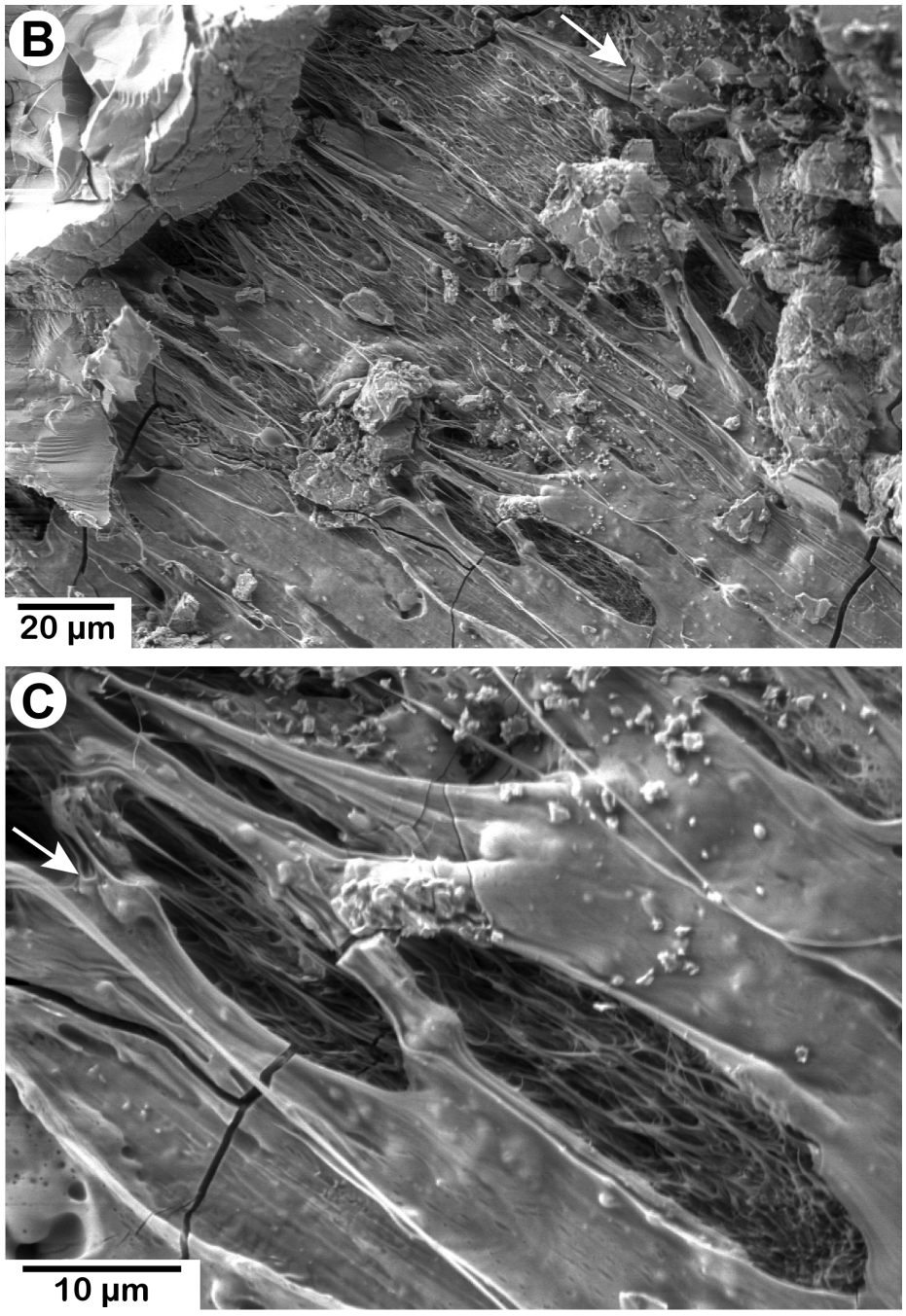

Figure 511-7.—Continued. *B*, *C*, Highly porous, filamentous textures exposed in ellipsoidal openings (perhaps stretched vesicles) beneath a thin coating of glass. The fracture surfaces of a possible quartz crystal in the upper left corner of *B* have textures similar to those in figure 511-5.

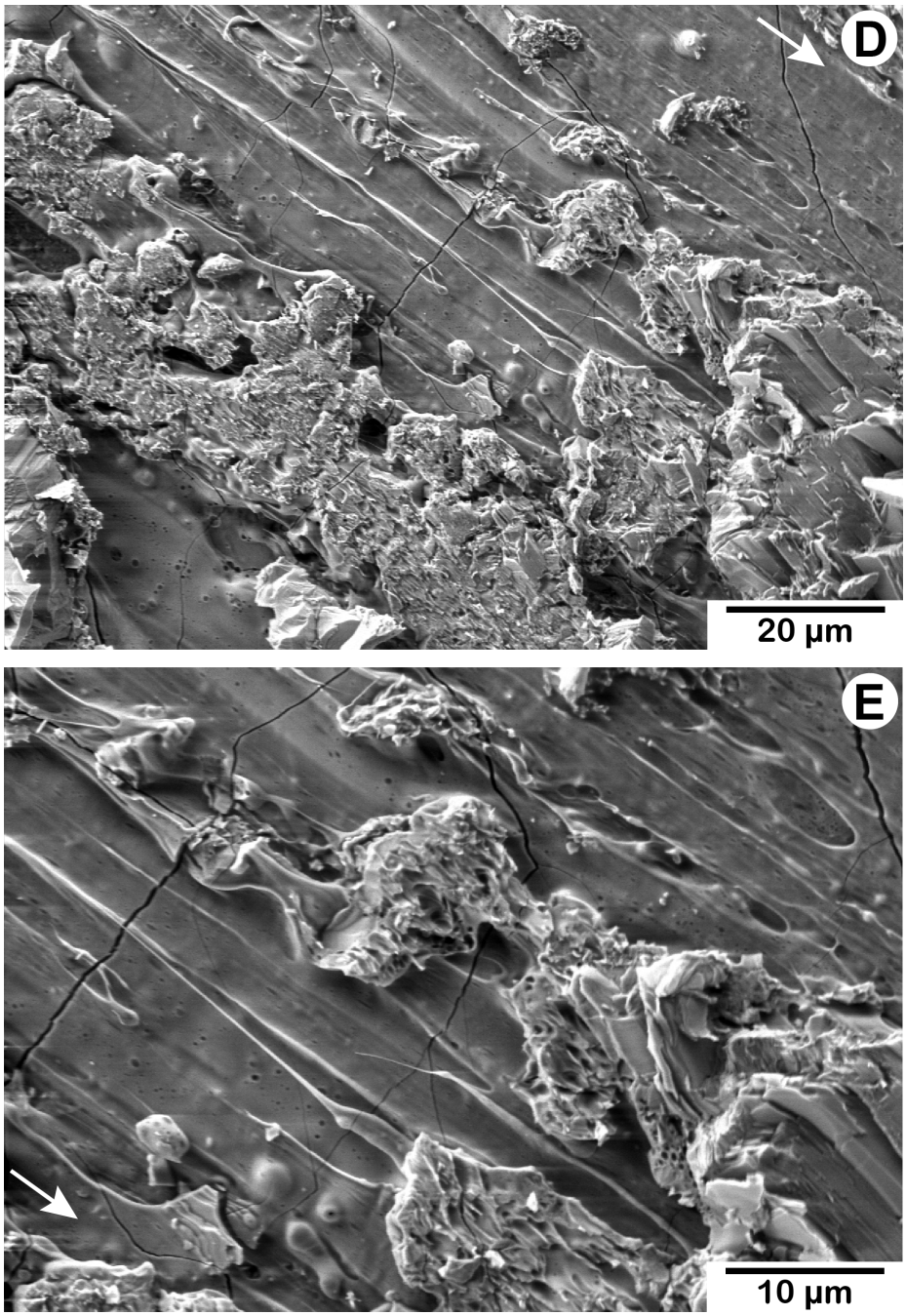

Figure 511-7.—Continued. *D*, *E*, Material above the striated, solid glassy layer. The flat, matted surface in *D* suggests that this layer was at or near the upper sawcut surface. The matted material is vesicular (best seen in *E*), with many smaller scale examples of the ridges and stretched vesicles aligned in the shearing direction. Planar features in the overlying material on the right side of both images may be glassy layers similar to the main exposed glassy surface.

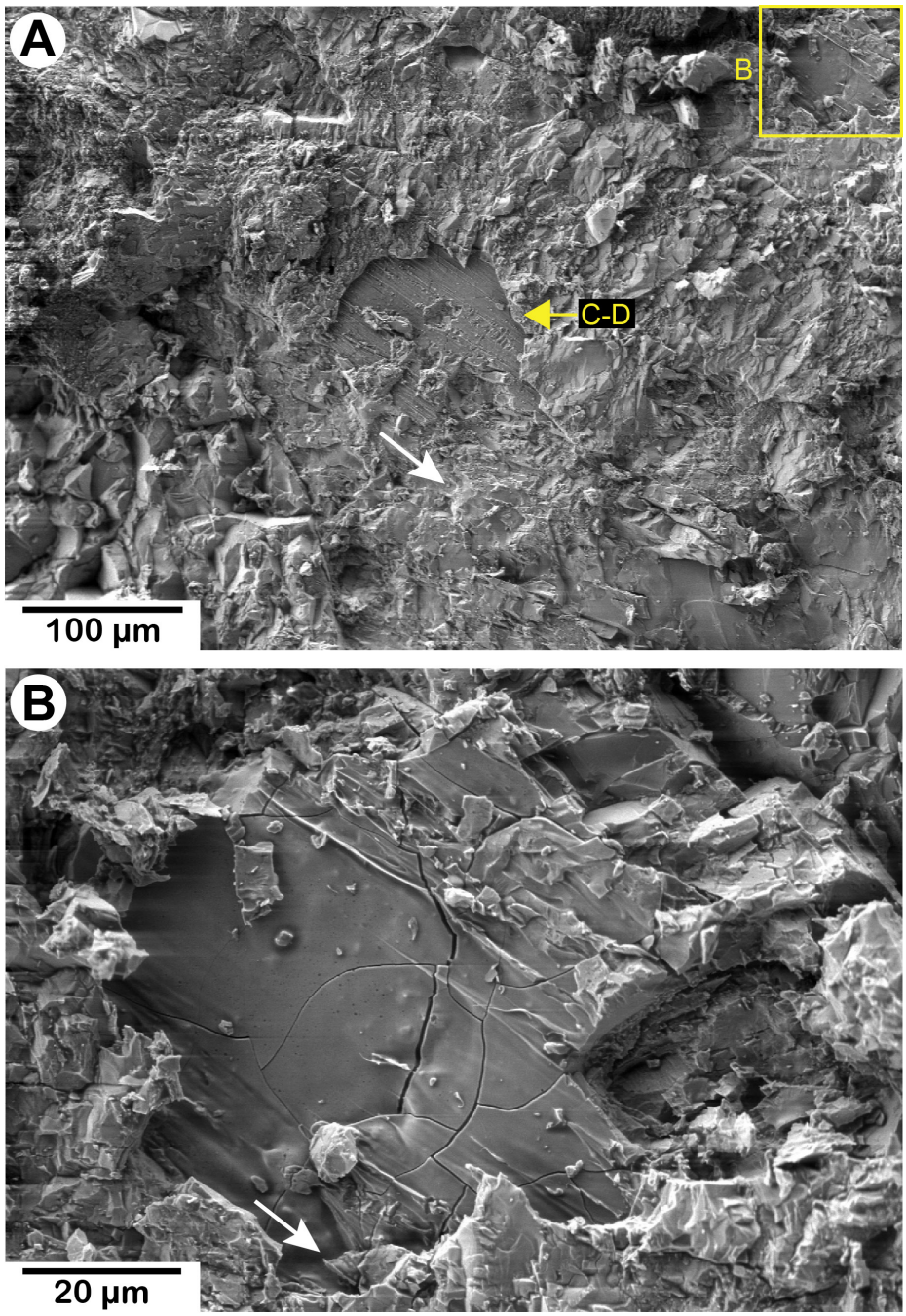

Figure 511-8. Secondary-electron images of two relatively solid layers of glass exposed on the sawcut surface. White arrows show shear direction of driving block. *A*, Low-magnification view shows locations of *B*–*D*. *B*, The very smooth, flat surface in the upper right corner of *A* has only a few linear trends and very few vesicles.

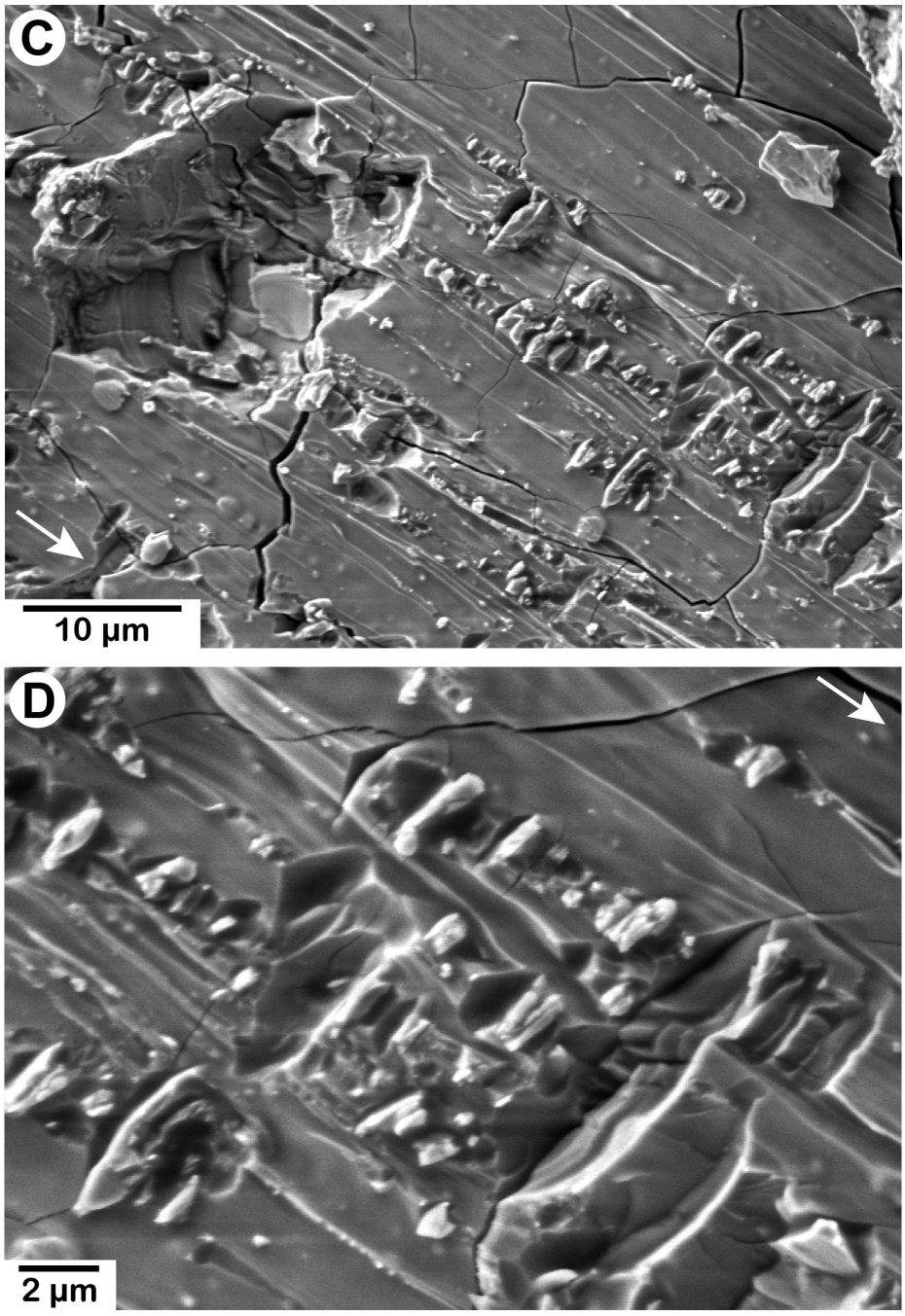

Figure 511-8.—Continued. *C*, *D*, The "window" in the center of *A* contains a number of notches oriented perpendicular to the shear direction. Some of them contain thin mineral slivers. The empty notches may be associated with crystal fragments that remained attached to the overlying driving block when the two sides were separated. Many of the linear trends in the glassy layer emanate from the notched areas, suggesting that the crystal fragments impeded flow of the melt.

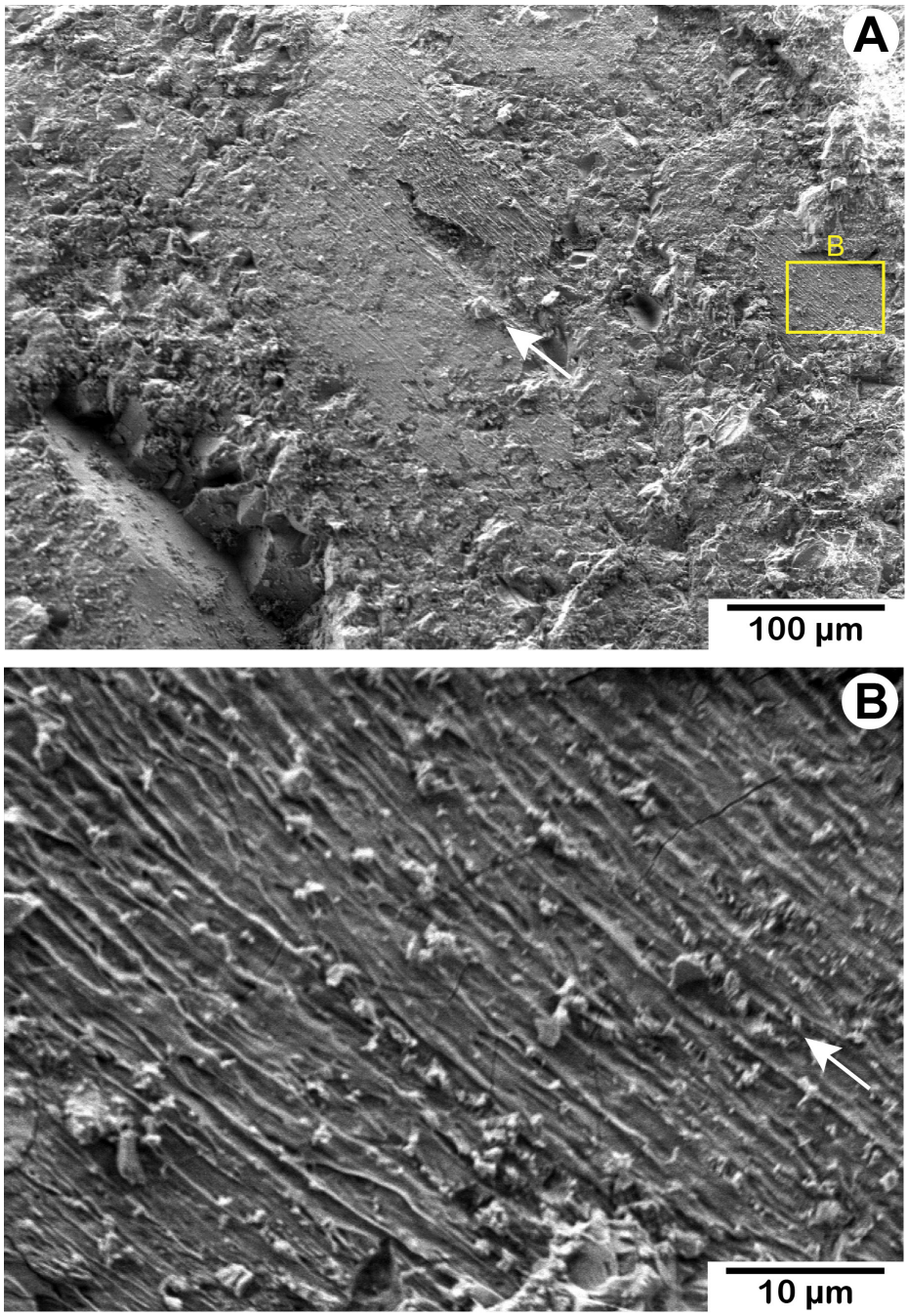

Figure 511-9. Secondary-electron images showing relatively viscous melt of contrasting texture to figure 511-8. White arrows show shear direction of driving block. *A*, Low-magnification view shows location of *B*. Relatively extensive layer of striated glass is exposed in *A*, although it is surrounded and overlain by clumps of mineral fragments in a matrix of vesicular glass. *B*, Viscous-looking, finely striated glass containing numerous tiny clasts.

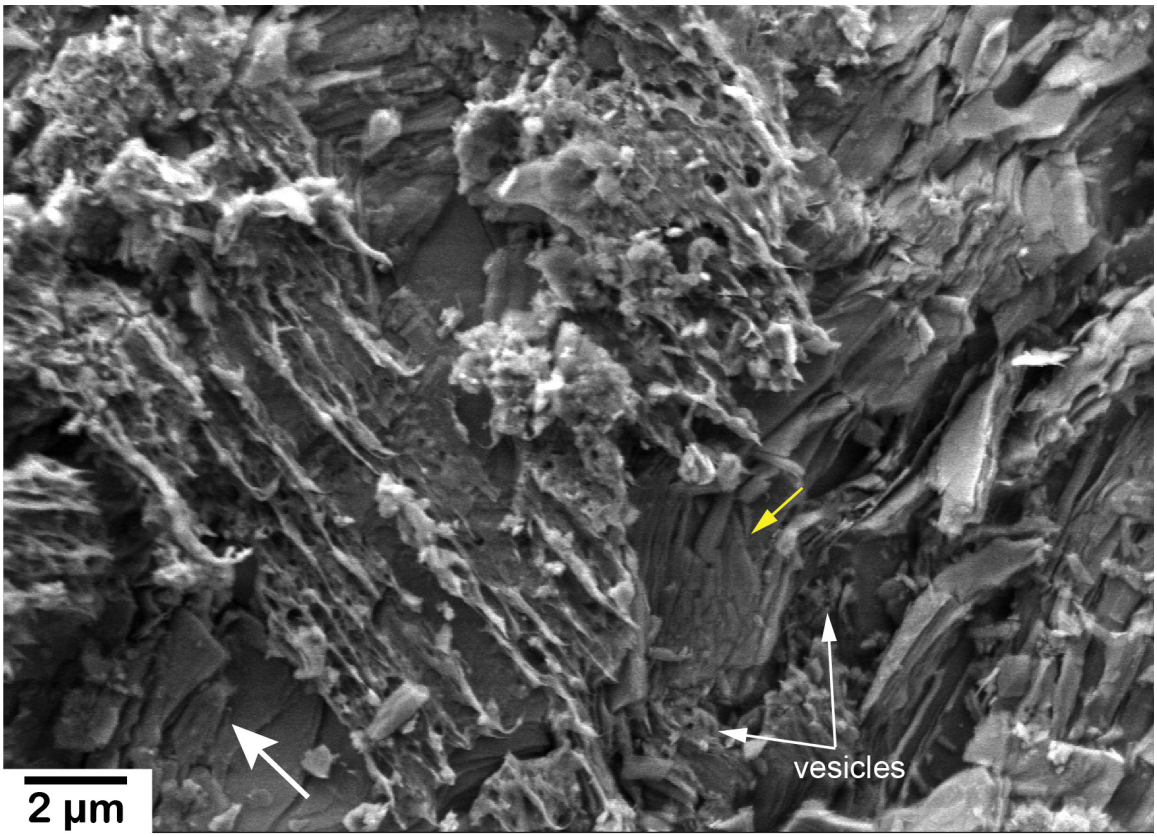

Figure 511-10. Secondary-electron images showing smears of very viscous, clast-filled glass on a crystal with platy cleavage; likely a phyllosilicate mineral. Larger white arrow shows shear direction of driving block. Some of the mineral layers immediately below the shear are fragmented (yellow arrow) and intermixed with patches of vesicle-filled material.

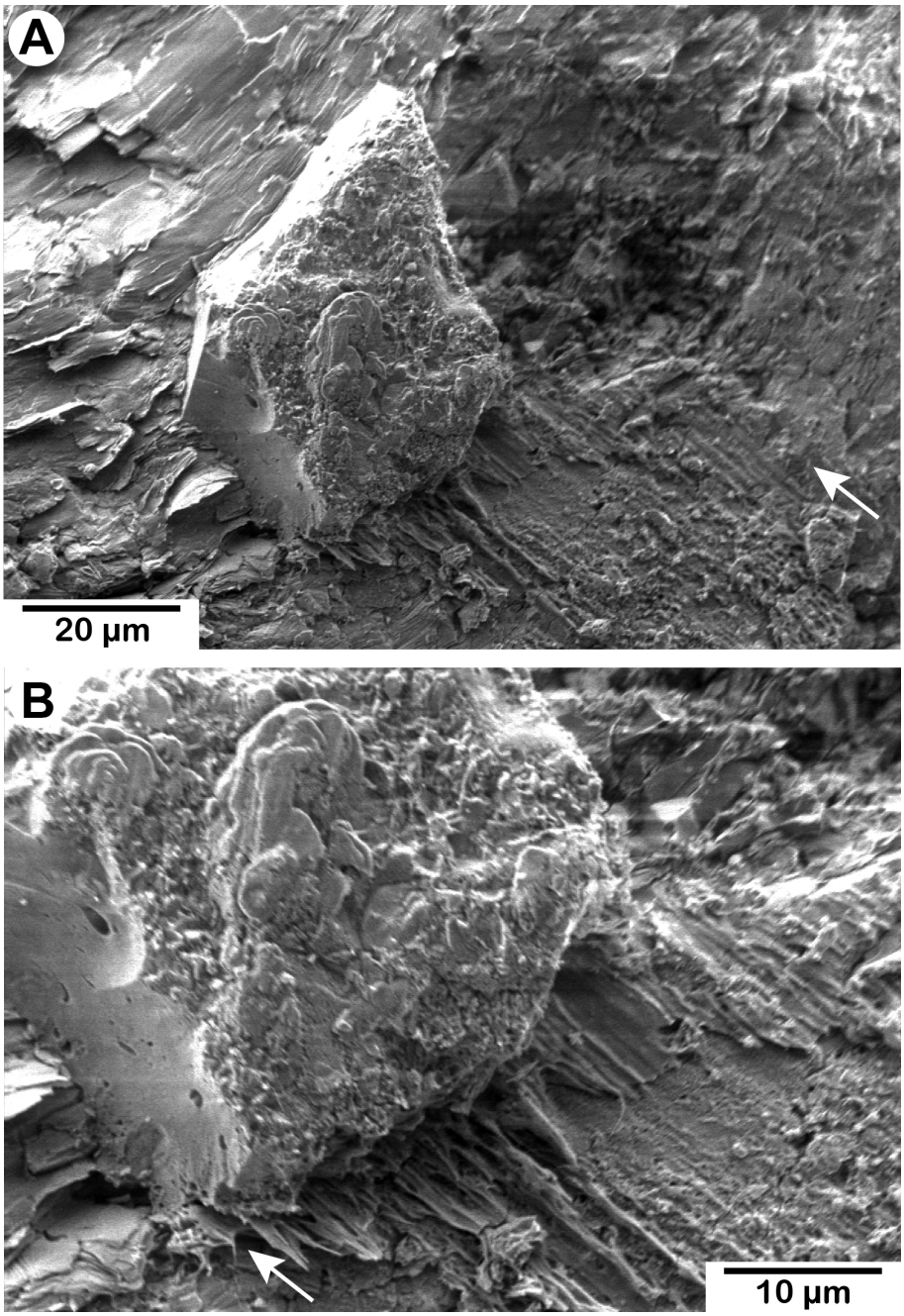

Figure 511-11. Secondary-electron images of a fragment sticking out above the driving block show the thickness of the glassy shear band on its left side. White arrows show shear direction of driving block. *A*, Lower magnification image shows how the projecting piece sits between a mineral face exposed at upper left and a glassy surface at lower right. *B*, Higher magnification image shows that the conchoidally fractured left side of the large piece is very dense across much of its width, with only a few stretched vesicles oriented parallel to the shear direction. Porosity increases downwards and the lower surface is very irregular, apparently because melt migrated into the damaged rock adjacent to the shear band. The transition in porosity on this face is at the level of the fingers of glass that extend out to the lower right from the base of the clast. Much of the upper surface of this piece is covered by a mixture of small clasts and vesicular glass; the tips of larger mineral fragments are rounded.

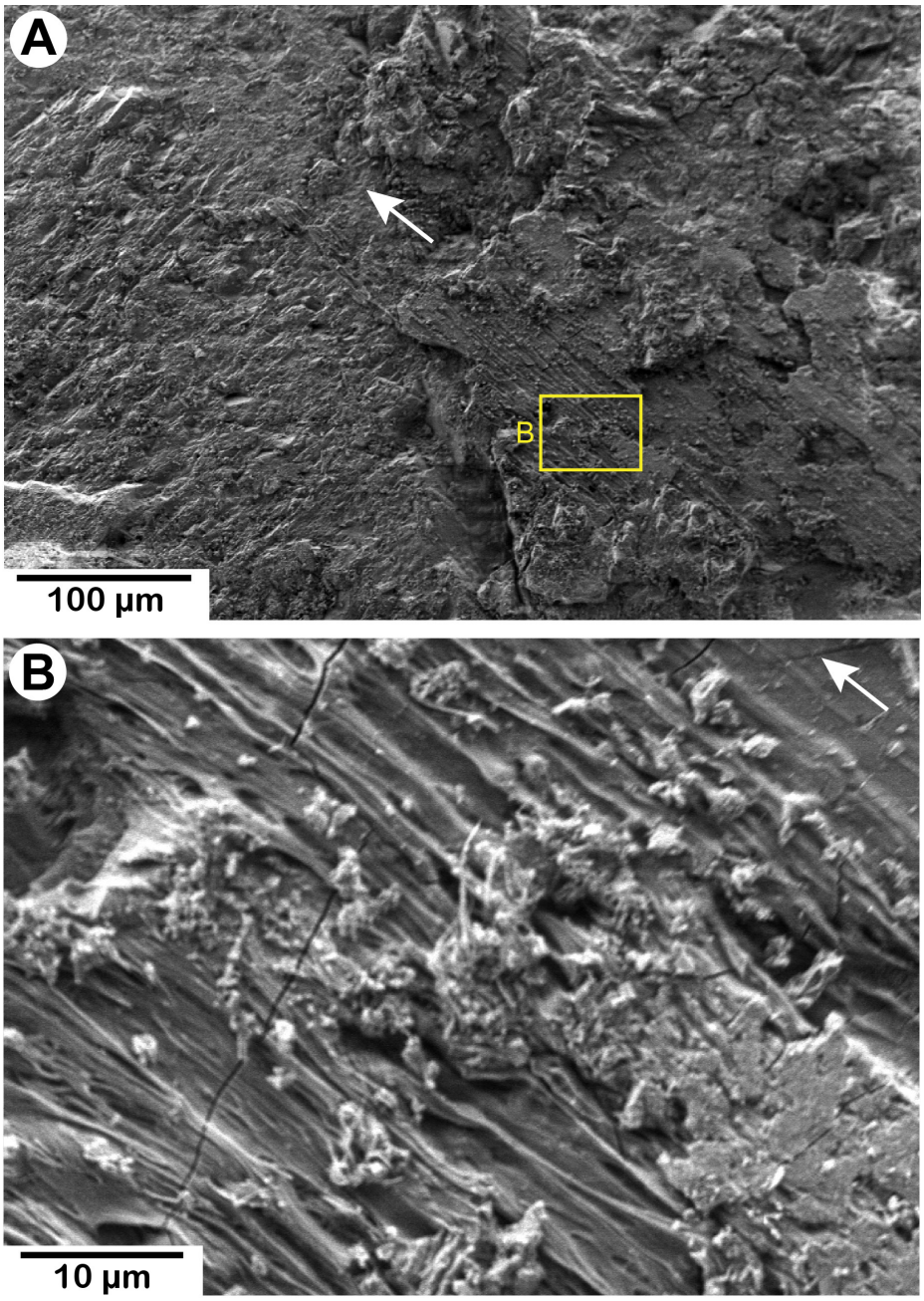

Figure 511-12. Secondary-electron images of a striated glassy surface exposed in a rough but relatively low-topography area. White arrows show shear direction of driving block. *A*, Low-magnification view shows location of *B*. *B*, The glassy surface is highly stretched out and appears to be a composite of many thin glassy strands. Those near the lower left corner are hairlike. The striae are overlain by matted material similar to that in figure 511-7*D*.

DL504—400 MPa

This was the first sample that was examined with the SEM for evidence of melt generation using secondary-electron techniques. Aside from verifying the presence of glassy textures, this sample was not examined petrographically in any detail. The experiment was characterized by three total stress drops (250–320 MPa), in contrast to the other examined 400-MPa samples. If melting occurred during each of the stick-slip events with total stress drops, then textural evidence of the multiple melting episodes may be preserved. This sample, or others like it, thus deserves further study. The narrow end of one driving block (fig. 504-1) was mounted on a glass slide for SEM examination. The sample orientation in figure 504-1 is roughly the same as that in the SEM images, with movement towards the lower left.

Figure 504-1. Photograph showing the narrow end of one driving block from experiment DL504 that was studied. Black arrow shows offset direction of this piece.

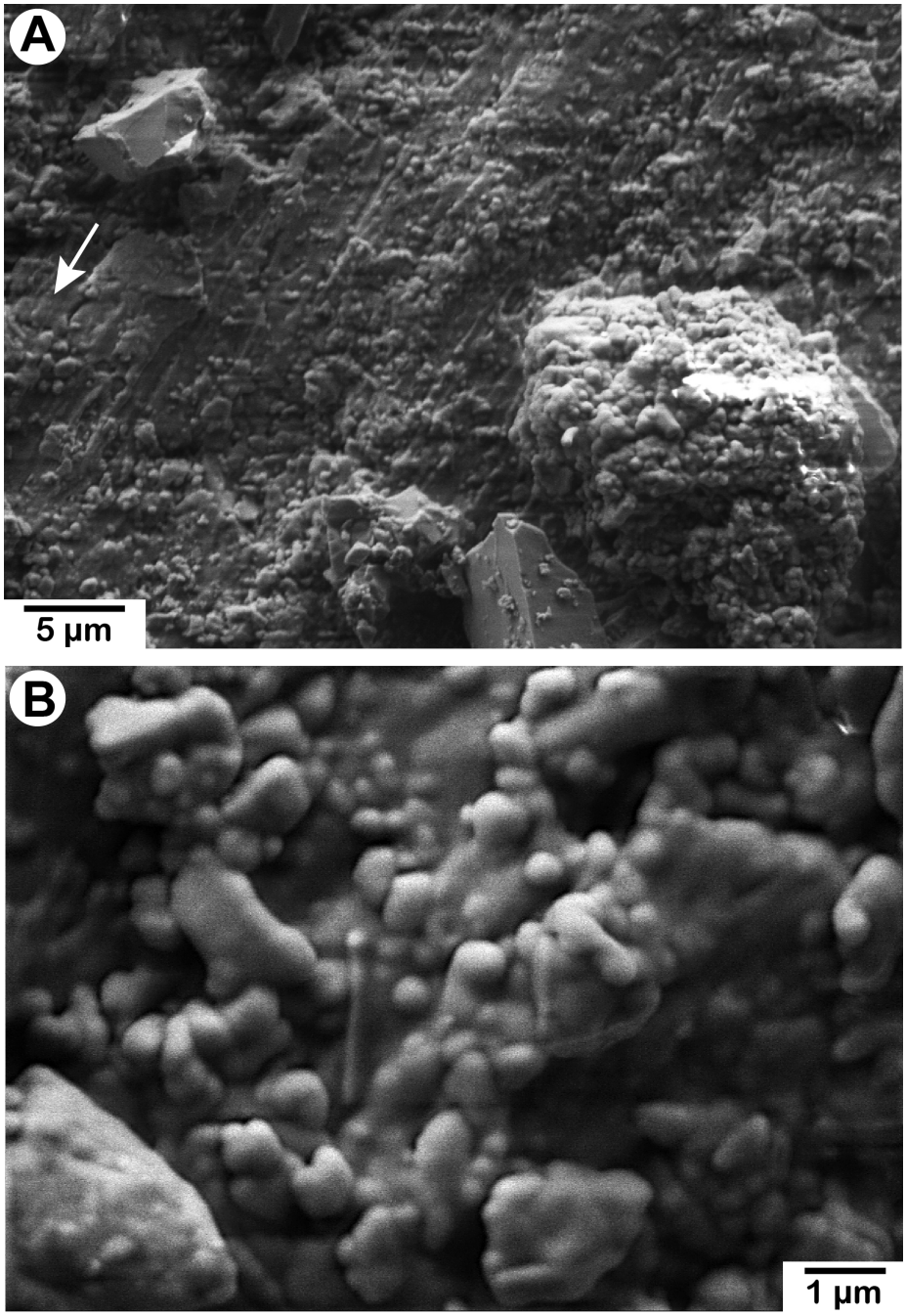

Figure 504-2. Secondary-electron images of a relatively rough, locally slickensided shear band. *A*, The large mineral fragment at lower right is covered with small, rounded grains coated with glass. White arrow shows shear direction of driving block. *B*, This higher magnification image was taken slightly below and to the left of the larger grain in *A*. The rougher parts of the shear band have a similar texture to that of the large coated grain. The many rounded grains, visible beneath the glassy coatings, were not commonly observed in sample DL511. These rounded grains may perhaps reflect the progressive rounding of the brecciated minerals adjoining the sawcut and their incorporation into the melt during later slip events.

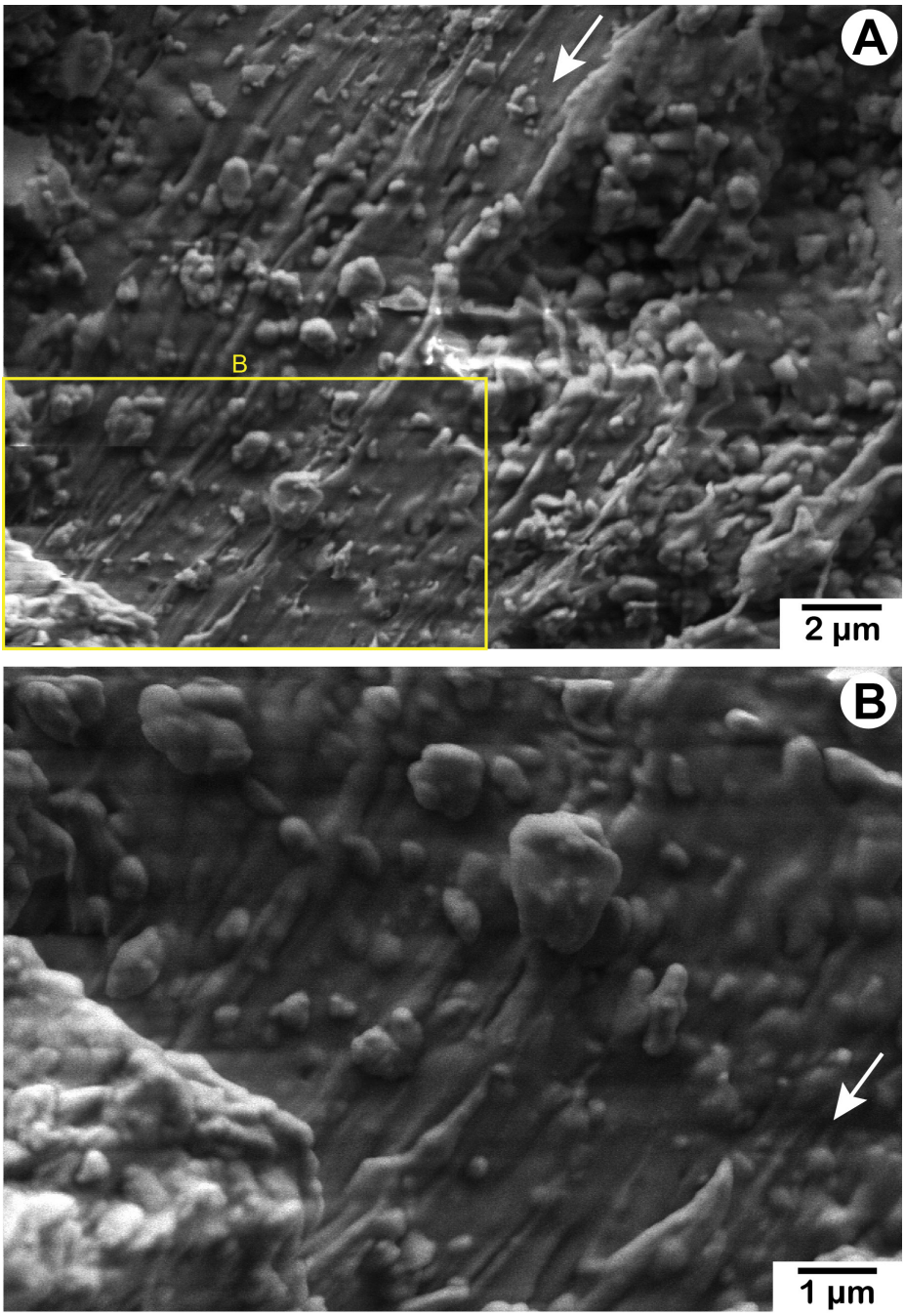

Figure 504-3. Secondary-electron images of a somewhat streaky, glassy surface at high magnification. White arrows show shear direction of driving block. *A*, Lower magnification view shows location of *B*. *B*, Loose clasts of various sizes on top of the striated shear band are typically clusters of spherical grains covered by a thin coating of glass. Numerous other rounded grains are embedded in the striated surface.

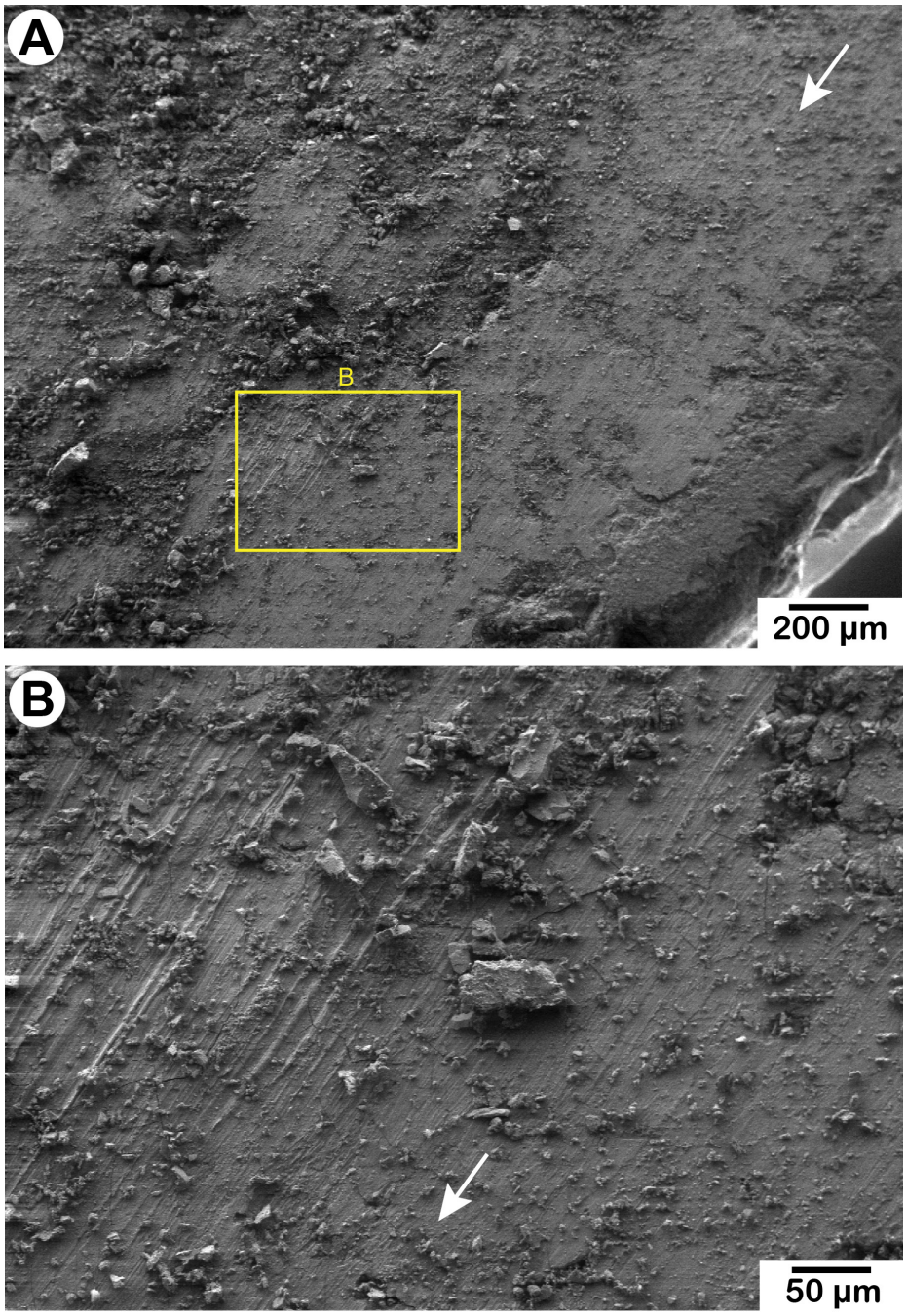

Figure 504-4. Secondary-electron images showing shear textures near the edge and towards the tip of the driving block. White arrows show shear direction of driving block. *A*, Low-magnification view shows location of *B*. *A*, *B*, At lower magnifications, the surface shows no obvious signs of melting; the matted surface and the striations could be mistaken for slickensided, granular gouge.

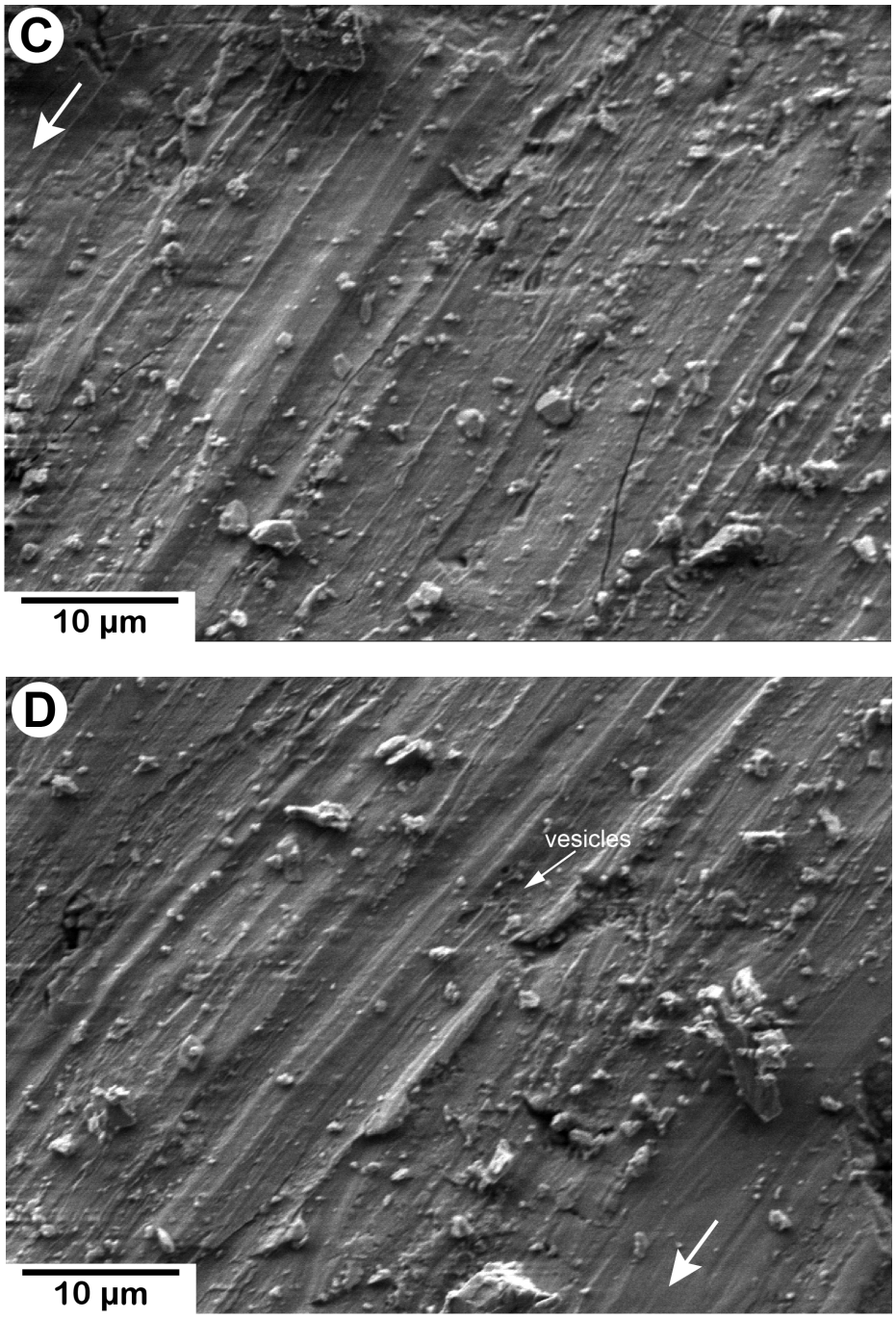

Figure 504-4.—Continued. Image *C* was located approximately halfway across the dull, matted band located on the right side of *A*, whereas *D* was close to the outer edge. Ridge and trough textures predominate, and a few vesicle-rich patches are present. The shear band in *C* is fractured in two places, suggestive of glass.

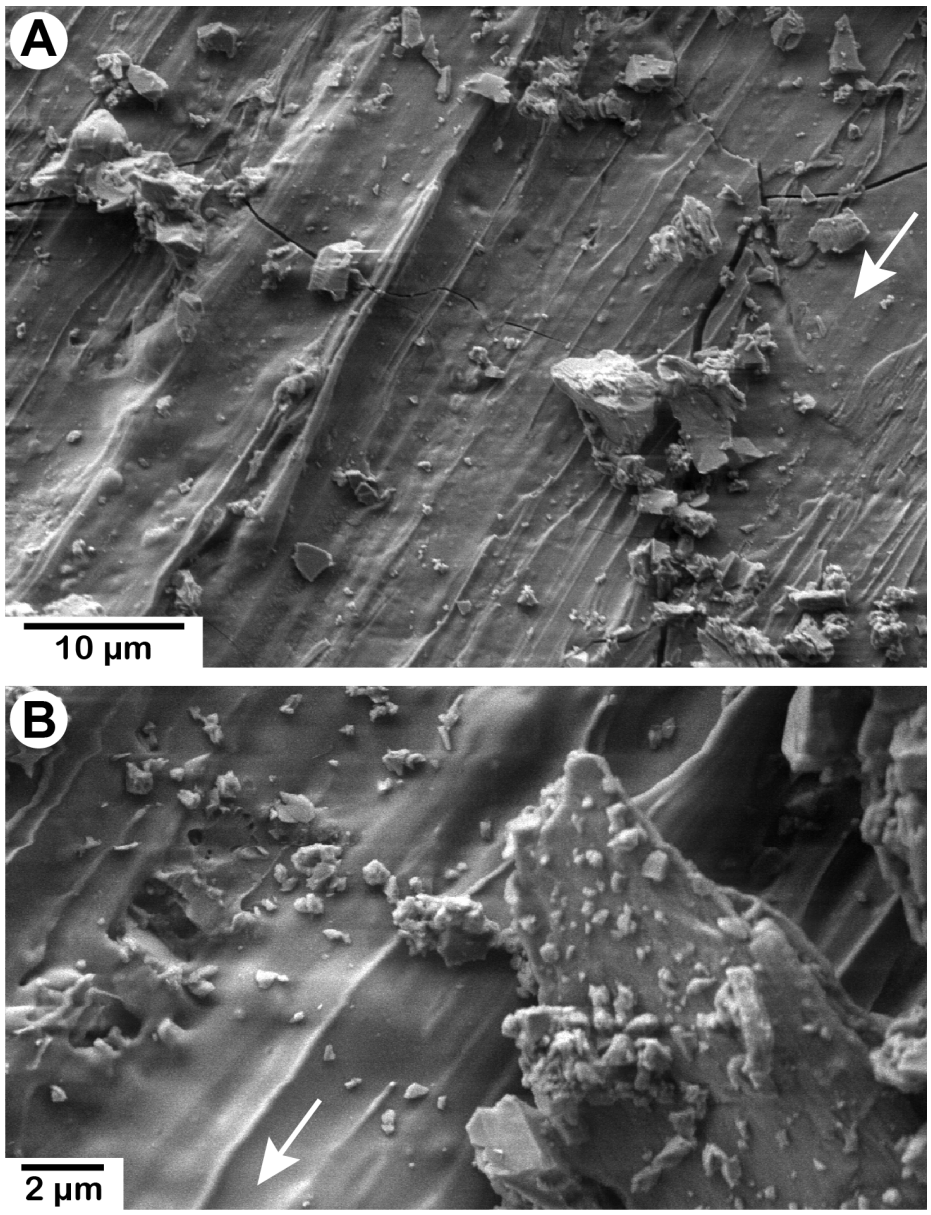

Figure 504-5. Secondary-electron images showing glass textures from different locations on the surface at high magnification. White arrows show shear direction of driving block. *A*, This spot is slightly inboard from the matted area shown in figure 504-4*A*. The surface of *A* is fractured in several places, and the narrow ridges have the irregular character seen on glass surfaces elsewhere. *B*, *C*, Images taken approximately halfway across the width of the sawcut. On the left side of *B* several pores are exposed at or just below the surface. The rubble on the surface in *C* includes several composite clasts containing small (<1-µm-diameter), spherical, glass-coated grains.

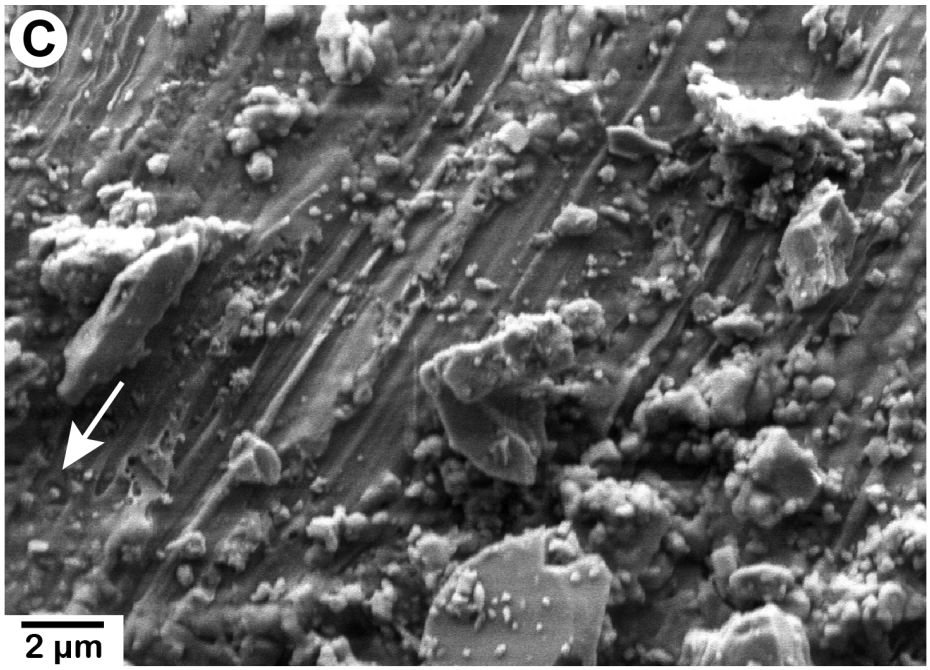

Figure 504-5.—Continued.

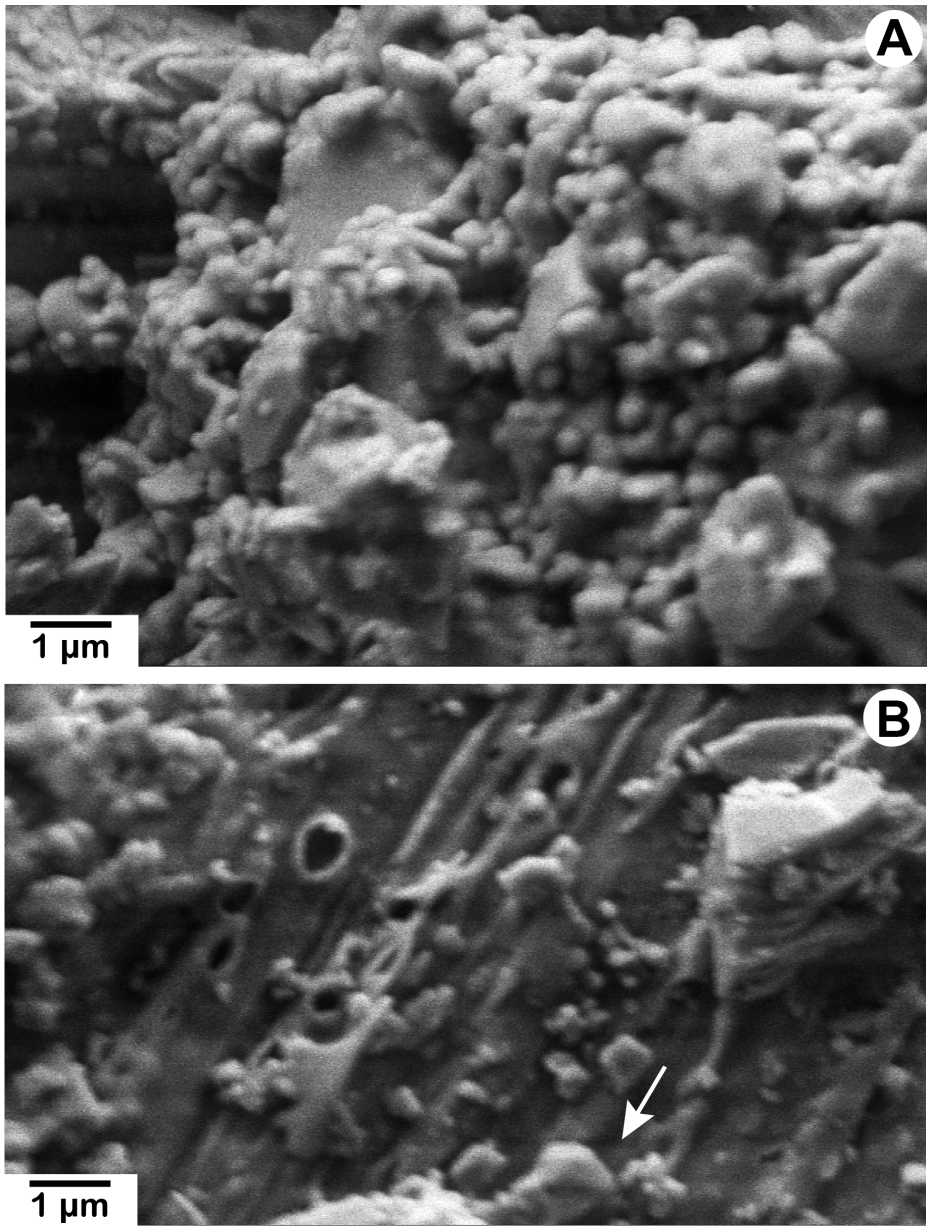

Figure 504-6. Secondary-electron images that are at high magnification and slightly out of focus. *A*, Rounded grains encased in glass in a rubbly area. *B*, Numerous vesicles on a striated, clast-rich, glassy surface. White arrow shows shear direction of driving block.

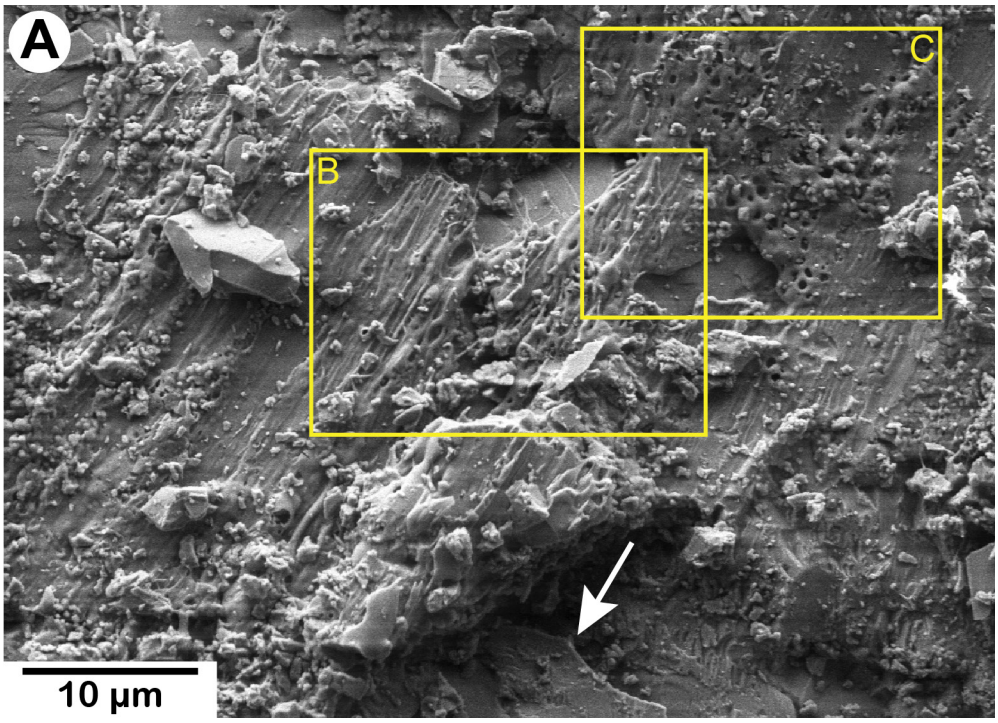

Figure 504-7. Secondary-electron images of an area rich in glassy textures. White arrows show shear direction of driving block. *A*, Lower magnification view shows locations of *B*, *C*. Textures range from vesicle-rich blobs of glass to flatter, well-striated surfaces with a few 2–4-µm-long hairs of glass. Glimpses of crystal surfaces are visible beneath the glassy coverings.

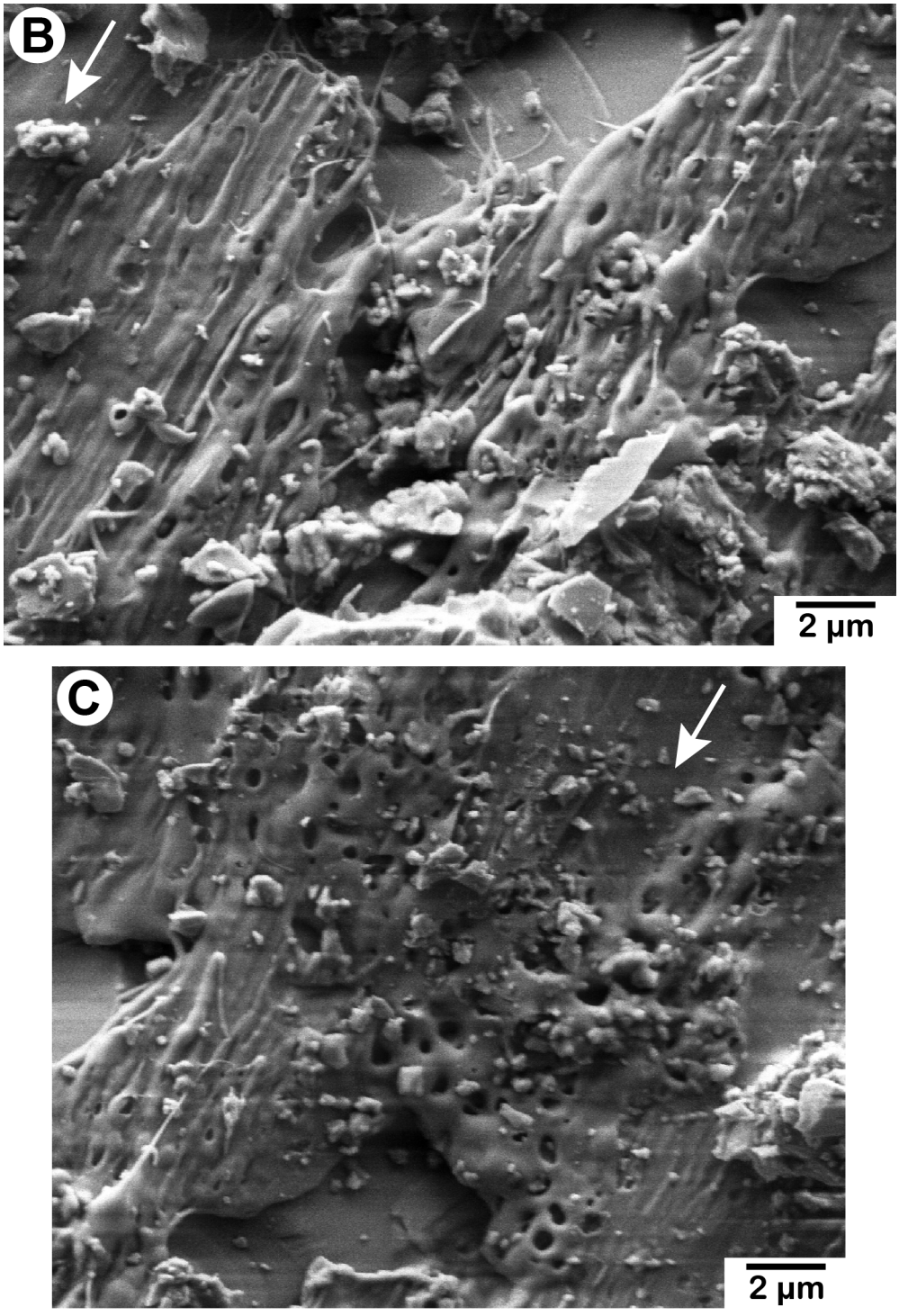

Figure 504-7.—Continued.

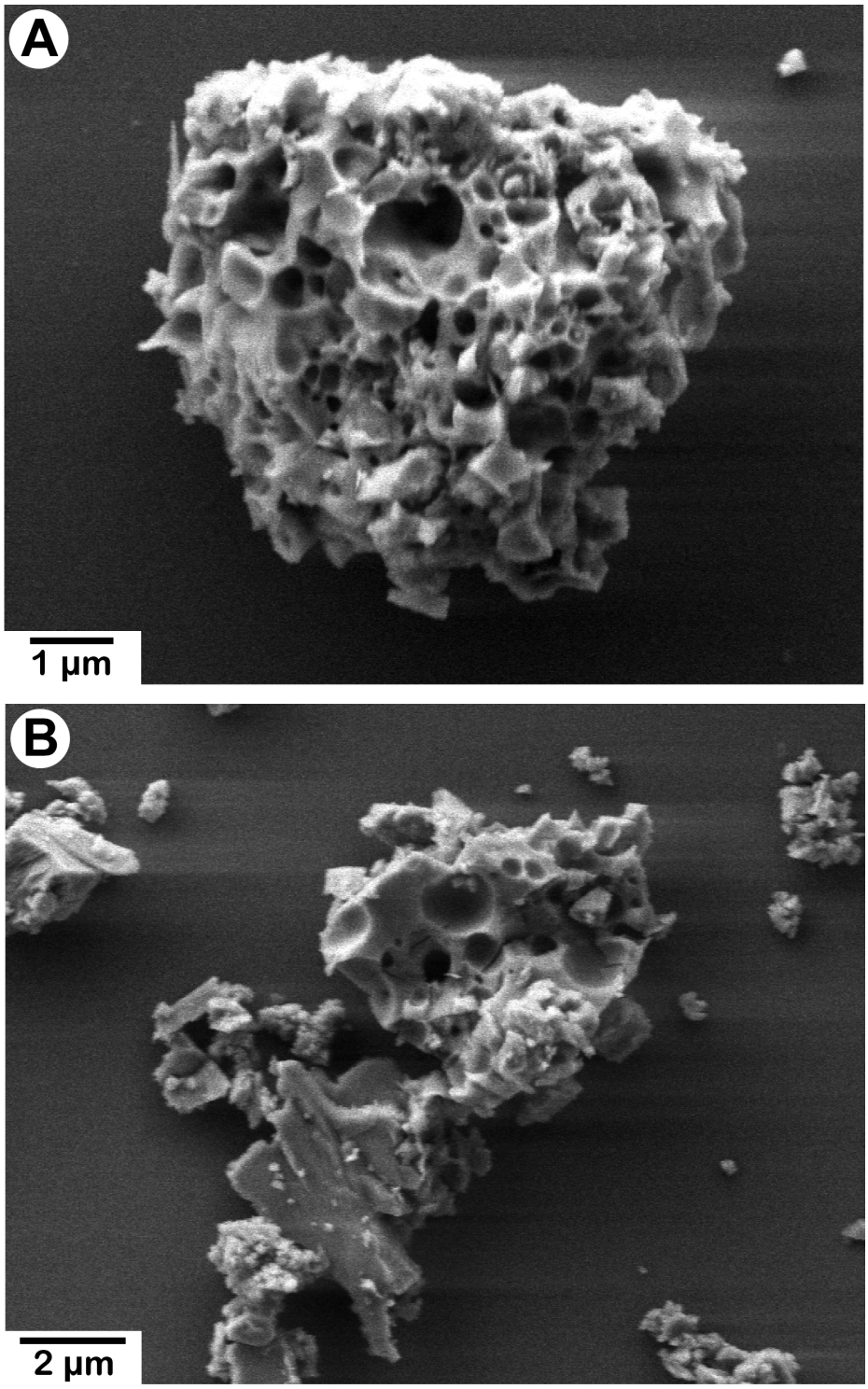

Figure 504-8. Secondary-electron images of loose pieces from the sample that were mounted on a glass slide for study. The grain in *A* and the largest grain in *B* have scoriaceous textures. Maximum vesicle diameter in these grains is ~2 µm.